AD-A036 302 GENERAL RESEARCH CORP MCLEAN VA WASHINGTON OPERATIONS F/G 17/8
COAT: MODAL-ZONAL COMPARISON.(U)
AUG 76 J RADLEY, N NOMIYAMA, J WILSON N60921-76-C-0122

UNCLASSIFIED NL

1 OF 2
AD-A
036 302

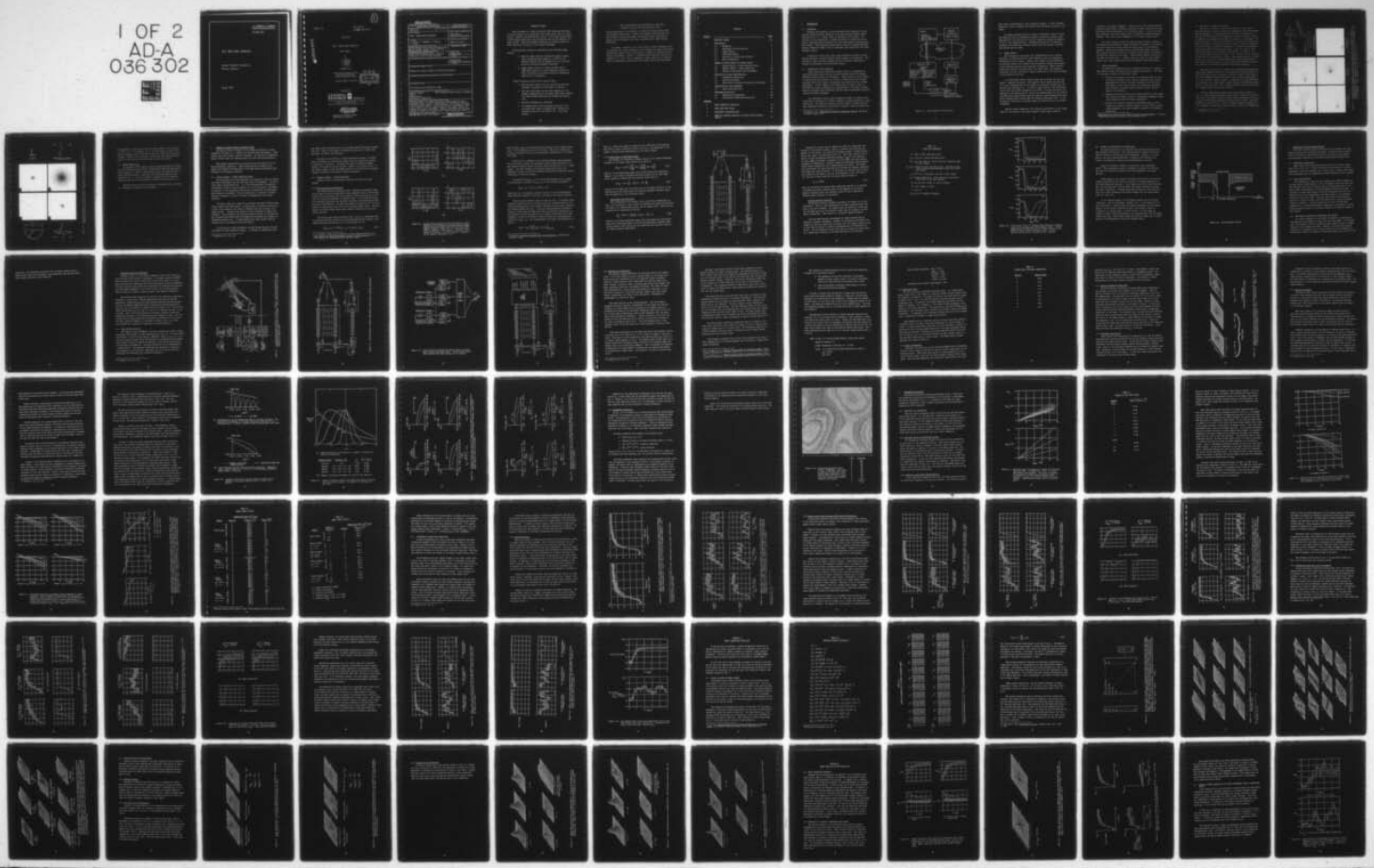

U.S. DEPARTMENT OF COMMERCE
National Technical Information Service

AD-A036 302

COAT: MODAL-ZONAL COMPARISON

GENERAL RESEARCH CORPORATION
McLEAN, VIRGINIA

AUGUST 1976

August 1976

WGRC 76-4482

Copy 2 of 50 Copies

911-01-CR

AD A036302

COAT: Modal-Zonal Comparison

Final Report

by

J. Radley
N. Nomiyama
J. Wilson
G. Gurski

Prepared for:

Naval Surface Weapons Center
White Oak Laboratory
Silver Spring, MD 20910

Contract N60921-76-C-0122

DDC
RECEIVED
MAR 1 1977
D

Prepared by:

GENERAL RESEARCH CORPORATION
WASHINGTON OPERATIONS
7655 OLD SPRINGHOUSE ROAD
WESTGATE RESEARCH PARK, MCLEAN, VA 22101

REPRODUCED BY
NATIONAL TECHNICAL
INFORMATION SERVICE
U.S. DEPARTMENT OF COMMERCE
SPRINGFIELD, VA. 22161

Approved for public release;
distribution unlimited

UNCLASSIFIED

SECURITY CLASSIFICATION OF THIS PAGE (When Data Entered)

REPORT DOCUMENTATION PAGE		READ INSTRUCTIONS BEFORE COMPLETING FORM
1. REPORT NUMBER 911-01-CR	2. GOVT ACCESSION NO.	3. RECIPIENT'S CATALOG NUMBER
4. TITLE (and Subtitle) COAT: MODAL-ZONAL COMPARISON		5. TYPE OF REPORT & PERIOD COVERED Final Report 6. PERFORMING ORG. REPORT NUMBER
7. AUTHOR(s) J. Radley, N. Nomiyama, J. Wilson, G. Gurski		8. CONTRACT OR GRANT NUMBER(s) N60921-76-C-0122 New
9. PERFORMING ORGANIZATION NAME AND ADDRESS General Research Corp.-East, Washington Operations, Westgate Research Park, 7655 Old Springhouse Rd., McLean, VA 22101		10. PROGRAM ELEMENT, PROJECT, TASK AREA & WORK UNIT NUMBERS
11. CONTROLLING OFFICE NAME AND ADDRESS Naval Surface Weapons Center, White Oak Laboratory, Silver Springs, MD 20910		12. REPORT DATE August 1976 13. NUMBER OF PAGES v + 105
14. MONITORING AGENCY NAME & ADDRESS(if different from Controlling Office)		15. SECURITY CLASS. (of this report) Unclassified 15a. DECLASSIFICATION/DOWNGRADING SCHEDULE

16. DISTRIBUTION STATEMENT (of this Report)

Approved for public release; distribution unlimited.

17. DISTRIBUTION STATEMENT (of the abstract entered in Block 20, if different from Report)

Cont'd from P.1

18. SUPPLEMENTARY NOTES

This research was sponsored by ARPA.

19. KEY WORDS (Continue on reverse side if necessary and identify by block number)

Optics, Adaptive
Lasers
Modal Control
Atmospheric Compensation
COAT (Coherent Adaptive Optics Technique)

20. ABSTRACT (Continue on reverse side if necessary and identify by block number)

The performance of a modal multidither Coherent Adaptive Optics Techniques (COAT) System is investigated via simulations with distributed dynamic targets. Target influence on performance is shown to be similar to that of zonal systems in that target effects can degrade and prevent convergence. However, additional design alternatives are shown to be possible with a modal system that cannot be achieved with a zonal system.

DD FORM 1 JAN 73 1473 EDITION OF 1 NOV 65 IS OBSOLETE

UNCLASSIFIED

SECURITY CLASSIFICATION OF THIS PAGE (When Data Entered)

EXECUTIVE SUMMARY

The performance of a modal multidither COAT system has been found to be quite similar to an equivalent zonal system with respect to target effects. However, the whole-aperture control of the modal system results in both design complications and alternatives that are not apparent for zonal systems. These are especially important in scenarios where low-order aberration correction is the primary requirement.

All multidither systems are influenced by the following target effects:

1. When the target spectrum overlaps the dither channels with a normalized power density $S_c \geq (G^2\Delta f)^{-1}$, the affected channels will be dephased (G is the loop gain and Δf is the noise equivalent bandwidth).
2. Large targets introduce a dither reduction factor (DRF) which results in a non-optimum gain causing delayed convergence and increased residual uncompensated phase error at convergence.

A modal transmitter differs from a zonal in that:

1. Whole-aperture control does not dictate the loop gain increase in proportion to the number of channels.
2. The lower order modes are much more important in turbulence compensation than the higher order modes, whereas in a zonal system essentially all channels are equivalent.
3. The DRF is different for each mode.
4. The maximum return from an extended target may occur at a point other than a converged beam. However, the observed effects have been small (i.e., $\lesssim \lambda/10$ peak offset).

5. Dither amplitudes must be different for each mode in order to achieve the same modulation level.

The non-equivalence of each channel in a modal system does create additional design complications. However, the unequal correcting power and whole-aperture control does present interesting design trade-offs for adaptive gain and channel allocation in scenarios with target-limited performance.

In summary: results of this study indicate a modal transmitter will be equivalent to a zonal transmitter in the presence of target effects (and perhaps more complex) when a large number of channels is required to meet mission requirements. However, in scenarios where low-order correction is adequate (i.e., tilt, focus, astigmatism) a modal system can be conceived which is fundamentally superior and less complex than a zonal equivalent.

CONTENTS

SECTION			PAGE
	EXECUTIVE SUMMARY		iii
1	INTRODUCTION		1
	1.1	Background	1
	1.2	Description of COAT Operation	1
	1.3	Target Effects	3
	1.4	Study Requirements	4
	1.5	Selection of Targets and Scenarios	5
	1.6	Report Organization	8
2	SUMMARY OF TARGET EFFECTS ON DITHER SYSTEMS		9
	2.1	Spatial Effects - Dither Reduction Factor	9
	2.2	Temporal Effects - Target Modulation	10
	2.3	Summary of Multidither COAT Performance	18
3	COMPARISON OF SYSTEM CHARACTERISTICS		20
	3.1	Atmospheric Compensation	20
	3.2	Beam Control/Dither	20
	3.3	Beam Control Influence on Electrical Loop Design	20
4	SIMULATION BASE-LINE PARAMETERS		22
	4.1	Modal System Base-Line	22
5	PERFORMANCE EVALUATION		44
	5.1	Open-Loop M-D Comparisons	44
	5.2	Illustrative Closed-Loop Simulations	53
APPENDIX			
A	MODAL TRANSMITTER SIMULATION		70
B	MODAL BASE-LINE SYSTEM		85
C	ATMOSPHERIC TURBULENCE MODEL		92
D	EFFECT OF APERTURE AVERAGING ON SPECKLE POWER SPECTRAL DENSITY		97

1 INTRODUCTION

1.1 BACKGROUND

Technical data generated by the COAT-Modal-Zonal Comparison Program, Contract N60921-76-C-0122, sponsored by the Naval Surface Weapons Center, monitored by Mr. W. P. Altman, NSWC, is presented in this report. The objective of this program was to assess the effects of target-COAT interactions comparing modal multidither with zonal multidither and phase-conjugate systems. This program paralleled efforts with the on-going RADC/ARPA Contract F30602-75-C-0086,[1] which is supporting zonal multidither and phase conjugate studies.

A potential problem exists when target modulation overlaps the COAT sensing bandwidth, causing erroneous control signals to be generated. Differences in modal and zonal transmitters are of potential importance in closed-loop performance with distributed targets.

1.2 DESCRIPTION OF COAT OPERATION

A COAT system uses closed-loop feedback control to compensate for time-varying phase distortions which would otherwise reduce the maximum achievable energy density at the aimpoint. These systems are also capable of fine pointing and tracking, but require a strong return from a highly localized area on the target's surface near the optical axis for optimum performance. A block diagram of the COAT process is shown in Fig. 1-1. Two different sensing techniques are considered here, one based on energy detection (outgoing wave multidither) and the other on heterodyne detection (return-wave phase conjugate).

In a multidither system, each transmitter element (or vibrant structural mode) is dithered at a distinct frequency to phase modulate the transmitted beam. The radiation scattered from the target is energy detected; then synchronous detection at each dither frequency is used to recover the

[1] J. Radley et al., COAT-Target Interactive Modulation Effects, GRC Report 571-02-TR, August 1976.

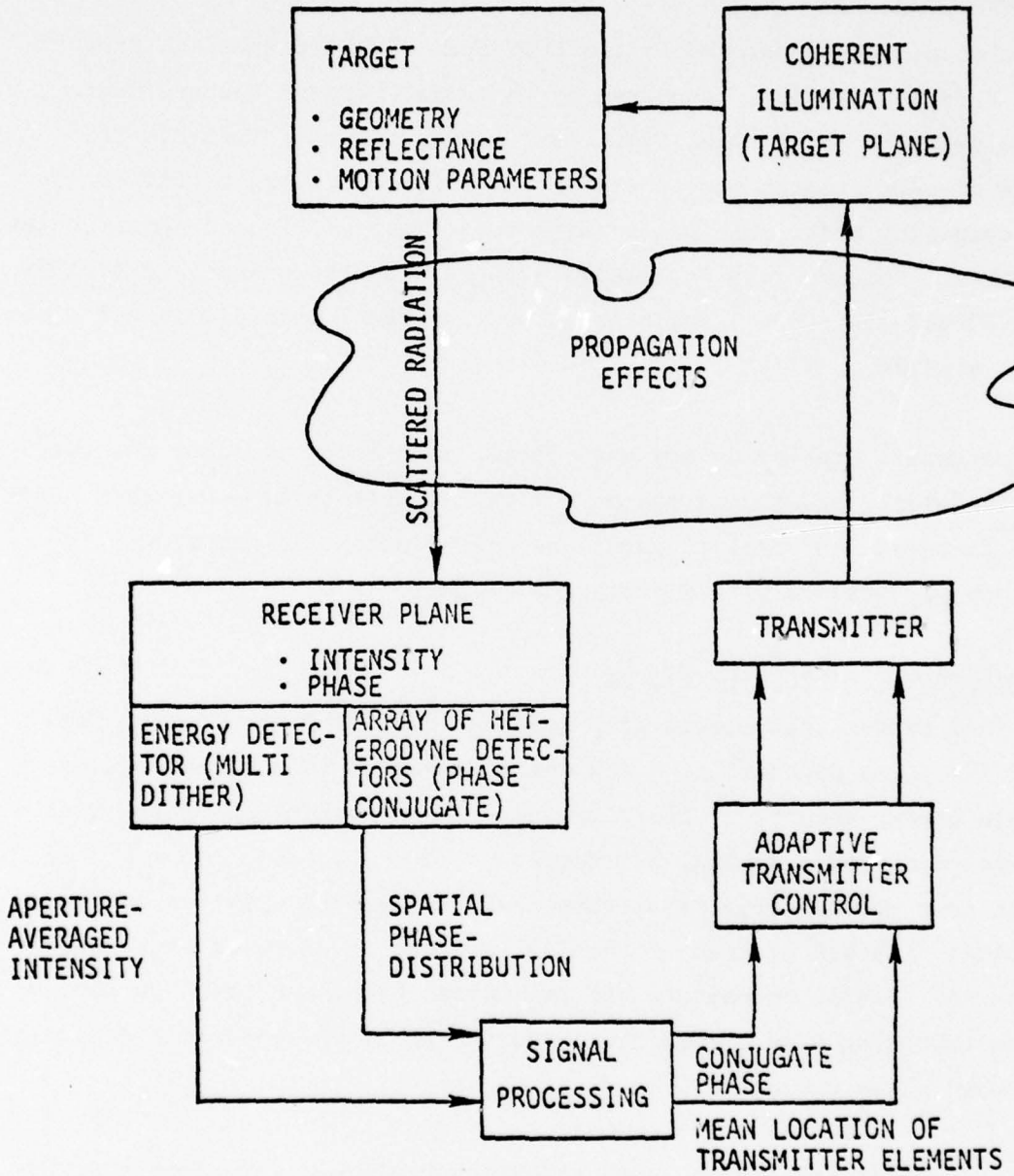

Figure 1-1. Block Diagram of COAT Process

error signal corresponding to each transmitter element. A "hill climbing" algorithm is used to maximize the received power and hence the power on the target.

In a phase conjugate system, an array of heterodyne receivers, which are coincident with the transmitter elements, measures the spatial phase distribution of the returned wave from the target and applies the negative of this to the transmitted beam. Assuming reciprocity of the phase disturbances, the transmitted wavefront cancels them and produces a diffraction-limited beam on target.

1.3 TARGET EFFECTS

Both systems have been shown, both experimentally and by computer simulation, to perform well with laser wavefront errors and atmospheric turbulence for point targets. However, real targets are distributed and not optically smooth, and therefore produce spatially complex interference in the scattered radiation when coherently illuminated. Target rotation causes this spatially varying pattern to be swept across the receiving aperture(s) in time, resulting in temporal modulation of the received signal in both intensity and phase.

In a multidither system, target effects may be placed into two categories: temporal and spatial. The temporal effects depend upon the size (D) of the illuminated area on the target, its effective rotation rate (Ω) and the laser wavelength (λ). In terms of power spectrum, the target modulation (TM) noise covers frequencies up to $2\Omega D/\lambda$. For the high dither frequencies the TM spectrum may not overlap the sensing bands, but the analysis and simulations presented here show that there is noise centered about each dither frequency which reduces SNR and increases convergence time. If the TM spectrum overlaps all the dither bands, the system can fail to converge altogether.

Spatial effects depend upon the brightness distribution of the target, which in turn depends on the target geometry, aspect angle, material

reflectance, and surface roughness. Adaptive optics (A/O) systems perform optimally against highly localized, single-glint targets because these give the largest dither modulations of the received signal. If the size of the glint increases, the dither signal level is reduced and system performance degrades. This effect occurs independent of the target dynamic motion.

In a phase conjugate system, an extended target produces a phase in the receiver plane which has a random distribution unrelated to the desired correction phase and a spatial scale the same as that of the intensity speckles. Target motion produces both a translational Doppler frequency shift from the optical carrier and a frequency spread around this caused by the effective rotation of the target. These produce temporal variation of the phase in each detector. A target which has a glint of large spatial extent causes large random phase errors and degrades system performance.

1.4 STUDY REQUIREMENTS

The Modal-Zonal Comparison Program addressed the effect of targets on COAT systems through both open-loop and closed-loop simulation. The scope of the program consisted of three major tasks:

1. Develop the formalism to describe the vibrational modes in terms of Zernike polynomials, which would be compatible with computer implementation; simulate the modal transmitter with the proper algorithms to permit both open-loop and closed-loop operation; and incorporate the MOWACS (Modal Wavefront Control System)[1] modes in the simulator.

2. Examine the open-loop dither error signals against a point target and a variety of complex targets, to determine fundamental differences between the modal and zonal transmitters.

3. Evaluate illustrative closed-loop performance against a point target and a variety of complex targets with and without a phase screen atmosphere, and apply parametric analysis to performance predictions.

---

[1] Modal Wavefront Control Systems (MOWACS) Phase II Interim Report, C. Neufeld, Perkin-Elmer Corporation Report 12700, September 1975.

1.5 SELECTION OF TARGETS AND SCENARIOS

The particular choice of targets and scenarios for this study is important because it serves as a basis for comparing the three COAT systems under consideration. It is apparent from the variety of scenarios envisioned for COAT systems[1] that undertaking a parametric study of performance against all combinations of targets and scenarios is a monumental (and unnecessary) effort. Much of the interest is in the tactical encounter for which the atmospheric effects can be severe and hence adaptive compensation can make the biggest performance improvement. For these cases atmospheric absorption necessarily limits useful ranges to less than 20 km, so that usually only a portion of the target is illuminated. In addition, the target aspect angle is often near nose-on (±30°) for many tactical scenarios, and hence can be represented as a simple, single dominant feature, as shown in Fig. 1-2. In this way, COAT performance can be better quantified in terms of the effective glint size on the target, which depends on the surface radius of curvature and its material reflectance properties.

This does not mean that all targets can be adequately represented by simple sphere segments and that it is unnecessary to accurately model the particular complex target of interest. However, the goal of this study is of a more fundamental nature and is meant to be of greater applicability than to a particular class of targets. In addition, if a COAT system does not perform well on a simple sphere segment having a single maximum radiance located on the optical axis, then it almost certainly will not perform well on a complex target having multiple features.

The four single-feature targets used in this study are shown in Fig. 1-3. The distributed radiance of each target is shown on a 14-level gray scale. The display scales are linear, and much of targets A and C are a factor of 20 below the peak value and hence are not visible. The sizes and radii of curvature (0.2, 1, and 4 m) selected roughly correspond to a nose, fuselage, and wing section of an aircraft or missile, and demonstrate

---

[1] J. Radley et al., op. cit.

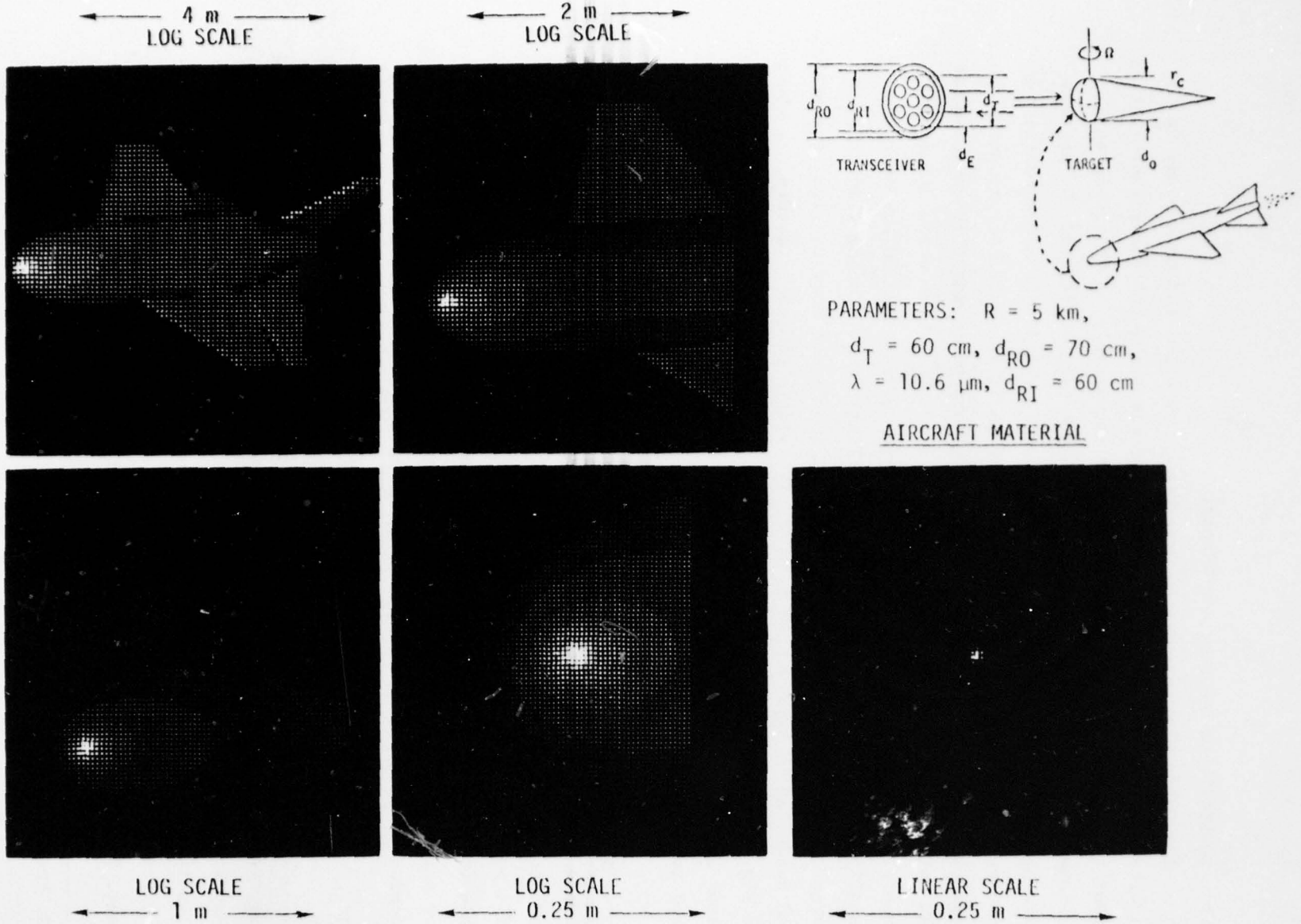

Figure 1-2. Tactical Scenario Parameters for Closed-Loop Simulations and Distributed Radiance of Styx Missile with Uniform Illumination. The log intensity scale spans a dynamic range of approximately 30 dB. Transmitter subaperture diameter d_E = 20, 12, 8.6 cm for 7, 19, 37 elements. Target parameters (d_0, r_c) given in Fig. 1-3.

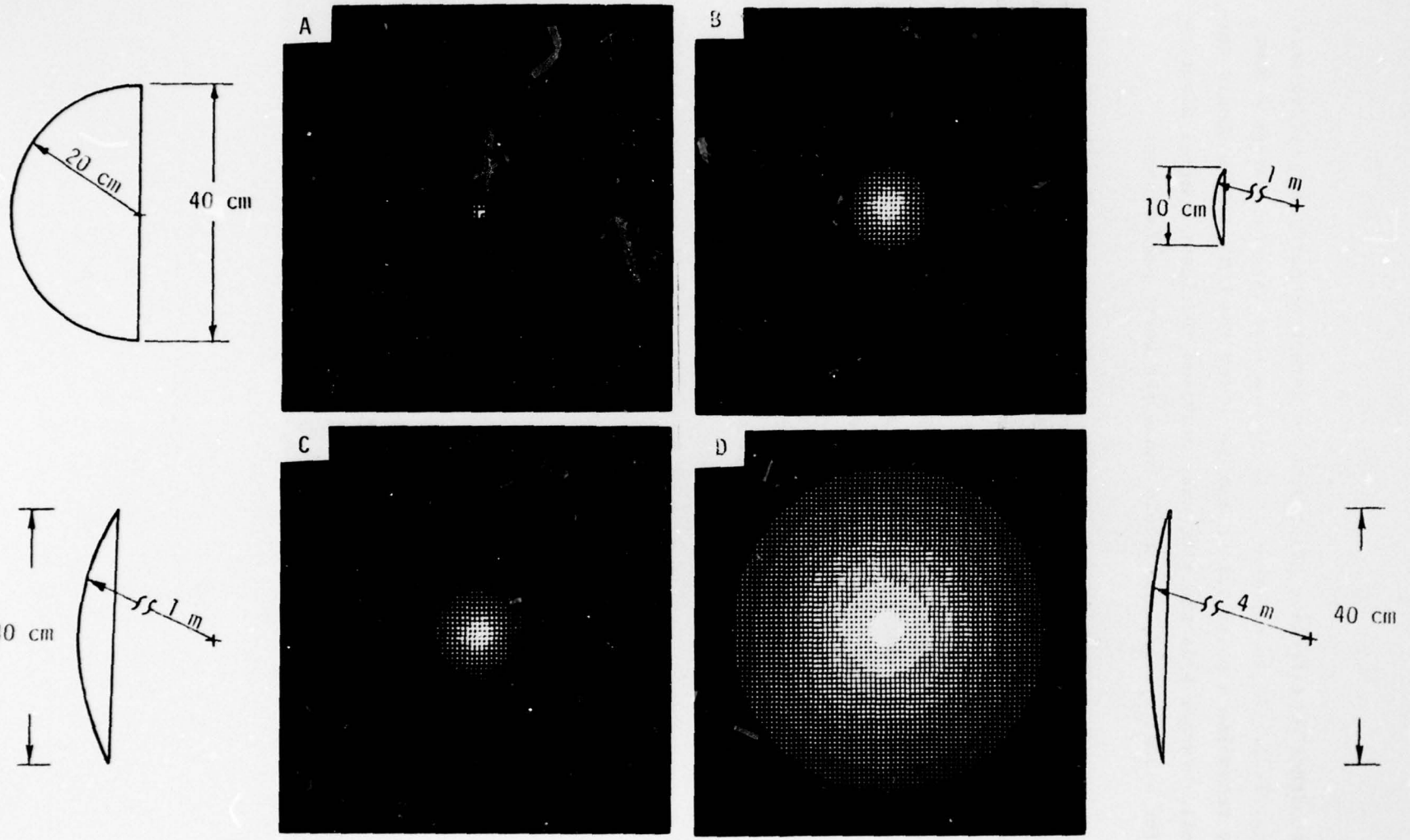

Figure 1-3. Distributed Radiance of Single-Feature Test Targets for 10.6-μm Uniform Illumination. Display is 14-level linear gray scale. Target surface is aircraft aluminum.

the dependence of effective glint size on target geometry and reflectance (cf. Fig. 1-3). It is apparent that, of the four targets, target A most closely resembles a point target against which the COAT system should perform well. Target D is the flattest, provides the least spatial discriminant for a COAT system, and should cause the worst performance.

1.6 REPORT ORGANIZATION

The remainder of this report contains a general description of target effects on COAT systems and specific comparisons of modal and zonal multidither approaches. Section 2 summarizes the nature of target influence on dither system performance. Modal and zonal system characteristics are compared in Sec. 3. Section 4 provides a description of the simulation parameters utilized for the performance evaluation presented in Sec. 5.

Additional data on the modal simulation, atmospheric model, and aperture averaging is contained in the Appendixes.

2 SUMMARY OF TARGET EFFECTS ON DITHER SYSTEMS

The spatial extent of targets and the temporal variations in their backscatter patterns (i.e., speckle) can influence COAT performance. These effects have been studied in detail[1] elsewhere. The results are summarized below to form a basis for comparing modal and zonal COAT characteristics.

Real dynamic targets must be characterized by both spatial and temporal backscatter properties. These properties may be related to the spatial and temporal resolving power of the COAT system to determine their influence on convergence properties.

2.1 SPATIAL EFFECTS - DITHER REDUCTION FACTOR

The system gain and dither amplitudes are selected in order to achieve the desired convergence time and the final level of convergence. Two first-order design considerations are: (1) a hill-climbing servo can approach the maximum to within a small increment (ε), and as the gain is increased ε is reduced; (2) the convergence time may *also* be reduced if the gain-bandwidth product is increased. Thus the dither level is selected in concert with gain parameters in order to achieve the maximum gain with stable operation.

The finite extent of a target will influence the depth of dither modulation sensed by the COAT system. As target size is increased from that of a point, the strength of the dither is modified such that the gain is no longer optimal. In general the modulation level decreases as target size increases. This influences the system performance exactly in the same manner as reduced gain which delays convergence and increases the residual uncompensated phase error ε. In most instances the delay rather than the residual error is of greatest practical concern.

In the case of a zonal transmitter the DRF (Dither Reduction Factor) is similar for each transmitter element. It becomes of significance when

---

[1] J. Radley et al., op. cit.

the target extent approaches that of the single element diffraction limited spot size. Thus, as the number of channels increases (for a fixed total aperture), the DRF is less important.

The effect is the same for a modal transmitter; however, its magnitude is different for each control channel since the diffraction pattern of each mode is different. In general the lower the spatial frequency content of the mode the greater the DRF. However, as is shown in Sec. 3, the relative impact on the nine MOWACS modes (all of which have low spatial frequency) depends on the specific target distribution.

2.2 TEMPORAL EFFECTS - TARGET MODULATION

Temporal effects are essentially identical for modal and zonal systems.

2.2.1 Target Backscatter Modulation

The complex wavefront emanating from a coherently illuminated target is the result of both the macroscopic surface geometry which is much larger than an optical wavelength and the microscopic surface which may be on the order of an optical wavelength or slightly larger. The surface microstructure produces random phase and intensity variation in the backscatter which is noise to COAT systems. The phase and intensity profiles in the receiver plane are illustrated in Fig. 2-1 for two different target sizes. As anticipated, the larger target yields higher spatial frequencies in the backscatter patterns.

The spatial power spectral density (PSD) $S_I(f_x, f_y)$ associated with the speckle intensity incident on the receiving aperture is related to the target brightness distribution I(u, v) and its mean $\langle I \rangle$ by[1]

$$S_I(f_x, f_y) = \langle I \rangle^2 [\delta(f_x, f_y) + \Gamma_I(\lambda R f_x, \lambda R f_y)] \qquad (2\text{-}1)$$

[1] J. W. Goodman, "Statistical Properties of Laser Speckle Patterns," in Laser Speckle and Related Phenomena, Topics in Applied Physics, Vol. 9, J. C. Dainty, ed. (Springer-Verlag, New York, 1975).

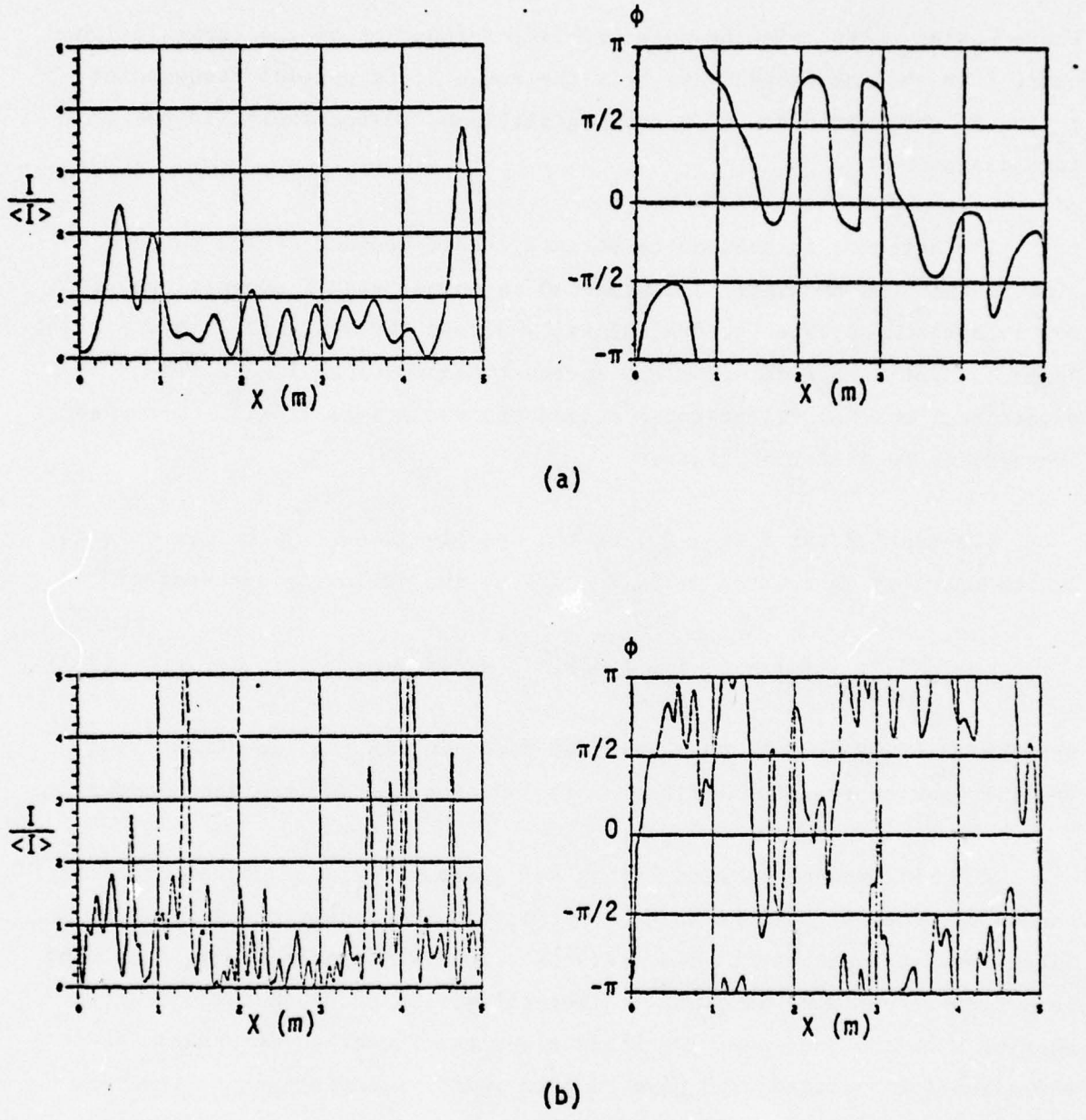

Figure 2-1. Receiver Plane Intensity ($I/\langle I\rangle$) and Phase (ϕ) Corresponding to Two Uniformly Illuminated Sphere Segment Targets Calculated Using Point Scatterer Model (PSM) Computer Program. Range = 5 km, λ = 10.6 μm; phase scale is modulo 2π. (a) Target B: diameter = 10 cm, radius of curvature = 1 m; (b) Target C: diameter = 40 cm, radius of curvature = 1 m.

where $\Gamma_I(\lambda R f_x, \lambda R f_y)$ is the autocorrelation function of the target brightness, λ is the wavelength, and R is the range. The spatial frequencies f_x and f_y correspond to the x and y directions, respectively, in the aperture plane.

The detector is assumed to be an aperture-bounded region perpendicular to the line of sight, and produces an output signal proportional to the integrated speckle pattern intensity across the aperture (i.e., a light bucket). For such a detector the aperture behaves much like a two-dimensional spatial filter which attenuates variations at different spatial frequencies to different degrees.

The spatial PSD $S_0(f_x, f_y)$ of the speckle intensity that is passed by the aperture is related to $S_I(f_x, f_y)$ by the following expression:[1]

$$S_0(f_x, f_y) = S_I(f_x, f_y)\left|H(f_x, f_y)\right|^2 \qquad (2\text{-}2)$$

where $H(f_x, f_y)$, the aperture transfer function, is the two-dimensional spatial Fourier transform of the pupil function of the receiver aperture.

Relative motion between target and aperture (e.g., a rotating target) causes the speckle pattern to be swept across the receiving aperture in a direction perpendicular to the target's effective rotation axis, resulting in a temporal-domain PSD $S_0(f)$. Since all spatial-frequency components sharing a common projected magnitude along the direction perpendicular to the effective rotation axis give rise to temporal variations at the same frequency, the PSD of the detector output is given by a one-dimensional integral of $S_0(f_x, f_y)$. For rotation about the y-axis, the expression for $S_0(f)$ is

$$S_0(f) = (v_x)^{-1}\left[\int_{-\infty}^{\infty} S_0(f_x, f_y)\, df_y\right]_{f_x = f/v_x} \qquad (2\text{-}3)$$

---

[1] A Papoulis, The Fourier Integral and Its Applications, (McGraw-Hill, New York, 1962).

where $v_x = 2R\Omega$ is the relative velocity in the x direction at the aperture and Ω is the target's effective rotation rate (i.e., the projection of the target's rotation vector perpendicular to the line of sight).

2.2.2 Noise Impact on COAT Beam Forming

The phasing of M transmitter elements results in an on-axis normalized intensity in the target plane (Strehl ratio) given by

$$\langle I/I_0 \rangle = (1/M^2) \left\langle \left[\sum_{m=1}^{M} \exp j\phi_m \right] \left[\sum_{n=1}^{M} \exp -j\phi_n \right] \right\rangle \qquad (2\text{-}4)$$

where ϕ_i is the target-plane phase of the field from the ith transmitter element. If we assume a Gaussian-distributed phase error in each transmitter channel of variance σ_ϕ^2, the resulting Strehl ratio is

$$\langle I/I_0 \rangle = \exp -\sigma_\phi^2 + (1/M)(1 - \exp -\sigma_\phi^2) \qquad (2\text{-}5)$$

Since it can be shown that the Strehl ratio is not highly sensitive to the distribution of the phase errors, the Gaussian assumption detracts little from the generality of the following results.

Multidither COAT with Noise

For a multidither (M-D) system, such as that shown schematically in Fig. 2-2, the variance in each channel is produced by at least three sources: (1) dither, (2) residual phase errors, and (3) target noise. Thus the total variance may be represented as follows:

$$\sigma_{\phi_i}^2 = (\beta^2/2) + (\sigma_i^2/G_L^2) + S_0(f_i) \cdot G_E^2 \cdot \Delta f \qquad (2\text{-}6)$$

where β is the dither modulation index, σ_i^2 is the variance of the initial phase error being compensated, Δf is the noise-equivalent bandwidth (NEB) of each channel, and G_L and G_E are the system loop and electronic gains of the control channels respectively.

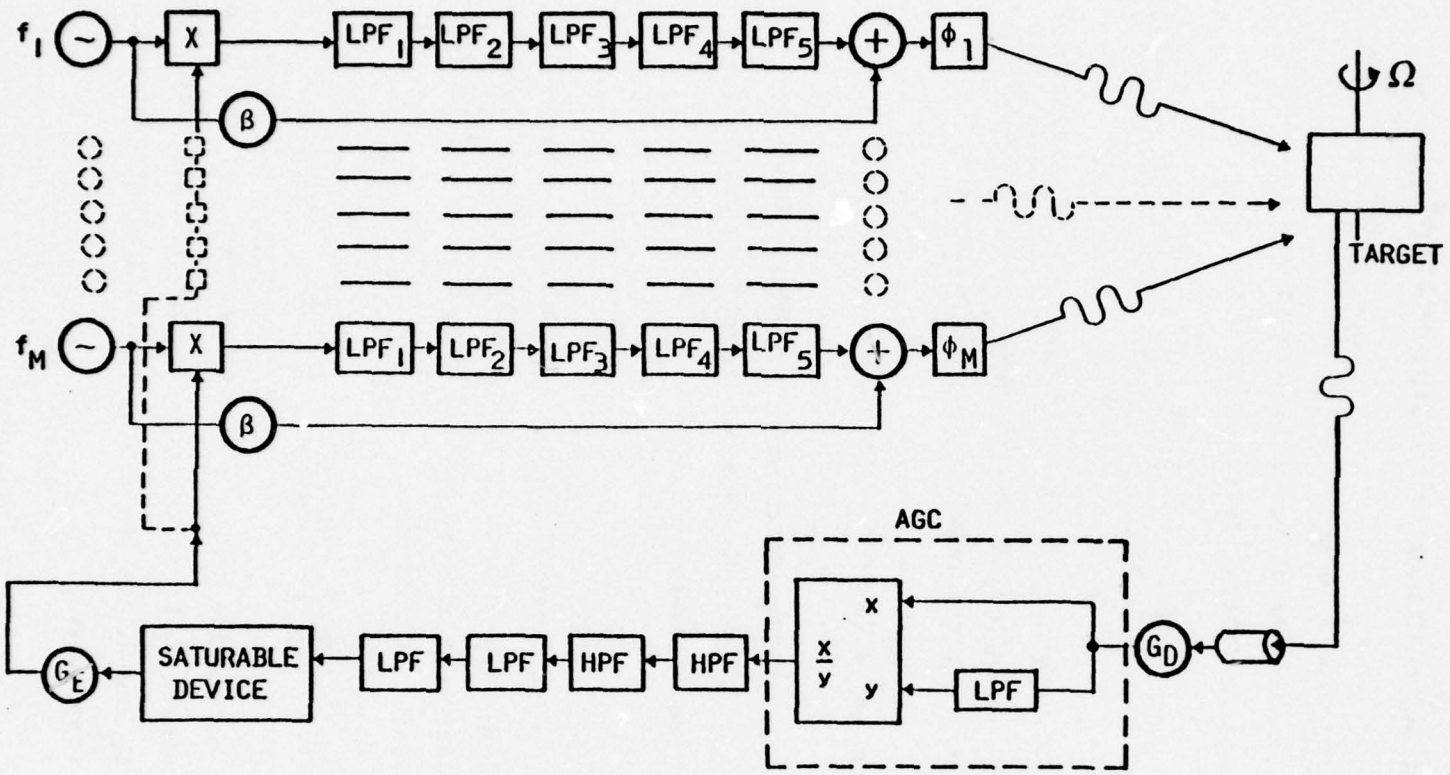

Figure 2-2. Block Diagram of Base-Line Multidither (M-D) COAT System: Important Parameters are Defined in Table 2-1

Equations 2-5 and 2-6 may be combined to yield the steady-state performance of a multidither system. Table 2-1 indicates the base-line parameters for the system. The resultant performance against a simple uniform square test target is illustrated in Fig. 2-3. The target rotation rate is varied to scale the maximum modulation frequency (f_{max}) in the spectrum. For this example the target is assumed to be very small such that aperture averaging is insignificant. Distinct regions of performance which approach nearly perfect phasing and total random phasing are evident. The transition occurs where the target spectrum $S_0(f)$ overlaps the sensing frequencies with high power spectral density. If we define the critical level of noise in a channel as that amount such that the exponential in Eq. 2-5 drops to e^{-1}, then the critical noise PSD to produce channel dropout is

$$S_c \approx 1/(G^2 \Delta f) \qquad (2\text{-}7)$$

Thus, by calculating the sensed target modulation spectrum it is possible to estimate the dither channels which will be dephased by the target. Aperture averaging, gain, and bandwidth trade-offs may be employed to minimize target influence on performance.

Initial Condition Threshold

The previous analytic treatments considered the targets to be fully illuminated. This is a good approximation for small targets and when the beam is not well converged. For targets which are physically larger than the converged spot size, the effective target size will change as convergence is approached. This results in a potential threshold process.

With the beam initially unconverged the target influence may be adequate to prevent convergence. However, if the system is initially converged the effective target size is smaller than the target's physical size. In this case the ability to maintain convergence may be dramatically improved. With intermediate initial conditions the system will either decay to a random phase condition or converge depending on the threshold.

TABLE 2-1

BASE-LINE PARAMETERS

$\beta = \pm 20°$ = dither modulation index

$\sigma_i = \pi/\sqrt{3}$ rad = initial RMS phase error

$\Delta f = 10\pi, 30\pi, 100\pi$ Hz = noise equivalent bandwidth (NEB) of each channel

G_L, G_E = system loop and electronic gains: selected to maintain a constant gain-bandwidth product as M and Δf are varied.

$\tau_c \simeq 10^{-3}$ sec = convergence time with a point target

f_D = dither frequencies: sine-cosine pairs starting at 8 kHz with 1.5 kHz pair spacing

M = 10, 30, 100 = number of control channels

R = 5 km = range to target

$\lambda = 10.6$ μm

d_T = 60 cm = transmitter diameter

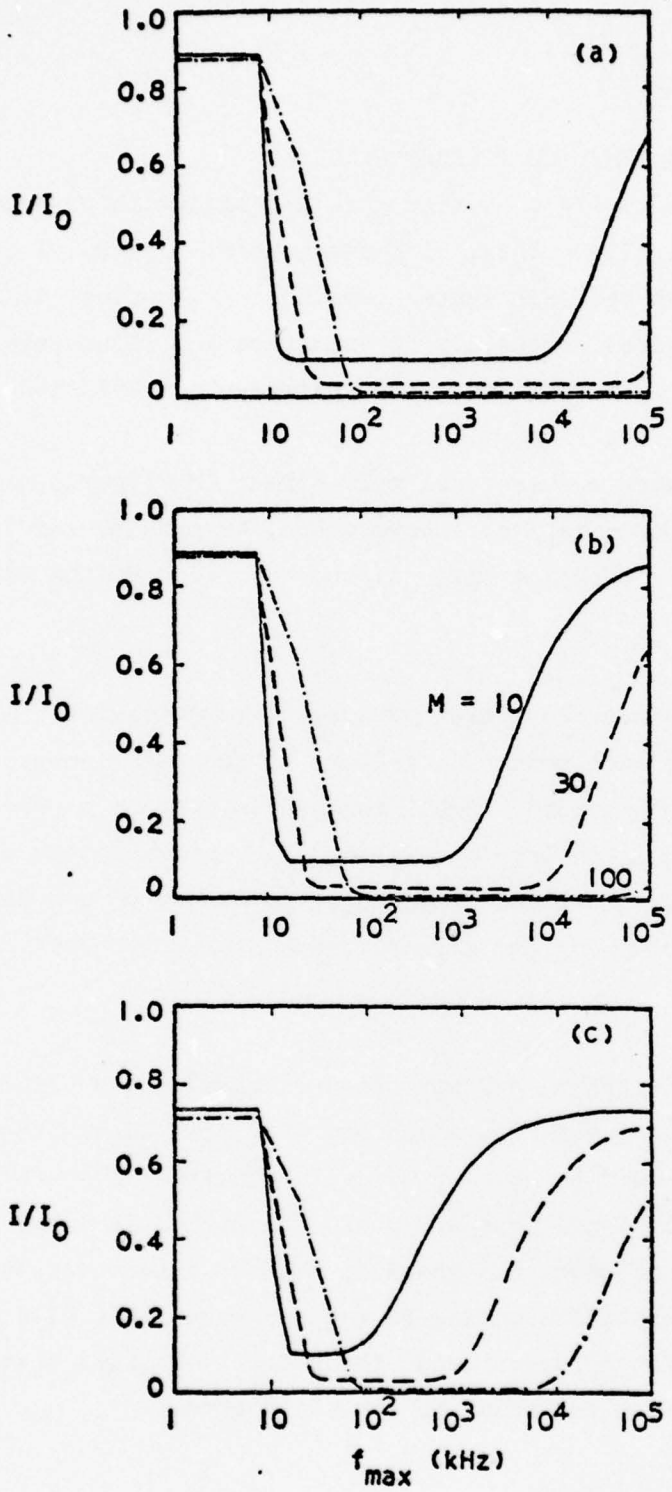

Figure 2-3. Strehl Ratio (I/I_0) vs. Maximum Target Modulation Frequency (f_{max}) for M-D System with Uniform Square Target. System noise equivalent bandwidth (Δf) is varied, and gain is adjusted to give constant convergence time ($\sim$ 1 msec). (a) $\Delta f = 10\pi$ Hz; (b) $\Delta f = 30\pi$ Hz; (c) $\Delta f = 100\pi$ Hz.

2.3 SUMMARY OF MULTIDITHER COAT PERFORMANCE

The extreme sensitivity to system gain and bandwidth parameters has been developed analytically. Thus, defining general regions of good performance depends on the specific system parameters. However, it is possible to map these regions adequately to summarize and illustrate the trends in performance as target and system parameters are varied.

Figure 2-4 presents a summary of multidither (M-D) performance trends. Three performance regions (convergence, threshold, and failure) are shown as a function of glint size and the bandwidth of the target spectrum.

Large targets do not provide an adequate discriminant for a M-D hill climbing algorithm and thus result in failure to converge independent of the target modulation bandwidth. Small targets do provide a good discriminant and the system will converge except when target modulation overlaps the dither frequencies. As shown previously the extent of the failure region due to noise overlapping the dithers depends upon the system parameters (cf. Fig. 2-3).

In the threshold region, M-D performance depends upon the initial conditions: level of convergence, aimpoint, etc. If the system is at or near convergence it should be able to maintain convergence in this region. However, if the initial conditions are poor, the system is likely to transistion to a failure mode. As shown in Fig. 2-4, this region is bounded by target sizes corresponding to the converged spot size and single element spot size. Within these bounds the effective target size is determined by the illumination and thus the threshold effect.

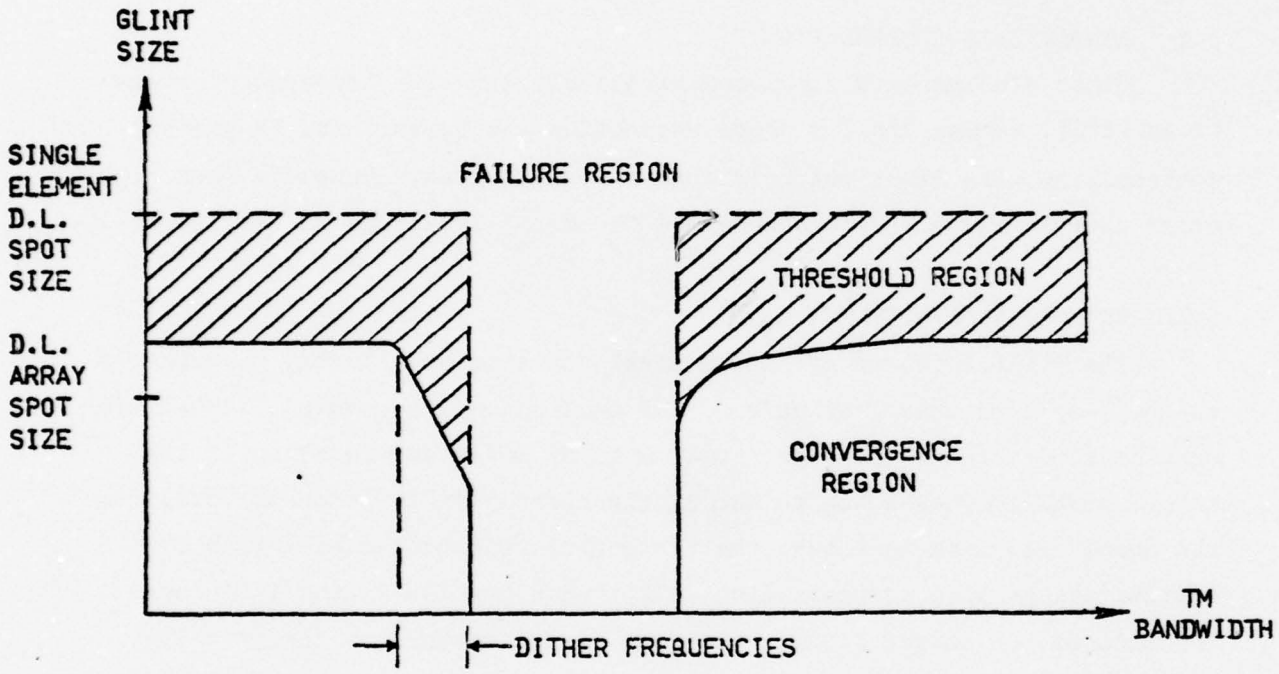

Figure 2-4. M-D Performance Regions

3 COMPARISON OF SYSTEM CHARACTERISTICS

Both modal and zonal systems considered here are based on the same signal processing and convergence algorithm. In this section the differences in transmitter characteristics and any restrictions they imposed on the parameter selection for the signal processing are briefly noted.

3.1 ATMOSPHERIC COMPENSATION

Other studies have shown quantitatively that for low-order corrections (tilt, focus, etc.) a modal correction can be tailored to provide compensation with fewer channels than a zonal system. However, when higher order aberrations must be compensated the modal advantage is lost entirely.

3.2 BEAM CONTROL/DITHER

The differences in modal and zonal concepts are clearly apparent in the beam control characteristics. For an M channel system each zonal element controls 1/M of the total power with an influence function in the target plane corresponding to the single-element diffraction pattern. In the modal case each mode perturbs the entire transmitted beam with the diffraction pattern corresponding to the mode profile as the influence function in the target plane. Thus each zonal channel is essentially identical in dither and beam control characteristics, whereas each modal channel is different. A modal transmitter will have the additional complexity of (1) different excitation amplitudes for each mode to achieve desired modulation depth, (2) different response to an extended target in each channel.

3.3 BEAM CONTROL INFLUENCE ON ELECTRICAL LOOP DESIGN

In a zonal transmitter as the number of channels is increased the loop gain must be increased to account for the lower signal. In the modal case, whole aperture control in principle would permit the gain to remain constant as more channels are added. However, in practice the residual modulation at convergence (due to dither) results in the requirement for reduced dither levels as channels are added and higher gain, just as in the

zonal case. The possibility does exist that the dither levels could be adaptive and reduce near convergence, thus permitting lower gain initially where target modulation is most important.

4 SIMULATION BASE-LINE PARAMETERS

As shown in Fig. 4-1, the computer simulator used in this study consists of three basic functional components: (1) target simulator (TARGSIM) which calculates the target's laser radar cross section based on its geometrical description, materials reflectance properties and motion parameters; (2) point scatterer model (PSM) which calculates the backscattered radiation from the target propagated to the receiver plane; and (3) COAT simulator, which includes the receiver, signal processor, and adaptive transmitter.

The following COAT simulators are used for the closed-loop comparisons presented in this section: MUDCATS (MUltiDither COAT Analysis Through Simulation), TOPCATS (The Optical Phase Conjugate Adaptive Techniques Simulation), and DEMCATS (DEformable Mirror COAT Analysis Through Simulation). The first two are described in complete detail by Radley et al.[1] and are only shown schematically here (in Figs. 4-2 and 4-3) to indicate how each is constructed. Some of the zonal multidither and phase conjugate closed-loop simulations presented in the reference are also presented in Sec. 5 for comparison with the modal multidither simulations accomplished for this study. The modal simulator (DEMCATS) is described in detail in Sec. 4.1, which also includes the rationale for selecting the system parameters.

4.1 MODAL SYSTEM BASE-LINE

The computer program (DEMCATS), which was constructed to model a modal multidither COAT system, is shown schematically in Fig. 4-4. The only difference between it and the zonal simulator (MUDCATS), shown in Fig. 4-2, is in the error signal processor which accomplishes the transformation from signal level (dither plus error signal) per channel to total mirror displacement (as described in Appendix A). The zonal transmitter can be represented by a similar matrix. The simulator description and selection of parameters are presented in the following. Additional data on the modal base line development and evaluation are provided in Appendix B.

---

[1] J. Radley et al., op. cit.

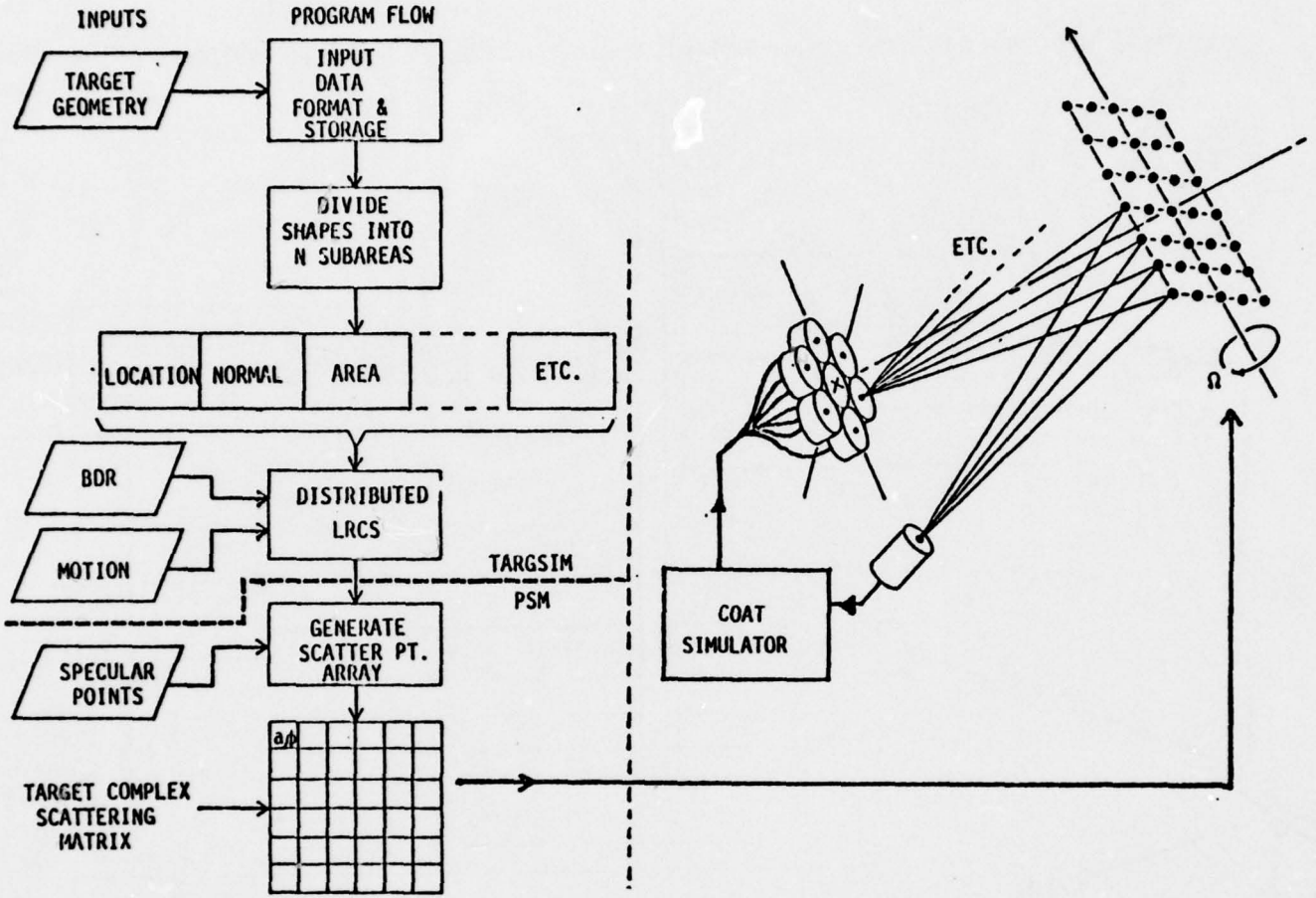

Figure 4-1. Scattering Model/COAT Simulator Interface. Receiver is depicted schematically only; extended and multiple receivers are included. Also, point scatterers are not necessarily in a regular array.

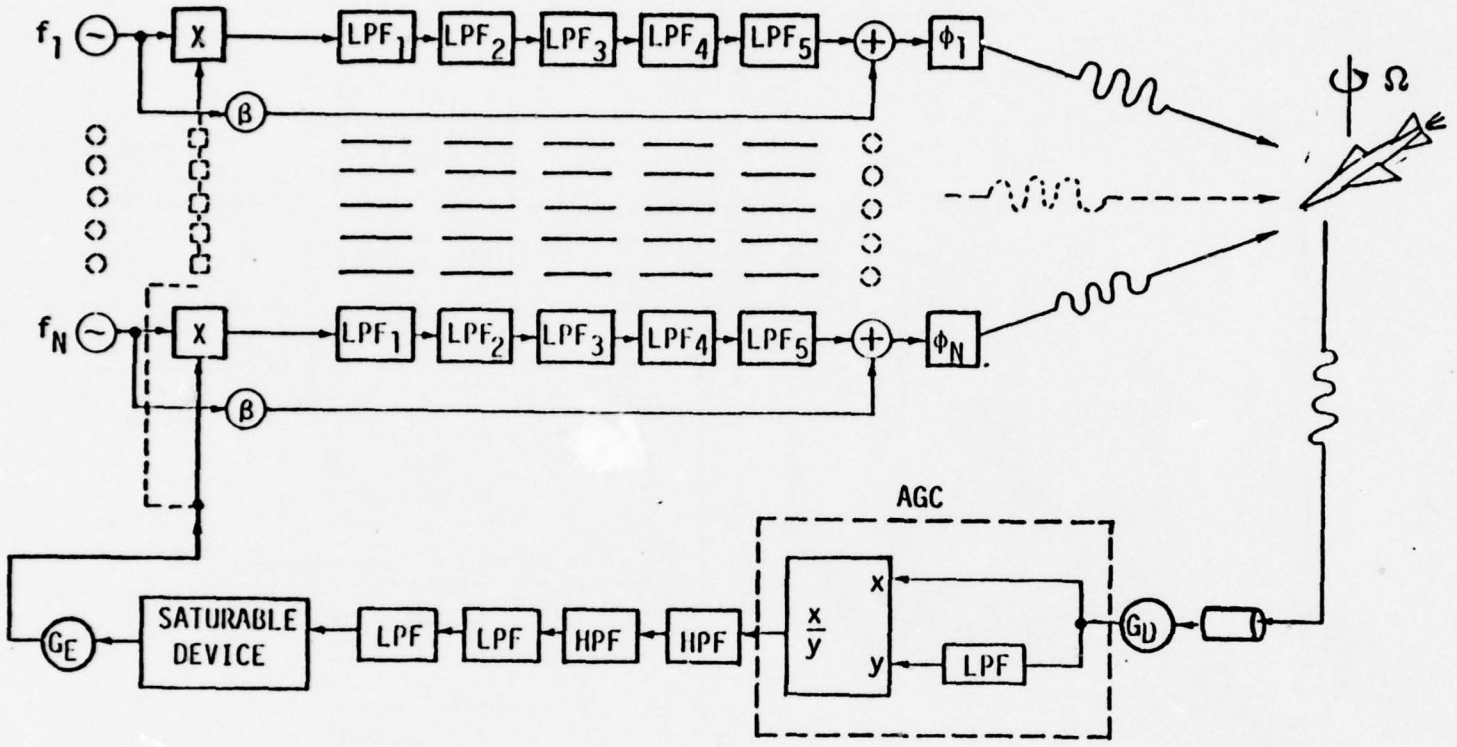

Figure 4-2. Block Diagram of MUDCATS (MUltiDither COAT Analysis Through Simulation)

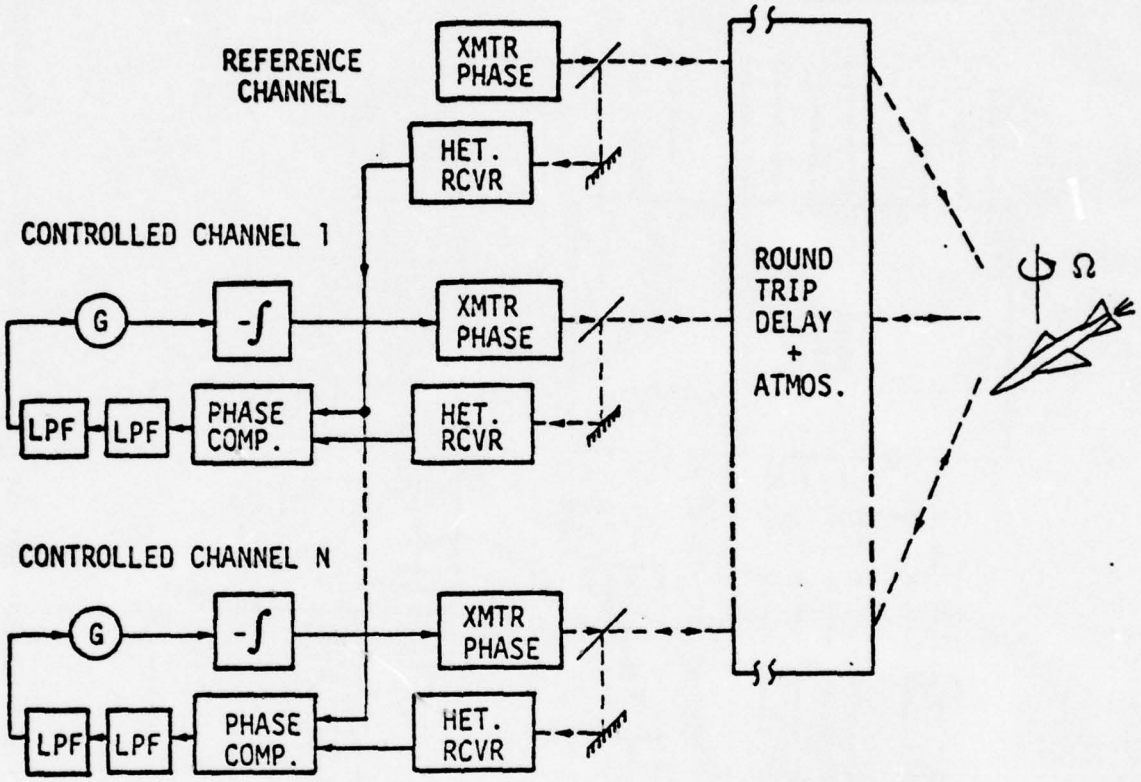

Figure 4-3. Block Diagram of TOPCATS (The Optical Phase Conjugate Adaptive Techniques Simulation). Ideal optical heterodyne receivers and phase comparators are assumed.

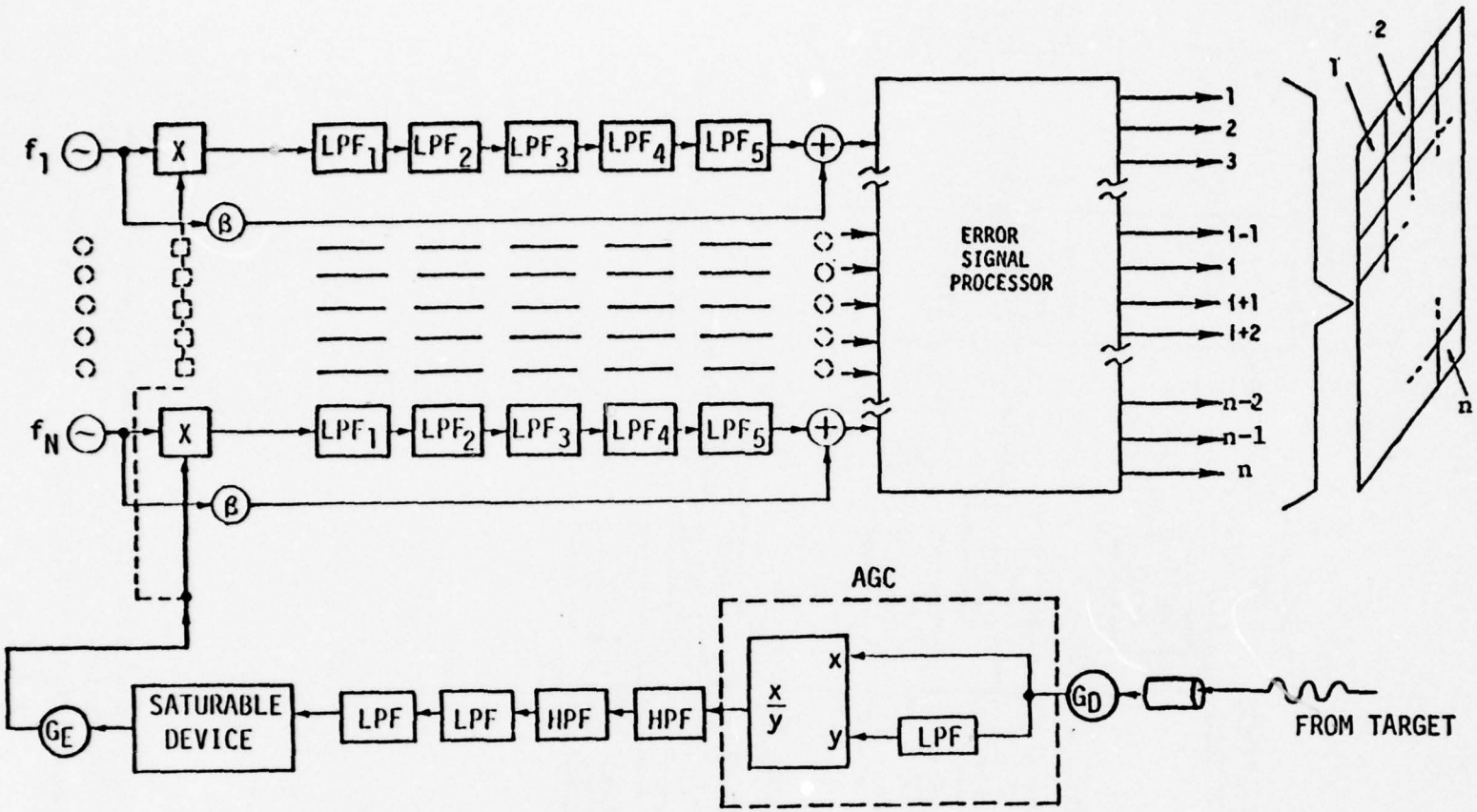

Figure 4-4. Block Diagram of DEMCATS (DEformable Mirror COAT Analysis Through Simulation)

4.1.1 Description of Simulator

The computer program DEMCATS has the following features and capabilities. It is fully closed loop with a complex target as an integral part of the system and incorporates all of the important signal processing features: energy detection with various aperture sizes and shapes (e.g., point, annulus, coincident, mesh), automatic gain control with signal clipping, synchronous detection, and bandpass filtering. The number of modes (each represented as a sum of Zernike polynomials) is selectable, as are the dither frequencies, interdither spacings, system cycle time, dither levels, system gains, and filter cutoff frequencies. Propagation is accomplished by a direct ray trace.

The system operates in the following manner. Once the scenario parameters and point-scatterer representation of the target have been determined, the initial phase error is applied to the system, usually by randomizing the phase of the individual transmitter modes from $-\pi/2$ to $\pi/2$, but in some cases by generating a phase screen atmosphere with the atmospheric model described in Appendix C. Perfect focus and no tilt error are assumed so that each mode has only to correct its phase error (except in the case of atmospheric phase error). Each mode undergoes both a high-frequency dither (8 kHz and above) and a lower frequency correction (~100-300 Hz).

This beam is propagated to the target and back to the receiver (usually an annulus with 1.2:1 ratio of O.D. to I.D.) which is assumed to have zero noise. This signal is then multiplied by the detector gain (G_D in Fig. 4-4) to convert target radiance to volts. The automatic gain control (AGC) is an analog divider which low-pass filters a portion of the received signal and divides this into the unfiltered component. This is necessary for stability considerations for large numbers of channels and for improved performance in the presence of target noise. The analysis of the AGC is reported elsewhere.[1]

[1] J. Radley et al., op. cit.

The high- and low-pass filters provide large attenuation at frequencies outside the dither frequency bands. The saturable device is a "soft" clipper which limits the signal for approximately the first 0.5 msec until the low pass filter in the AGC has had sufficient time to charge and provide a nonzero voltage. Otherwise, the initial instability drives one or more channels to a state which will produce only a local maximum at "convergence." The clipping mechanism is logarithmic rather than a sharp cutoff to reduce the characteristic high-frequency ringing which would extend into the dither bands.

After amplification by the electronic gain (G_E), the signal is then synchronously detected at each of the dither frequencies. This detection process selects only the signal at each particular dither frequency and shifts this to zero frequency. The error signal is then filtered by a series of five low pass filters. The most important filter is LPF_1 which has a 10 Hz break point and eliminates most of the noise which is at higher frequencies than the error signal (which is DC). The other filters have a substantially higher cutoff frequency and reduce intermodulation noise. The particular choice of these is discussed in detail in other reports.[1,2]

The dither signal, producing a modulation index β, is added to the error signal applied to each transmitter element in order to tag the error signal per channel prior to the next cycle. The convergence algorithm is a "hill climbing" type which seeks to minimize the error signal thereby maximizing the total received power.

This process is repeated every 10 μsec (the simulated cycle time) or less, depending upon the required sampling rate for dither or target modulation frequencies.

---

[1] W. B. Bridges et al., Coherent Optical Adaptive Techniques (COAT), Hughes Research Laboratories, Technical Reports No. 1 & 2, July and October 1973.

[2] J. E. Pearson et al., Coherent Optical Adaptive Techniques (COAT), Hughes Research Laboratories, Final Technical Report, RADC-TR-75-46, January 1975.

The selection of system parameters for all closed loop simulations is based on the following criteria:

a. The parameters are the most favorable to performance against an ideal (point) target, for which a convergence level of at least 90% must be attained within 2 msec.

b. They are physically realizable using present or anticipated state-of-the-art hardware.

In order to isolate only the effects of target noise and provide errors which the systems should be capable of correcting, the following conditions are incorporated in the simulators: infinite detector signal-to-noise ratio, no tilt error, and a lens at the transmitter focused on the target. The base-line system utilizes the first 9 MOWACS modes. The overall transmitter diameter, 60 cm, is within the 50-150 cm range proposed for most scenarios.

The base-line initial condition is random peak mode amplitude distributed $-\pi/2$ to $\pi/2$ in phase with no atmosphere. This represents a phase error which each mode is able to correct. Because the RMS phase error characterizes the initial level of convergence and because only nine samples of a uniform distribution can give significantly different RMS on each run, the same initial phases were used for the base-line system simulations. This phase distribution has an RMS error of 1.7 rad and a peak-to-peak error of 6.28 rad.

Refer to Fig. 4-4; the following parameter values were chosen:

Number of channels = 9

Dither frequencies = 8-20 kHz, Δf = 1.5 kHz

Gains: β = 0.503 ($\pm 28.8°$ dither modulation for Mode 1)

G_D = 12,000

G_E = 500

Filter break frequencies: LPF_1 = 10 Hz
LPF_{2-5} = 5 kHz
AGC LPF = 1 kHz
2 HPF's = 1 kHz
2 LPF's = 50 kHz

Saturable device cutoff (logarithmic) = 50 V

4.1.2 Modulation Index

The first step was to determine the dither level. In a zonal multi-dither system this is ±20° based on a trade-off between required signal level and linearity of operation. The amount of control of on-axis power on target is shown in Sec. 5 for 7, 19, and 100 channels each with the same overall transmitter size. As expected, the percent modulation decreases with the number of elements. For 7 elements, a ±20° dither at 90% convergence corresponds to ±6.4% power modulation. This value and an alternative dither level equivalent to the 19-channel zonal transmitter was sought to match the MOWACS transmitter. To compensate for a decrease in dither level for the 19 channel case, a proportional increase in signal gain was made.

Each MOWACS mode has a different spatial structure and hence produces a different amount of target plane power modulation for a given amount of dither. To make a modal-zonal comparison, we chose the amount of dither for each mode to give the same signal modulation at the same convergence level. Each mode was assigned a different peak dither amplitude (±29° for mode #1, ±9° for mode #4, etc.) so each would possess the same "optical" gain, i.e., the same power modulation on a point target. The dither levels in mode amplitude are listed in Table 4-1.

4.1.3 Dither Frequencies

Initially, the intent was to use the actual MOWACS dither frequencies (2.28-13.3 kHz); however, this was not done for initial comparisons for the following reason. More target noise occurs at lower frequencies for all target rotation rates, hence the low dither channels encounter more target noise. Thus the same frequencies and interdither separations as the zonal

TABLE 4-1

DITHER LEVELS FOR MODAL TRANSMITTER

Mode No.	Dither (±deg)
1	28.8
2	13.5
3	13.5
4	9.2
5	10.7
6	12.1
7	12.1
8	15.3
9	13.5

case were used (f_d = 8-20 kHz, Δf = 1.5 kHz). This permits a direct comparison of full aperture modal beam control vs. segmented control. The 8-kHz lowest dither frequency creates a region where low-frequency target noise does not overlap the dither frequencies. This permits a clearer illustration of the target effects as dynamic rates are varied.

4.1.4 Initial Transmitter Phase Error

The next step was to determine an initial phase error comparable to that assumed in the zonal case (random 0 to 2π per element). Also the spatial frequency could not exceed the correction capability of the first nine MOWACS modes. The peak mode error was random $-\pi/2$ to $\pi/2$ and a number of randomizations were made to select the same initial RMS error as the zonal case with a nonzero initial error for each mode. However, a major difference between modal and zonal is the modulo 2π factor. In the zonal case, an element can be 2π out of phase with the other elements and still produce near-diffraction-limited performance because each is independent (spatially) of the others. In the modal case, the mode errors are additive, which can lead to peak-to-peak errors too large for the system to correct. One mode 2π out of phase produces a large reduction in the power on target. (See Appendix B, Sec. B.2, for sensitivity to phase error.) Figure 4-5 illustrates the target plane beam profiles which were used in the comparison between modal, zonal, and phase conjugate closed-loop performance. Final modal runs used the transmitter with ϕ_{p-p} = 6.28 rad.

4.1.5 Automatic Gain Control

Zonal results also demonstrated the importance of an AGC for minimizing system gain variation resulting from the low-frequency signal modulation caused by low target rotation rates. An AGC was also found to improve zonal multidither COAT performance against targets producing higher frequency noise. Hence, it was included in DEMCATS prior to making any complex target runs. Basically, the AGC divides the received signal by a 1-kHz low-pass-filtered version of the same signal. In this way, signal fluctuations are normalized to the mean of the received signal.

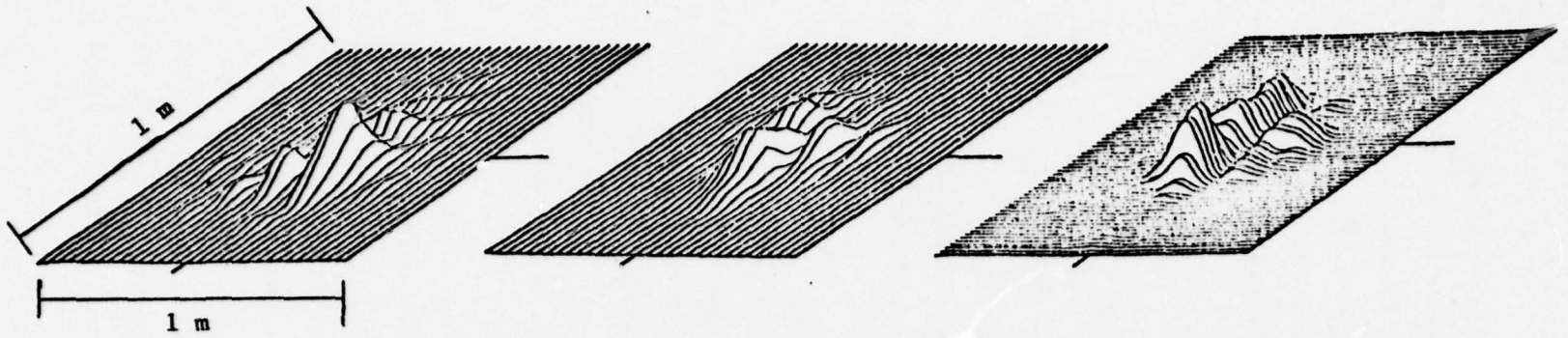

ϕ_{p-p} = 6.28 rad

ϕ_{p-p} = 6.50 rad

9-MODE MOWACS

ϕ_{p-p} = 4.34 rad

7-CHANNEL ZONAL
(multidither and phase conjugate)

Figure 4-5. Target Plane Beam Profiles for Transmitters with Equivalent Phase RMS ($\cong$ 1.7 rad), but Different Peak-to-Peak Wavefront Distortion (ϕ_{p-p}). Parameters are: range = 5 km, λ = 10.6 μm, transmitter diameter = 0.6 m.

To prevent initial instability caused by large gains from an uncharged LPF in the AGC, the error signals are disabled for the first 0.125 msec. Any further instabilities incurred during the engagement due to signal dropout (speckle nulls) are checked by a "soft" voltage clipper. The soft clipper is logarithmic for voltages above the clipping level. Its main purpose is to limit large gain fluctuations created by the AGC (during signal dropout).

4.1.6 Aperture Averaging

Multidither COAT systems (both modal and zonal) sense the intensity or power of the radiation scattered from the target and use synchronous detection to selectively measure the signal modulation at each of the separate beam tagging (or dither) frequencies. Any spurious intensity modulation at these frequencies is noise which competes with the signals in the affected channels.

Most real targets are not optically smooth and hence produce a spatially random intensity pattern in the receiver plane which can be characterized by a probability density function and a power spectral density (or its Fourier transform, the autocorrelation function).[1] Any method which reduces the dynamic range of these fluctuations and its extent in the frequency domain reduces its impact on multidither system performance.

Aperture averaging is one such method of reducing target noise. In fact, a larger receiver aperture is also beneficial in terms of increasing the received signal level with respect to the detector and system electronic noise. One of the easiest to implement from an optical design standpoint is an annular receiver which is coaxial with the transmitter. In this way, the same beam-expanding telescope can be used to transmit and receive. A configuration which is much more difficult to implement is a receiver which is coincident with the transmitting aperture. In this case, a high-power beam splitter is required and the optical system is faced with some of the

[1] J. Radley et al., op. cit.

same problems as return-wave phase conjugate. It has been shown elsewhere[1] that both configurations are nearly equal in terms of reducing target modulation noise.

Rather than make a large number of closed-loop simulations, it is more instructive and considerably more efficient to use the techniques for calculating open-loop aperture-averaged PSD, probability density, and contrast ratio developed in Appendix D to determine the effect of aperture averaging and provide an initial estimate of which targets and rotation rates are potentially most stressful to system performance.

Briefly summarized, the target spatial PSD is the sum of a DC component and higher frequency component calculated from the autocorrelation of the target brightness distribution. It requires an additional step if the spatial structure of the adaptive illumination is to be included, but for this analysis it has little effect and uniform illumination is assumed. (This is valid provided that the beam is larger than the target, which is the case here when the beam is unconverged.)

The spatial PSD is then multiplied by the magnitude squared of the aperture transfer function, and this is integrated in the spatial frequency component which corresponds to the direction parallel to the target's rotation axis. Integrating the spatial PSD in both the x and y spatial frequencies gives the number of correlation cells in the aperture and hence the speckle probability distribution and contrast ratio (cf. Appendix D).

Finally, it is scaled by $2R\Omega$ to transform it into the temporal frequency domain. This process has been programmed on a digital computer and makes extensive use of fast Fourier transforms so that parametric variation of target geometry, receiver geometry, and scenario parameters (range and wavelength) is fast and efficient. Finally, this analytic method produces ensemble average results without the necessity of generating a large number of statistical samples to adequately predict expected performance.

[1] J. Radley et al., op. cit.

The following receiver geometry is considered here: 70-cm o.d., 60-cm i.d. annulus. Both a one-dimensional cut and the y-spatial-frequency-integrated, aperture-averaged PSD's are shown in Fig. 4-6a. Note that the latter is the aperture-averaged PSD (in the spatial frequency domain) for an infinite, uniform target rotating about the y axis.

The real test is how these perform in terms of reducing target noise. Rather than using uniform square targets of various sizes (whose PSD's are simply triangular) one of the targets used for the open-loop simulations in Sec. 5 is used here. This target is an intermediate case of those considered in this study. The aperture-averaged PSD is shown in Fig. 4-6b.

However, the PSD is only half the story. The probability density function shows which values of intensity are most probable, and the ratio of the RMS to the mean is defined as the contrast ratio. Aperture averaging may produce a significant increase in the mean signal level and reduction in the fluctuations. The probability density functions are shown in Fig. 4-7.

In order to scale the target modulation spectrum (PSD) presented in Fig. 4-6b to the temporal frequency domain for comparison to the dither sensing frequencies, the spatial frequency scale must be multiplied by $2R\Omega$ and the vertical scale (PSD) divided by $2R\Omega$ (to keep the total integrated power constant) as described in Appendix D. These are presented in Figs. 4-8 and 4-9, for the four spherical targets considered in Sec. 5, at two different rotation rates. It is apparent from these that there is more target noise at lower frequencies for all cases; hence operation at higher dither frequencies is very desirable for reducing target effects. Also, when the adaptive beam is initially unconverged and illuminates a larger area of the target, as the extended target cases presented here, target noise may extend to tens of kilohertz for tenths of radians per second rotation rates. Hence, a system which can operate with fewer control channels and at higher dither frequencies will be able to operate above the target modulation frequencies encountered in many engagement scenarios. A 60-100-channel zonal multidither system, which is constrained to dither frequencies down to a few kilohertz, will suffer more severe performance degradation.

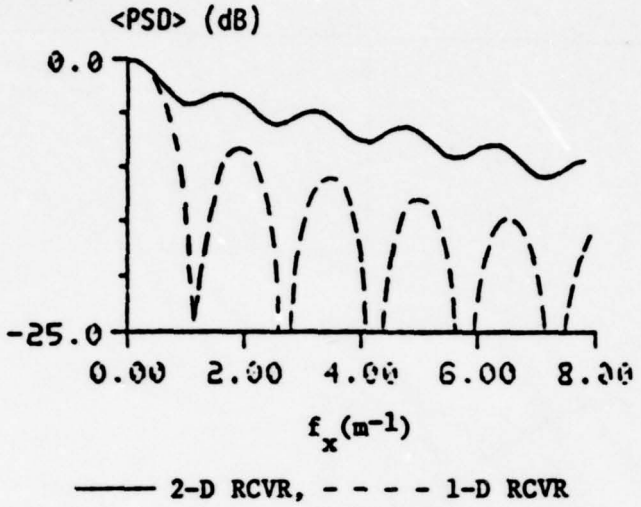

(a) One-Dimensional and Two-Dimensional PSDs of an Annular Receiver. The latter also corresponds to the target modulation spectrum for the idealized case of a uniform, infinite target rotating about the y axis.

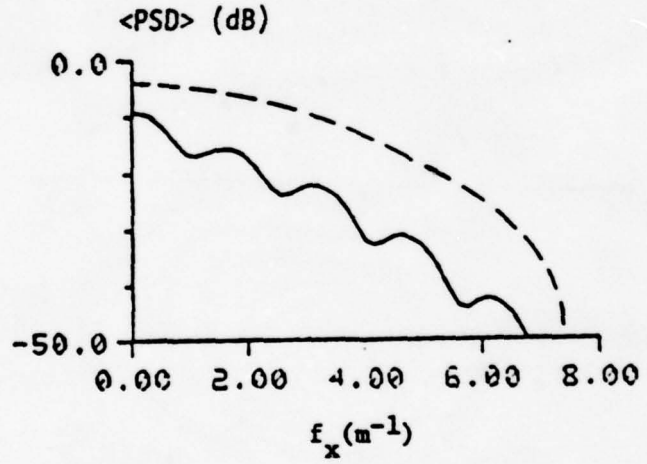

(b) Target Modulation Spectra for Two Receiver Geometries. Parameters: sphere segment target (d_0 = 40 cm, r_c = 1 m) uniformly illuminated, range = 5 km, λ = 10.6 μm.

Figure 4-6. Ensemble Average Power Spectral Densities (PSDs) Corresponding to an Annular Receiver (O.D. = 70 cm, I.D. = 60 cm).

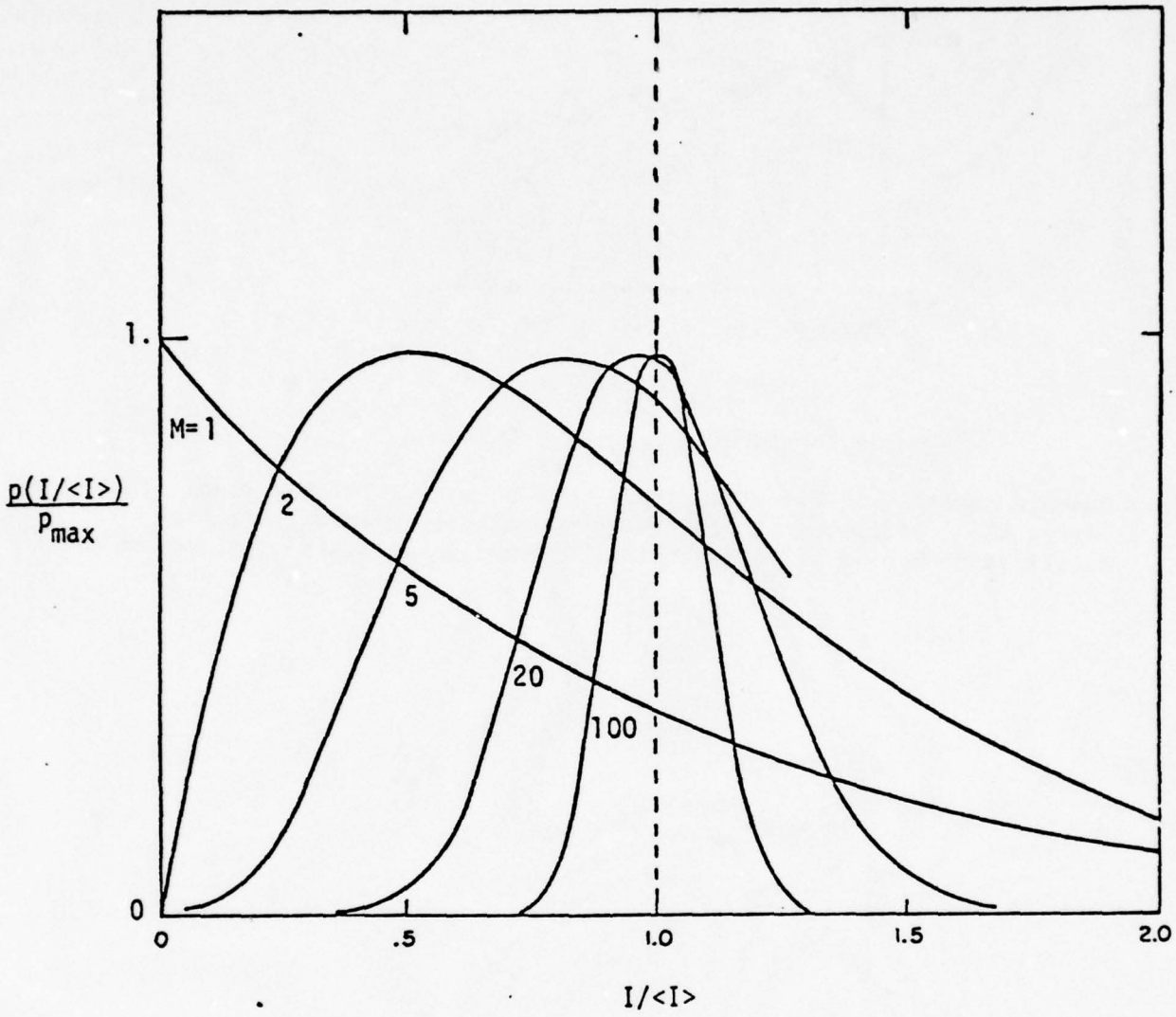

(a) Speckle probability distribution vs. number of correlation cells (M) in aperture.

Aperture Shape	Diameter (cm)	M	$C_R = \sigma_{I/<I>}$
Circular	60	7.58	0.364
Annular	o.d. = 85, i.d. = 60	12.05	0.288
Annular	o.d. = 70, i.d. = 60	9.47	0.325
Annular	o.d. = 61, i.d. = 60	8.56	0.342

(b) Computer calculated parameters (M, C_R) for each aperture.

Figure 4-7. Effect of Receiver Geometry On Probability Density Function of Direct Detected Signal. Parameters for (b) given in Fig. 4-6b.

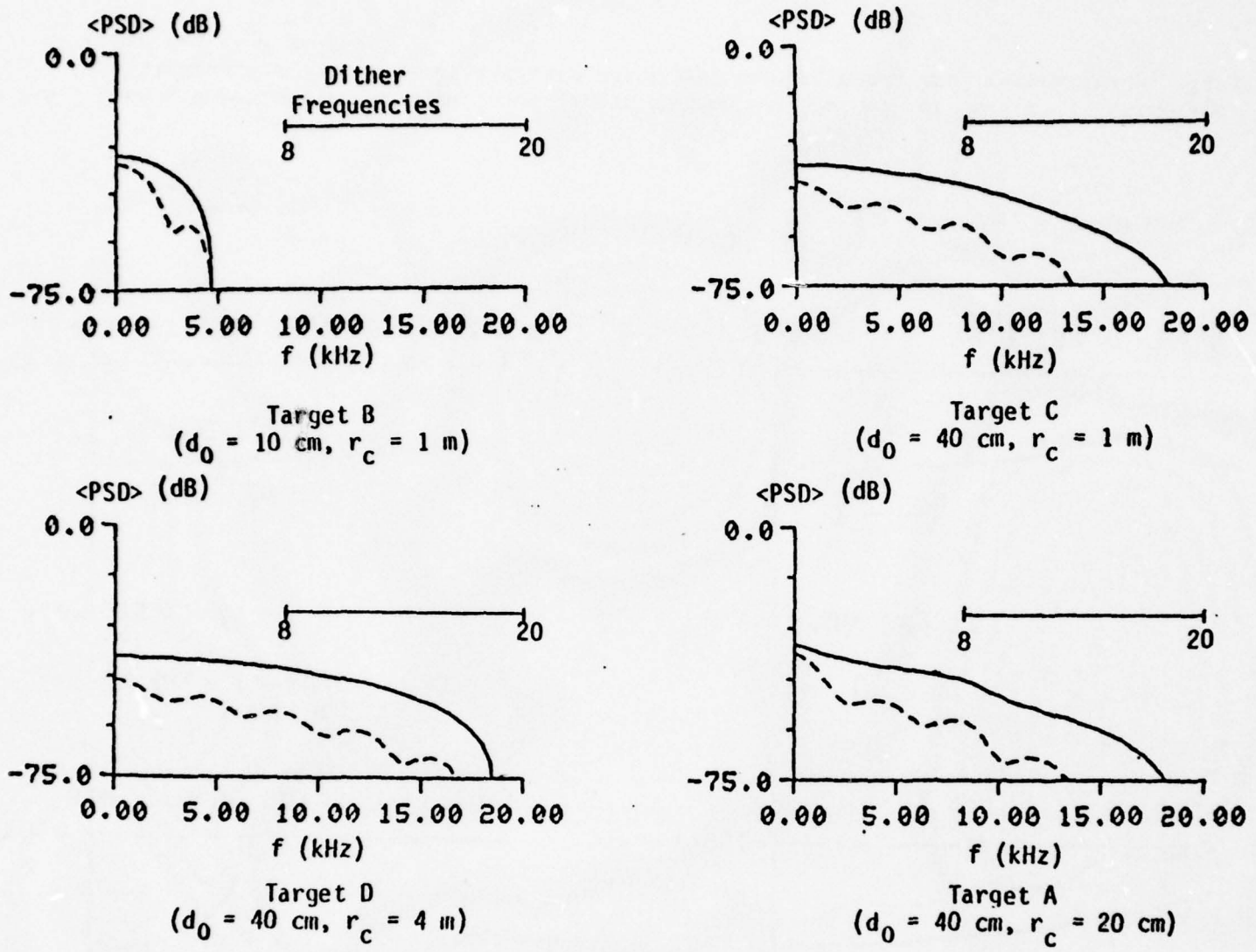

Figure 4-8. Ensemble Average Power Spectra of Target Modulation (Noise) for Uniform Illumination. Continuous and dashed lines indicate point and annular receivers, respectively. Target rotation rate is 0.25 rad/sec.

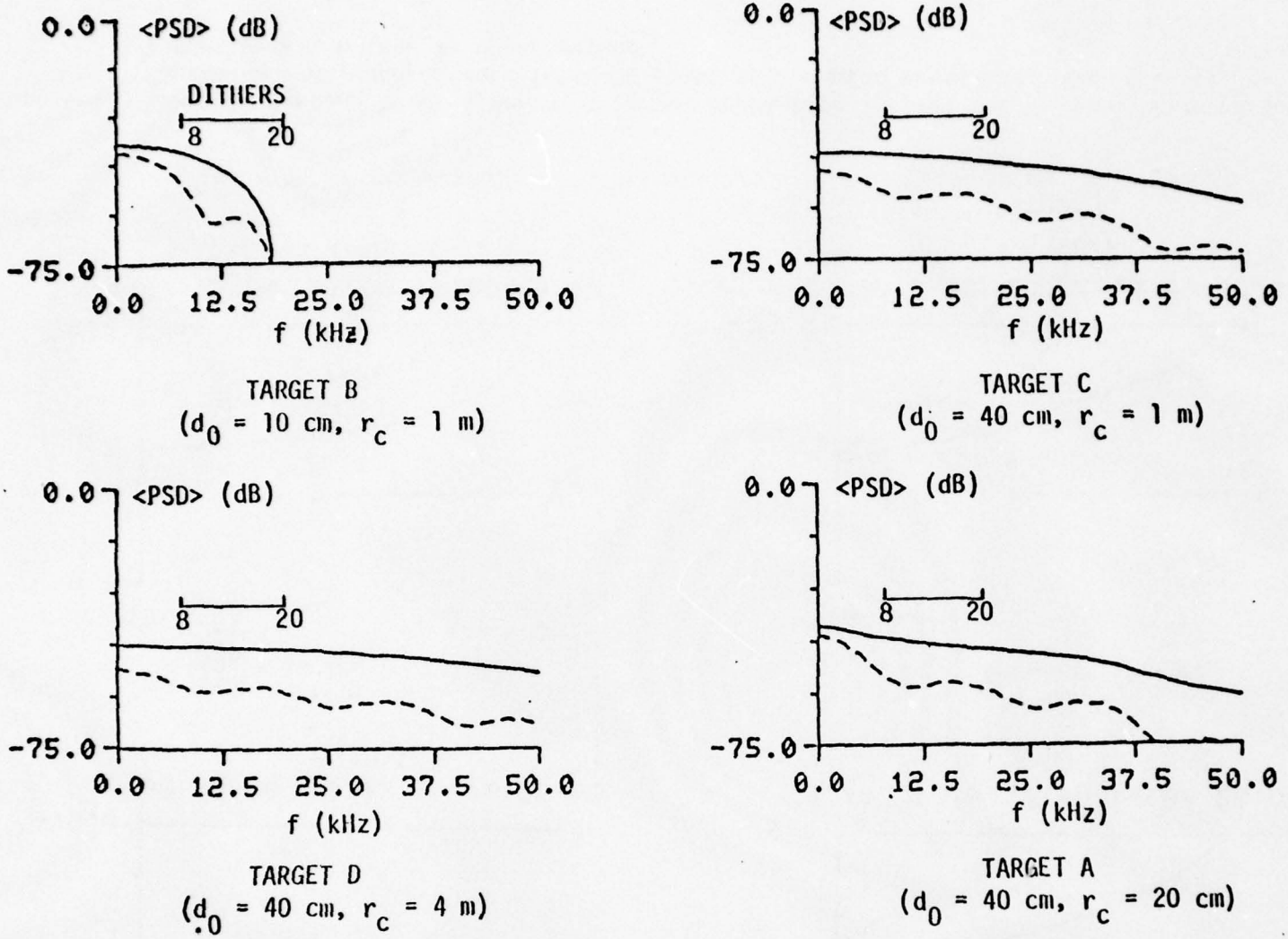

Figure 4-9. Ensemble Average Power Spectra of Target Modulation (Noise) for Uniform Illumination. Continuous and dashed lines indicate point and annular receivers, respectively. Target rotation is 1 rad/sec.

Computer run time requirements constrained us to use only the unresolved (d_0 = 10 cm) target for the illustrative closed loop simulations in Sec. 5. However, it is clear from the open loop PSD's in Figs. 4-8 and 4-9 that the cases where more surface area is illuminated or where the glint is less localized will be more stressful to system performance.

4.1.7 Atmospheric Turbulence

In Sec. 4.1.4 an initial set of random amplitude modal perturbations is applied to the transmitter surface to approximate an atmospheric phase screen. The implication is that such a two-dimensional perturbation in the transceiver plane accounts for most of the phase variations caused by propagation through the turbulent atmosphere. Using an atmospheric model described in Appendix C, two different atmospheric phase screens were generated for use in the modal, zonal, and phase conjugate COAT simulators.

The model parameters were assigned the following values:

1. Outer scale, L_0 = 10 m
2. Effective width of the phase perturbing region, d = 100 m
3. $C_n^2 = 10^{-13}$ $(m^{-2/3})$ - moderate turbulence
4. $C_n^2 = 10^{-14}$ $(m^{-2/3})$ - weak turbulence

Using the Fig. C-1, or Eq. C-1, the RMS phase fluctuations (σ_n values) for the moderate and weak turbulence are 1.19 rad and 0.376 rad, respectively.

The modal transmitter point locations were assigned phase screen values that corresponded to their physical location. As the modal correction is engaged, the phase screen is compensated by the negative wavefront of the transmitter. Using the same atmospheric phase screen for the zonal transmitter (and phase conjugate) requires sampling the phase screen at each of the transmitter element centers and determining the x and y phase slope across each of the elements. A simple linear approximation using two phase screen points for each orthogonal direction about each transmitter element center is employed. The mean phase slopes are applied to the diffraction

pattern of each transmitter element, but cannot be directly compensated for because of the single-direction, piston-like movement of the transmitter elements.

Figure 4-10 illustrates the atmospheric phase screen used in the COAT simulators. The values are normalized to the maximum phase excursion. The minus sign over some of the array values indicates negative phase values.

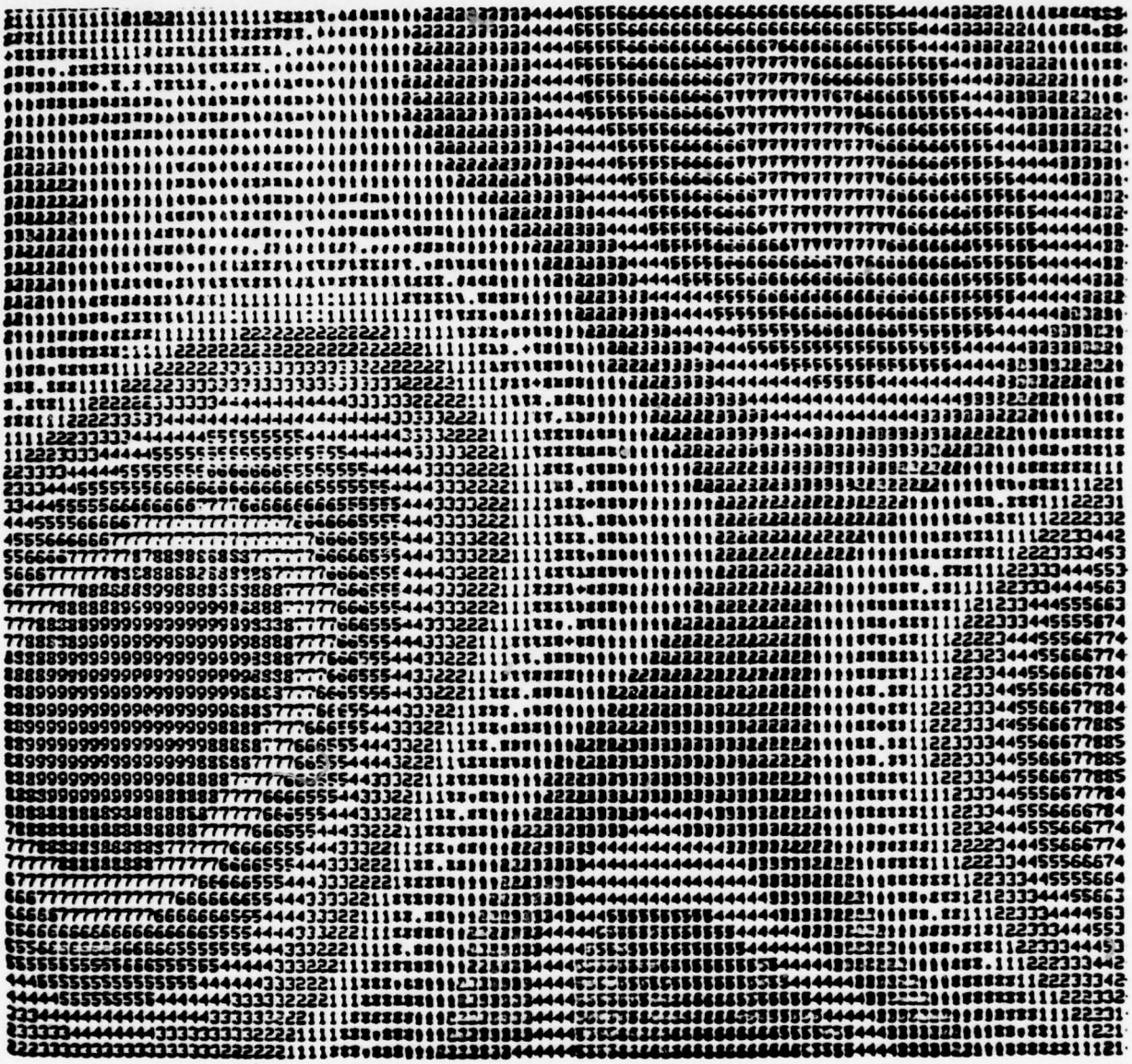

Level	% Maximum
0	100
9	90
8	80
7	70
6	60
5	50
4	40
3	30
2	20
1	10
*	1-10
•	0.1-1.0
+	<0.1

Figure 4-10. Normalized Atmospheric Phase Screen. Parameters: $L_0 = 10$ m, $d = 100$ m. For $C_n^2 = 10^{-14}$ $m^{-2/3}$, maximum phase excursion = 0.832 rad; for $C_n^2 = 10^{-13}$ $m^{-2/3}$, ϕ_{max} = 2.631 rad. Minus signs indicate negative phase values.

5 PERFORMANCE EVALUATION

Utilizing the simulation techniques described in Sec. 4 both open- and closed-loop evaluations are considered in this section to investigate the factors identified in Sec. 3. In addition to the modal and zonal multidither simulations, phase conjugate simulations are also provided to complete the COAT comparisons.

5.1 OPEN-LOOP M-D COMPARISONS

There are several important things to note from the open loop evaluations which follow: (1) each mode has a different optical gain (i.e., for the same peak dither amplitude with a point target a different modulation index results); (2) the ranking of modes by optical gain depends on the particular radiance distribution of the target; (3) for all of the distributed targets, some of the modes produce a maximum in the integrated radiance (and hence received signal) at nonzero mode amplitude; and (4) these three effects are different than for a zonal transmitter.

5.1.1 RMS Phase Error of Transmitter Surface

The fundamental difference between the modal and zonal transmitter is the control of the transmitter surface. Each control channel for the zonal transmitter affects a segment of the total laser energy incident across its aperture, whereas, in the case of the modal transmitter, the entire surface is controlled by each of the control channels. To determine the relative control over the transmitter surface, we can compare transmitter surface RMS vs. peak phase excursion plots for both modal and zonal transmitters. In Fig. 5-1 the transmitter RMS surface displacement vs. single mode (or element) displacement is presented. The data is tabulated for comparison in Table 5-1. Note that all nine MOWACS modes have steeper slopes than the zonal case, indicating a stronger control over the surface for equal peak displacement.

5.1.2 Modal Vs. Zonal Dither Characteristics

A fair comparison between the modal and zonal COAT systems requires the same dither frequencies and system parameters. The difference between

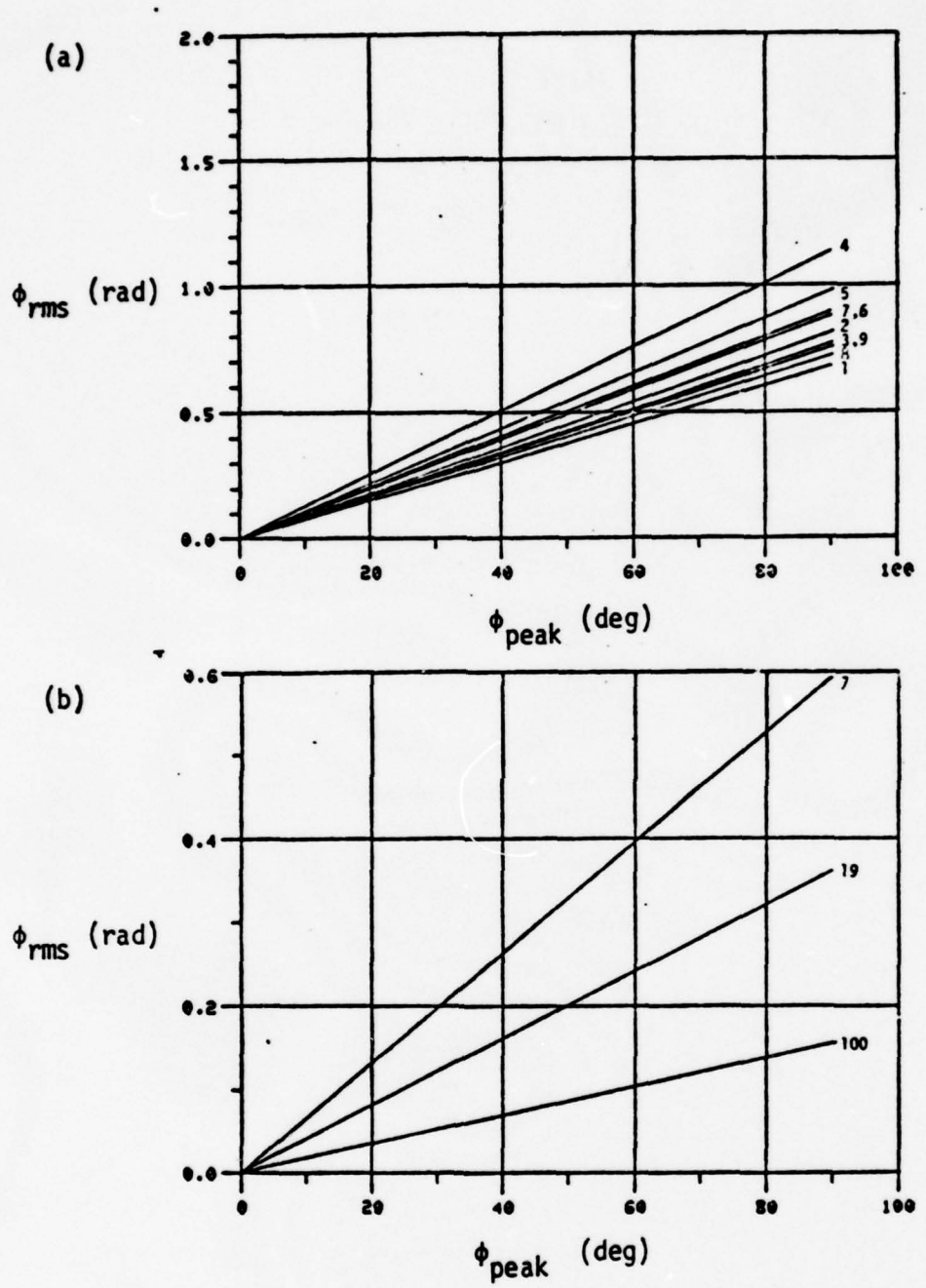

Figure 5-1. RMS Phase Error of Transmitter Surface for Both Modal and Zonal COAT. (a) Modes 1-9. (b) 7-, 9-, and 100-channel zonal elements. Each mode (or element) is individually stepped from convergence (phase amplitude = ϕ_{peak}), and surface statistics are calculated. (Note different scale factor on vertical axis.)

TABLE 5-1

TRANSMITTER RMS PHASE ERROR

CHANNEL	ϕ_{RMS} (@ $\phi_{peak} = 90°$)
Modal	
1	0.678
2	0.811
3	0.777
4	1.14
5	0.978
6	0.875
7	0.892
8	0.722
9	0.758
Zonal	
7	0.594
19	0.360
100	0.157

these two systems is their response to target spatial effects. As an individual channel (or mode) is dithered, the resulting far-field pattern spatially modulates the distributed radiance of the target which proportionally modulates the average received signal in the pupil plane. The results for a point target are presented in Fig. 5-2 for comparison with extended targets.

Open loop results which illustrate the target spatial effects for both zonal and modal COAT are presented in Figs. 5-3 and 5-4. The normalized power, which is computed by integrating the product of the far-field pattern of the transmitter and the target radiance, is plotted versus the mode amplitude, or transmitter element phase. In all cases for zonal COAT, a decrease in the slope of the curves (and hence dither signal level) occurs as the target increases in size and as it becomes flatter. Also, note that the maximum power occurs at zero phase excursion. For the modal transmitter, there is a similar reduction in dither signal level; however, the relative weighting of the modes changes and for several of the modes, the maximum power does not occur at zero mode amplitude. The implication here is that equalizing the gain, and hence dither signal levels, for each of the modes on a point target does not result in equal weighting for a distributed target. This is a fundamental difference between the modal and zonal multidither systems. In addition, depending on the target brightness distribution, a diffraction-limited spot size on the target may not be obtainable for several of the correction modes. The reason for this is that the transmitter will deform to maximize the received signal which may not necessarily produce a diffraction limited beam on target.

The open loop results shown graphically in Figs. 5-3 and 5-4 are quantitatively summarized in Tables 5-2 and 5-3. The numerical values given are the slopes of the curves at a convergence level of 95% (at convergence the slope is zero). The amount of modulation of the received signal for each mode or zonal element is directly proportional to the slope of the curves which depends on the level of convergence.

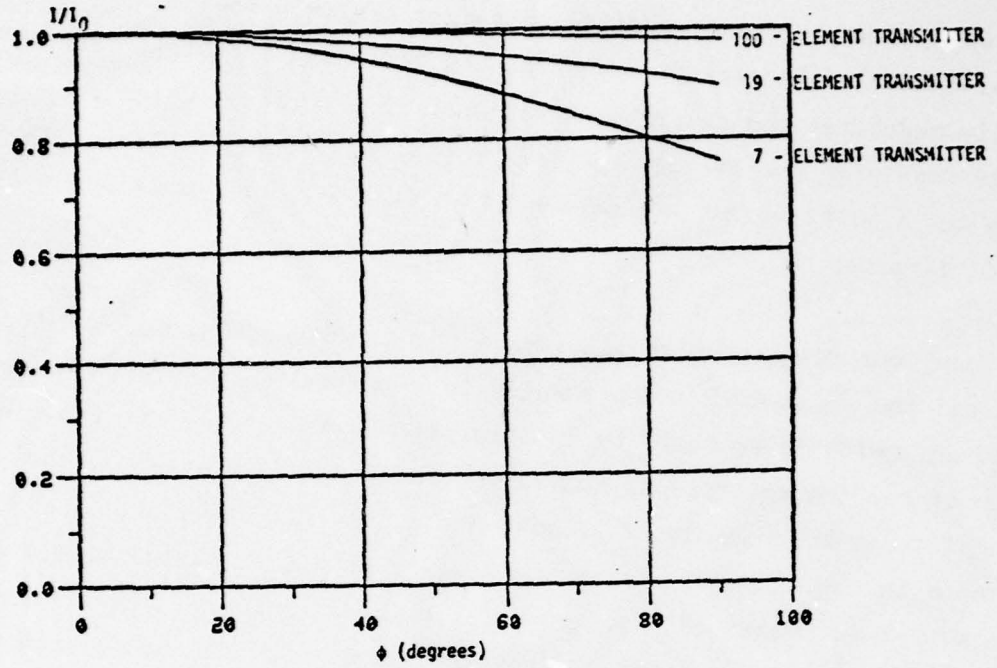

(a) Zonal Transmitter

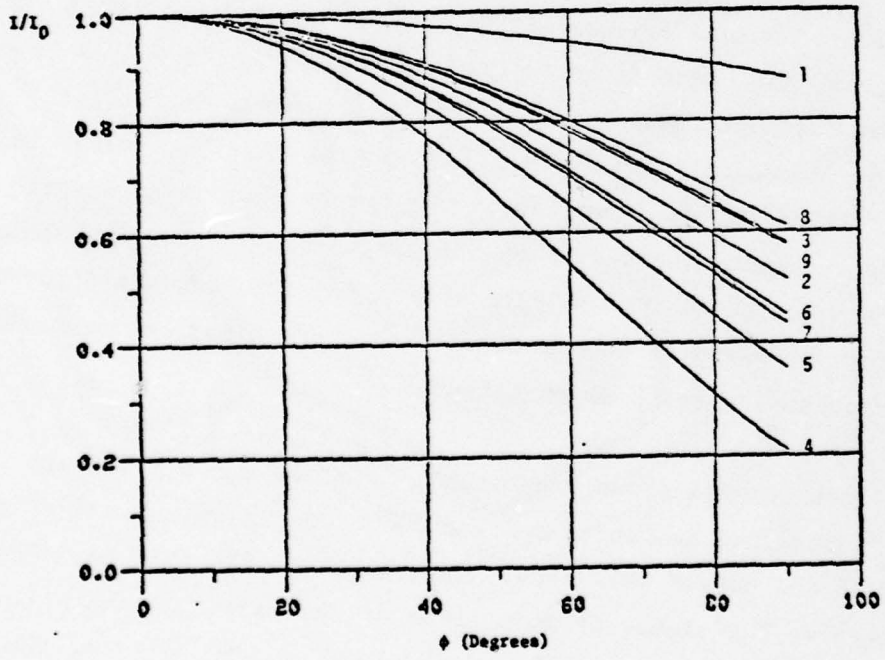

(b) MOWACS Transmitter

Figure 5-2. Normalized On Axis Power (Strehl Ratio) Vs. Single Transmitter Element or Mode Phase (from Convergence). Overall transmitter size is the same for all cases.

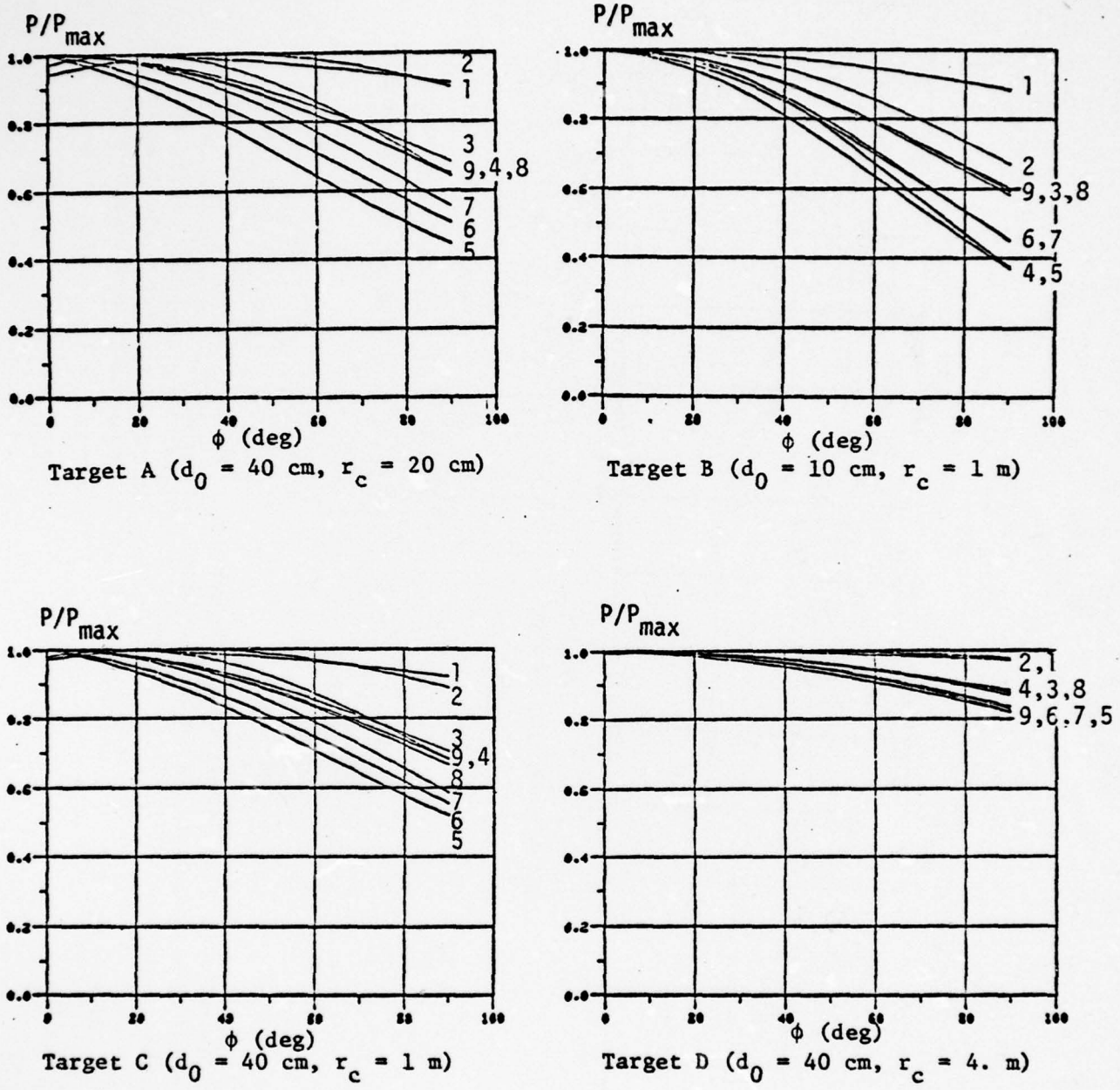

Figure 5-3. Integrated Radiance of Illuminated Sphere Segments Vs. Modal Amplitude. Each of MOWACS mode amplitudes is individually stepped in small increments from 0° to 90° and resulting integrated power (far-field pattern × target distribution) is plotted normalized to its peak value. Scenario parameters are: transmitter diameter (d_T) = .6 m, range (R) = 5 km, λ = 10.6 μm.

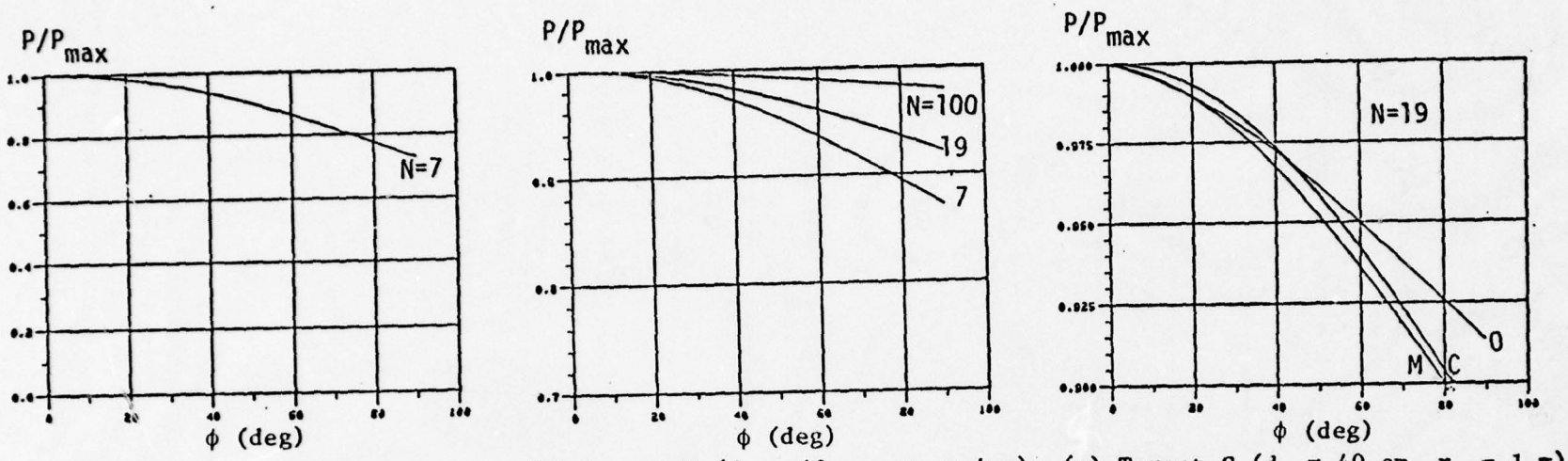

(a) Target B (d_0 = 10 cm, r_c = 1 m)

(b) Target D (d_0 = 40 cm, r_c = 4 m)

(c) Target C (d_0 = 40 cm, r_c = 1 r)

C - center transmitter element

M - middle ring element

O - outer ring element

Figure 5-4. Integrated Radiance of Illuminated Sphere Segments Vs. Zonal Element Phase (ϕ). In (a) and (b), the center transmitter element is stepped incrementally out of phase and the resulting integrated power (far-field pattern × target distribution) is plotted normalized to its peak value. Scenario parameters are: overall transmitter diameter (d_T) = .6 m, range (R) = 5 km, λ = 10.6 μm, N = 7, 19, 100 = number of transmitter elements.

TABLE 5-2

MODAL TARGET EFFECTS

Target	Mode No.	NORMALIZED SLOPE (10^{-5}/deg) $P/P_{max} = 0.95$	ϕ_{peak} (deg)
Point Target	1	173.1	0.
	2	371.3	0.
	3	332.3	0.
	4	517.1	0.
	5	460.3	0.
	6	400.9	0.
	7	416.9	0.
	8	332.4	0.
	9	345.7	0.
Sphere Segment d_0 = 10 cm r_c = 1 m	1	167.6	1.8
	2	320.8	9.0
	3	343.7	1.8
	4	469.4	5.4
	5	450.0	0.
	6	383.8	0.
	7	400.5	1.8
	8	335.1	1.8
	9	329.1	0.
Sphere Segment d_0 = 40 cm r_c = 20 cm	1	149.3	1.8
	2	298.2/241.2+	37.8
	3	295.7	0.
	4	389.4	18.0
	5	452.5	0.
	6	371.1	0.
	7	348.4	0.
	8	307.2	0.
	9	295.3	0.
Sphere Segment d_0 = 40 cm r_c = 1 m	1	136.6	1.8
	2	257.4	28.8
	3	296.2	0.
	4	354.1	16.2
	5	398.2	0.
	6	348.8	0.
	7	325.8	0.
	8	286.3	0.
	9	278.1	0.
Sphere Segment d_0 = 40 cm r_c = 4 m	1	82.2*	3.6
	2	95.1*	28.8
	3	125.7	0.
	4	174.2	0.
	5	187.4	0.
	6	216.7	0.
	7	202.4	0.
	8	189.8	0.
	9	217.9	0.

+Indicates slope on both sides of peak; *Mode amplitude extended greater than 90°.

TABLE 5-3

ZONAL TARGET EFFECTS

Target	Number of Channels	Element	NORMALIZED SLOPE (10^{-5}/deg) $P/P_{max} = 0.95$
Point Target	7	C	256.6
	7	O	256.6
	19	C	148.4
	100	C	*
Sphere Segment d_0 = 10 cm r_c = 1 m	7	C	262.4
	7	O	258.9
Sphere Segment d_0 = 40 cm r_c = 20 cm	7	C	268.3
	7	O	239.4
Sphere Segment d_0 = 40 cm r_c = 1 m	7	C	251.5
	7	O	213.6
	19	C	166.1
	19	M	158.2
	19	O	118.0
Sphere Segment d_0 = 40 cm r_c = 4 m	7	C	173.7
	7	O	120.7
	19	C	126.5
	100	C	†

C - Center transmitter element

M - Middle ring element

O - Outside ring element

* - Minimum $P/P_{max} = 0.96$ @ $\phi = 180°$

† - Minimum $P/P_{max} = 0.96$ @ $\phi = 178°$

Dither modulation of the received signal is largest when the illuminating beam is unconverged and goes to zero at convergence. The amplitude modulation of the received signal is calculated by multiplying the slopes (in Tables 5-2 and 5-3) by the dither amplitude in degrees. For example, for a point target, a ±20° dither amplitude for Mode 1 results in the following received signal modulation: (slope) × (dither)/(P/P_{max}) = $(173.1 \times 10^{-5})(20)/(0.95)$ = 0.036, i.e., 3.6% modulation at 95% convergence.

5.2 ILLUSTRATIVE CLOSED-LOOP SIMULATIONS

It must be emphasized that these closed-loop simulations represent illustrative examples of COAT performance and are not meant to be a complete set from which general conclusions can be drawn. However, they do give an indication of the performance with single-feature targets within the limits of variation for the statistical processes simulated. They have been selected to reflect the trends in the analytic results noted in Sec. 2.

The performance with real targets depends on the dither signal reduction by the target's brightness gradient, which is determined by its geometrical shape, size, and materials reflectance, and on the distribution of the target modulation (noise) in the frequency domain. For zonal multidither systems the performance is reduced as the number of transmitter elements (and hence control channels) is increased. Phase conjugate performance may be improved for more channels for some target sizes.[1]

Modal multidither (using the first nine MOWACS modes with the same interdither frequency spacing and lowest dither frequency) performance is comparable to a 7-element zonal system for a mode by mode (or element by element) initial phase error. However, it achieves better performance with the more physically realistic initial error of an atmosphere phase screen. This is because the modal shapes more closely approximate lower order aberrations than 7 zonal elements (in an hexagonal array). In fact, using only the first 4 MOWACS modes provides correcting power superior to that of a 7-element zonal system with respect to tilt and focus error.

---

[1] J. Radley et al., op. cit.

A 19-element zonal transmitter possesses approximately the same correcting power as the 9-mode MOWACS in terms of atmospheric phase perturbations, but performs significantly worse with target noise in the multidither implementation. It should be noted, however, that the modal system advantage is totally lost if higher order aberration correction is required. For a dither system with many channels (~ 50-100) modal and zonal performance should be comparable if the dither frequencies are the same.

5.2.1 System Parameters

There are a number of design details which must be considered in order to compare modal and zonal systems. For all these closed-loop runs, AGC, aperture averaging, and disabling the error-correction voltages to the mirror pushers for the first 0.125 msec were incorporated. Aperture averaging and AGC were found to improve zonal COAT performance by decreasing target modulation effects and thus were incorporated in the modal simulator with distributed targets. It was found that the performance of the modal transmitter was improved by limiting the gain of the AGC initially with a voltage clipper. In addition, by disabling the error-correction voltages for the first 0.125 msec, large initial transients in the correction voltages are not applied to the transmitter. Otherwise, the initial transients can drive the modes to a state which results in a local maximum at convergence.

Closed-loop comparisons between zonal and modal COAT require the same dither levels. Therefore, along with the equivalent of the 7-channel zonal dither level (±28.8° peak amplitude for Mode 1 and the others scaled to give equal modulation), an additional set of runs was made using the equivalent of the 19-channel zonal dither level (±17.1° for Mode 1).

Figures 5-5 and 5-6 illustrate the effects of target modulation. The smaller dither results in a higher convergence level with a point target, but performs worse with a distributed target when the modulation spectrum overlaps the dither frequencies as anticipated from gain considerations discussed in Sec. 2.

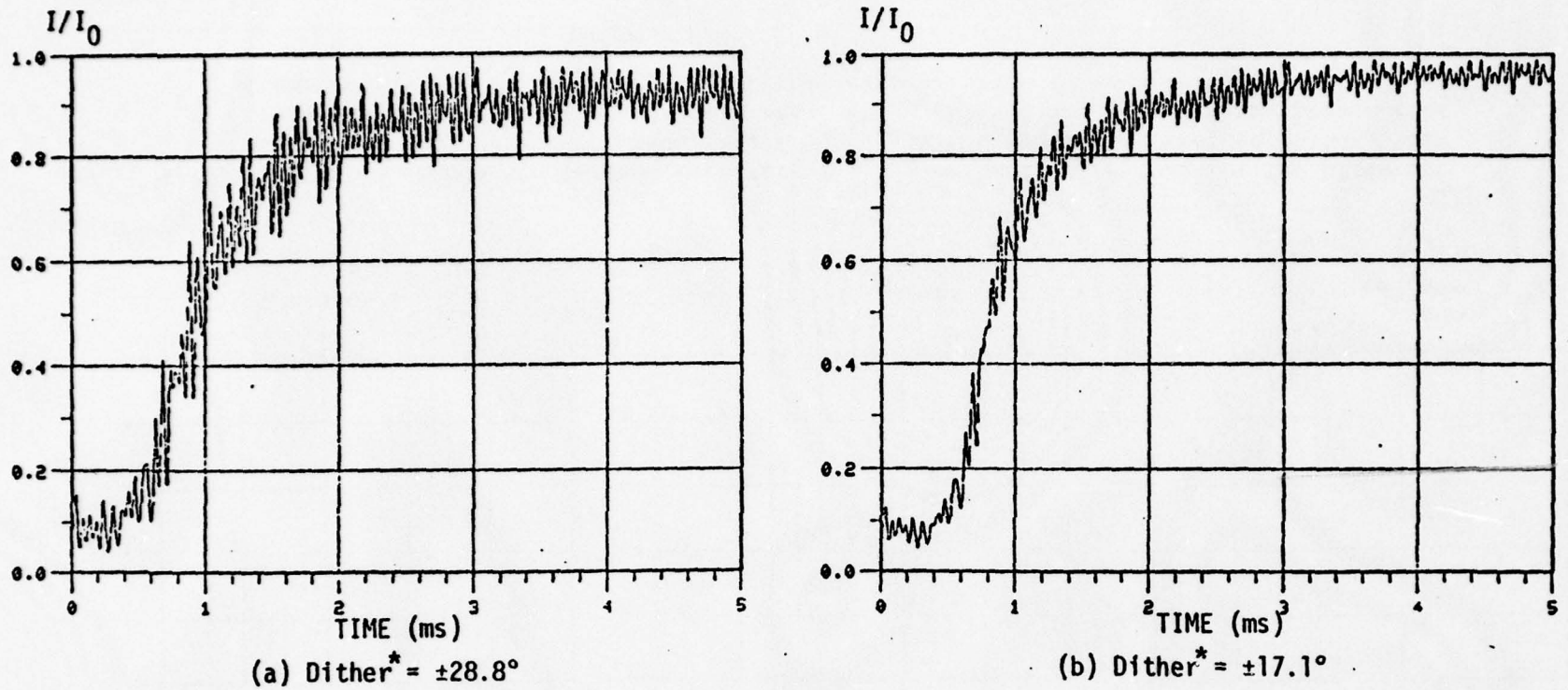

(a) Dither* = ±28.8°

(b) Dither* = ±17.1°

Figure 5-5. Modal Multidither COAT Closed-Loop Simulations with a Point Target for Two Different Dither Levels, Equivalent to the 7 (a) and 19 (b) Channel Zonal Transmitter. Target scenario parameters are: range = 5 km, λ = 10.6 μm, transmitter diameter = .6 m.

*For MOWACS mode 1; dither amplitudes of other 8 modes scaled to give equal received signal modulation for a point target.

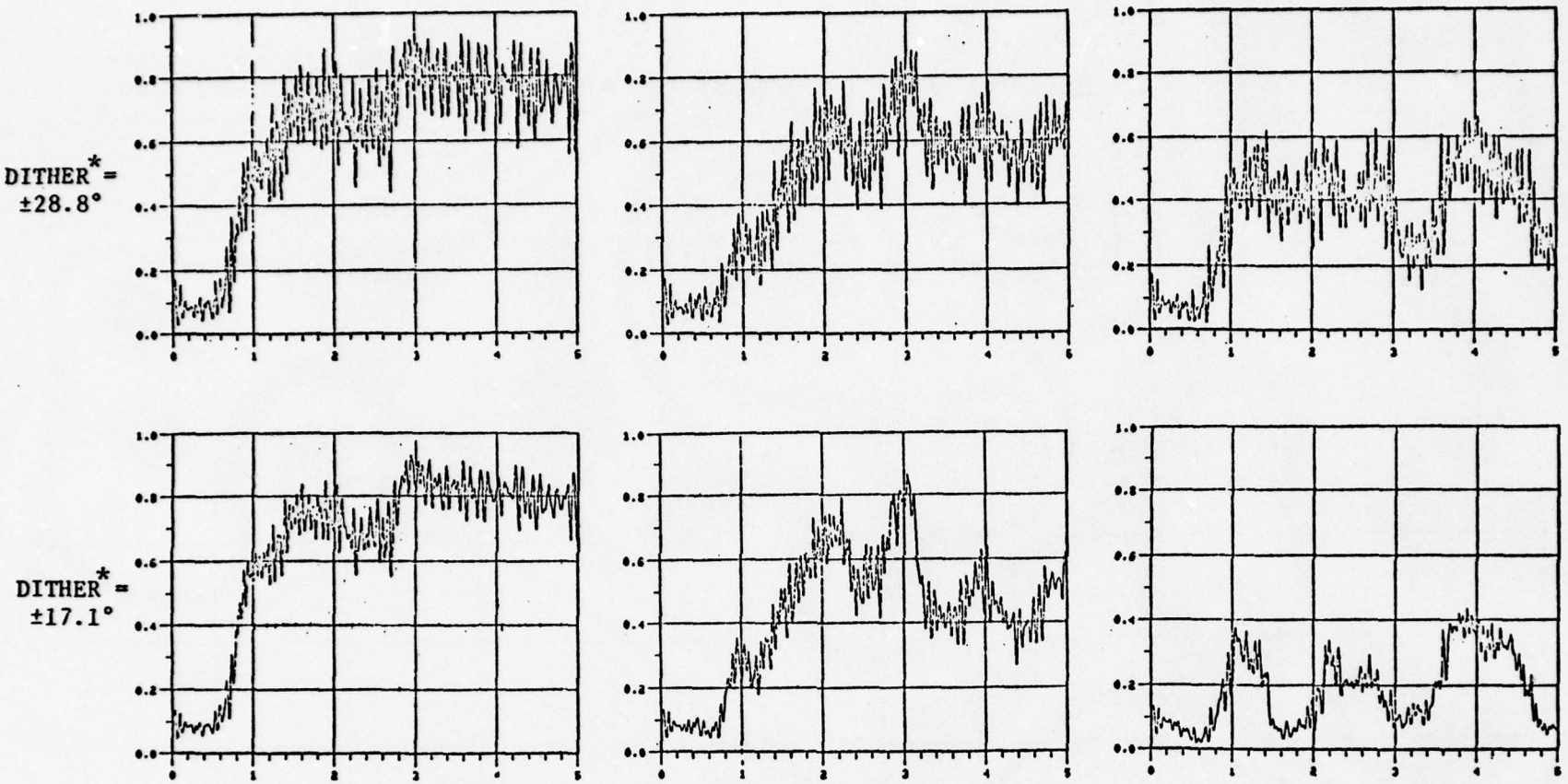

Figure 5-6. Modal Closed-Loop Simulations with Target B (d_0 = 10 cm, r_c = 1 m) for Two Different Dither Levels. Target rotation rate (Ω) and maximum modulation frequency (f_{max}) are listed under each case. Parameters are: range (R) = 5 km, λ = 10.6 μm, transmitter diameter (d_T) = .6 m. Curves are Strehl ratio vs. time (0 to 5 msec).

*Defined in Fig. 5-5.

5.2.2 Modal, Zonal, Phase Conjugate COAT Base-Line Comparison

As previously mentioned, equivalent system parameters were applied to the three COAT systems to present a fair comparison of their performance against varied target spatial effects.

Typical results and analysis indicate that phase conjugate COAT performs best at fast rotation rates, better than multidither COAT in this respect. However, for slow rotation rates, multidither COAT surpasses phase conjugate. The mechanism for these results is target modulation interfering with the signal processing. When target base-band noise overlaps the dither bands for multidither COAT, or falls within the filter bandwidth of the signal processor for phase conjugate, erroneous wavefront correction occurs, resulting in a degradation in performance. Figures 5-7 to 5-8 illustrate this effect. With no target modulation, as in the case of a point target, maximum performance is achieved for all COAT systems.

Another very important consideration is how the closed-loop performance scales with the number of control channels. Other studies have shown that as many as 60 to 100 transmitter elements (for a 1-m-diameter total aperture) may be required to provide adequate compensation for atmospheric phase perturbations along the propagation path. A modal transmitter requires fewer control channels for lower order aberration because each dithered mode controls the entire transmitter aperture which is better matched to the aberration than a zonal system. Consequently, a modal transmitter possesses higher correcting power for a small number of channels than an equal number of zonal elements. Therefore, it is not equivalent to compare the 9-mode MOWACS to only the 7-element zonal systems. However, when a large number of channels is required due to high order aberrations, equal numbers of channels are essentially equivalent.

The closed-loop performance of a 19-element zonal multidither and phase conjugate system is shown in Fig. 5-9. Note that the multidither performance is reduced from the 7-element case. Figure 5-10 shows the comparison to 37 elements. The reason for the reduction in a zonal multidither

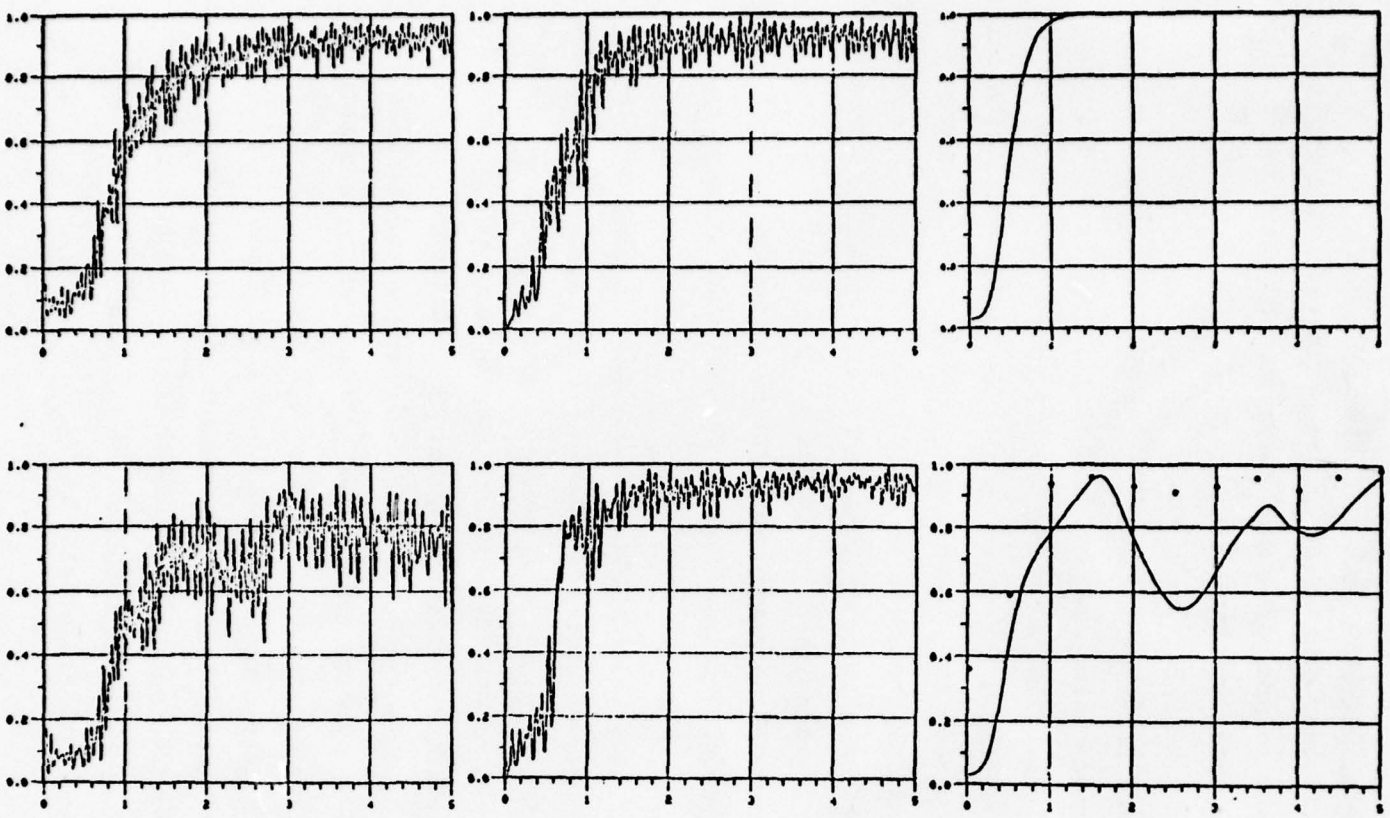

Figure 5-7. Modal, Zonal, Phase Conjugate COAT Closed Loop Simulations. Curves are Strehl ratio vs. time (0 to 5 msec). Dots are values of beam maximum (not necessarily on axis).

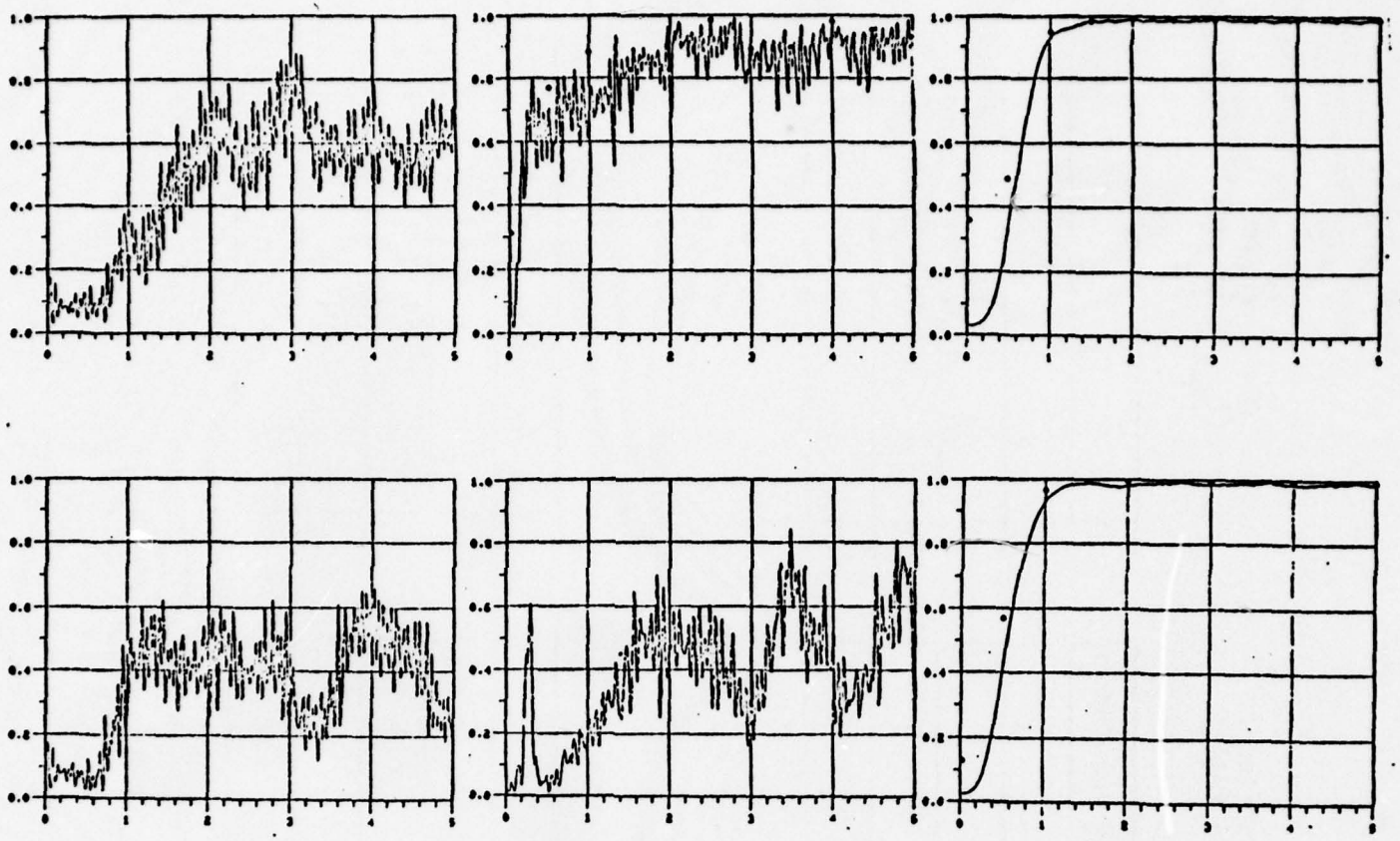

Figure 5-8. Modal, Zonal, Phase Conjugate COAT Closed Loop Simulations with Target B. Curves are Strehl ratio vs. time (0 to 5 msec). Dots show beam maximum.

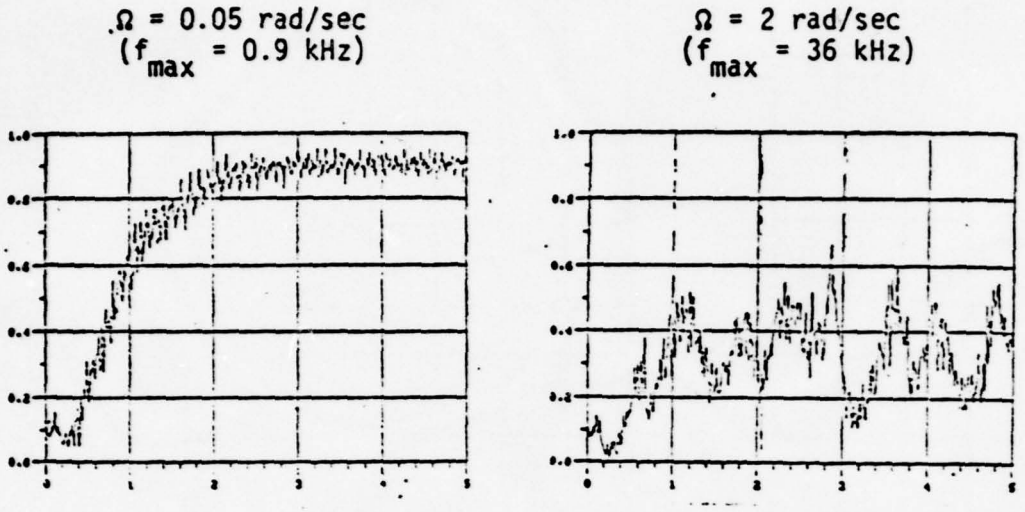

(a) Zonal Multidither

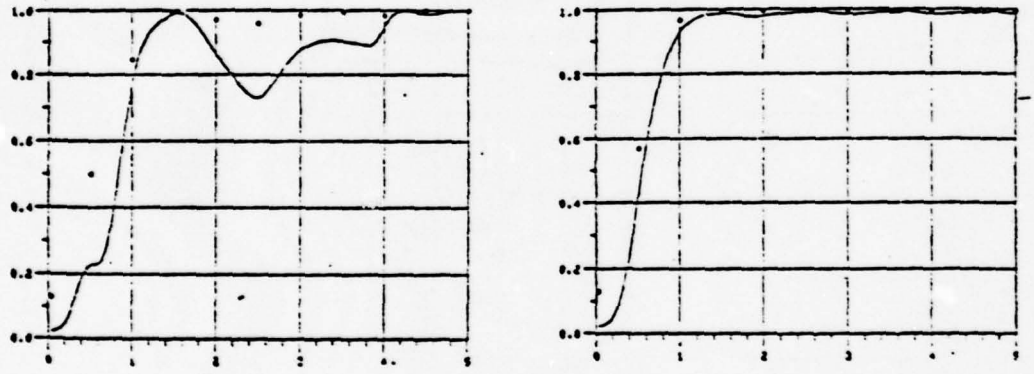

(b) Phase Conjugate

Figure 5-9. 19-Element COAT Performance with Target B (d_0 = 10 cm ≅ $\lambda R/d_T$, r_c = 1 m). Curves show Strehl ratio vs. time (0 to 5 msec). Dots show beam maximum.

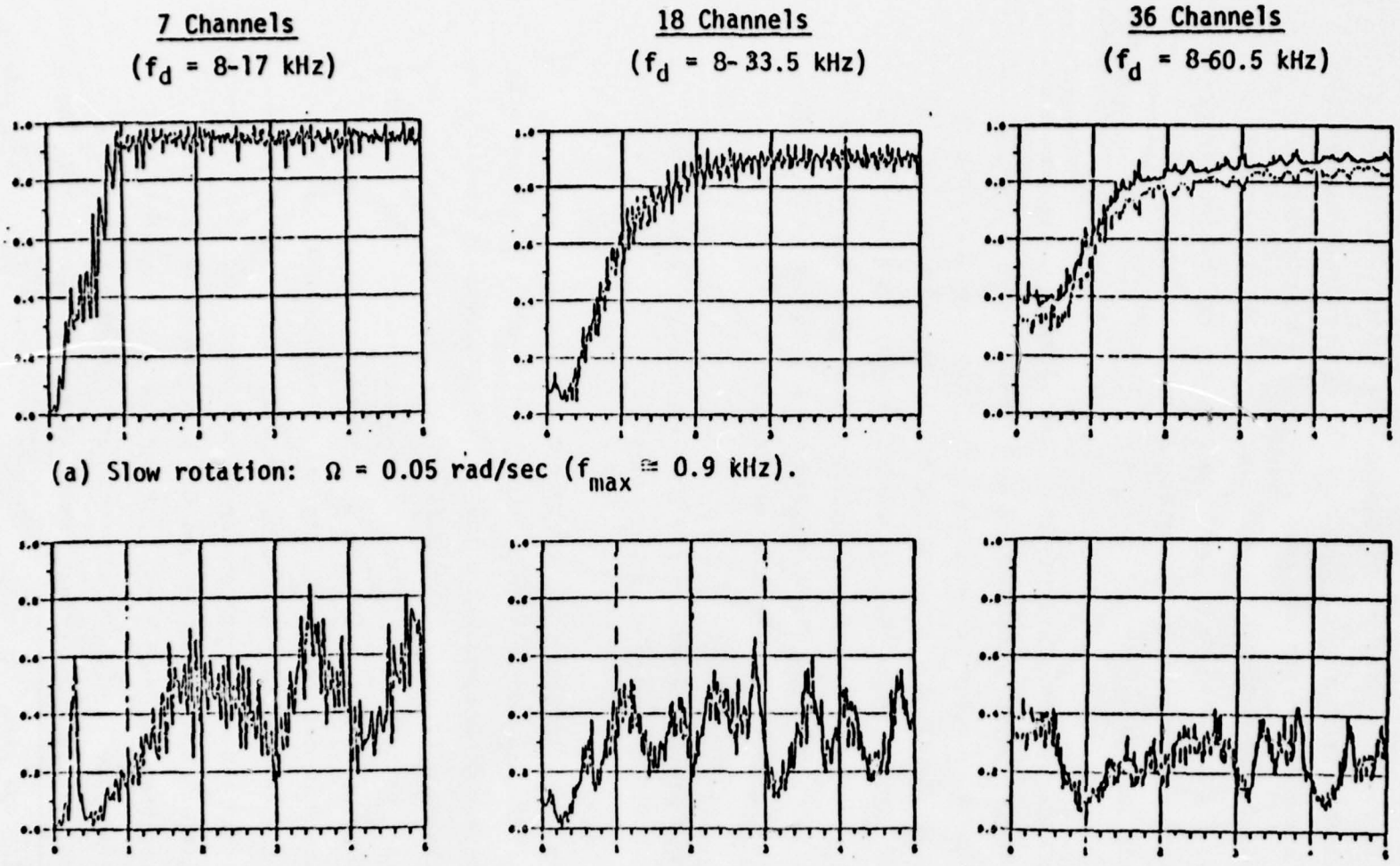

Figure 5-10. Comparison of Zonal Multidither Closed-Loop Performance with Target B (d_0 = 10 cm, r_c = 1 m) for Larger Numbers of Channels (total xmtr aperture diameter = 60 cm). TM generated open loop with annular receiver and used as multiplicative noise in closed loop run. Curves show Strehl ratio vs. time (0 to 5 msec). For 36 channels, error signals not applied to transmitter until t = 0.5 msec.

system is that the dither modulation of the received signal is reduced as the number of elements is increased, assuming the same overall transmitter size (cf. Secs. 2 and 3). Increased gain to recover adequate dither signals also amplifies the noise causing larger random phasing errors in each channel. Phase conjugate performance does not suffer for larger numbers of elements and in some instances may actually improve as the number of channels increases.[1]

The method used to accomplish the 19- and 37-element zonal runs was to generate the target noise separately in an open-loop simulation and then use it as multiplicative noise in the closed-loop simulations. This is valid provided that the target is unresolved by the transmitter aperture. Comparison to the target-in-the-loop closed-loop results and further description are given elsewhere.[1] Zonal and phase conjugate results are shown in Figs. 5-11 to 5-13 based on analysis which indicates that trends for a modal transmitter will be the same as the zonal.

The threshold process noted in Sec. 2 is illustrated clearly in Fig. 5-12 for both dither and conjugate systems.

5.2.3 Closed-Loop Comparison with an Atmosphere

Further performance comparisons between modal, zonal, and phase conjugate systems were made incorporating two static-phase screen atmospheres of different turbulence levels. These systems were exercised against two different targets: point target, and a rotating unresolved glint (sphere segment, d_0 = 10 cm, r_c = 1 m). For the distributed target, the most stressful rotation rate occurs when the target modulation overlaps the dither band for the two multidither systems, and for the phase conjugate when TM falls within the signal processing filter bandwidth. The appropriate target modulation extents were 36 and 0.9 kHz, respectively. This corresponds to rotation rates of 2 and 0.05 rad/sec. In the modal COAT system, ±28.8° (for Mode 1) dither performed better than ±17.7° dither against target modulation interference; hence it was used for these comparisons.

[1] J. Radley et al., op. cit.

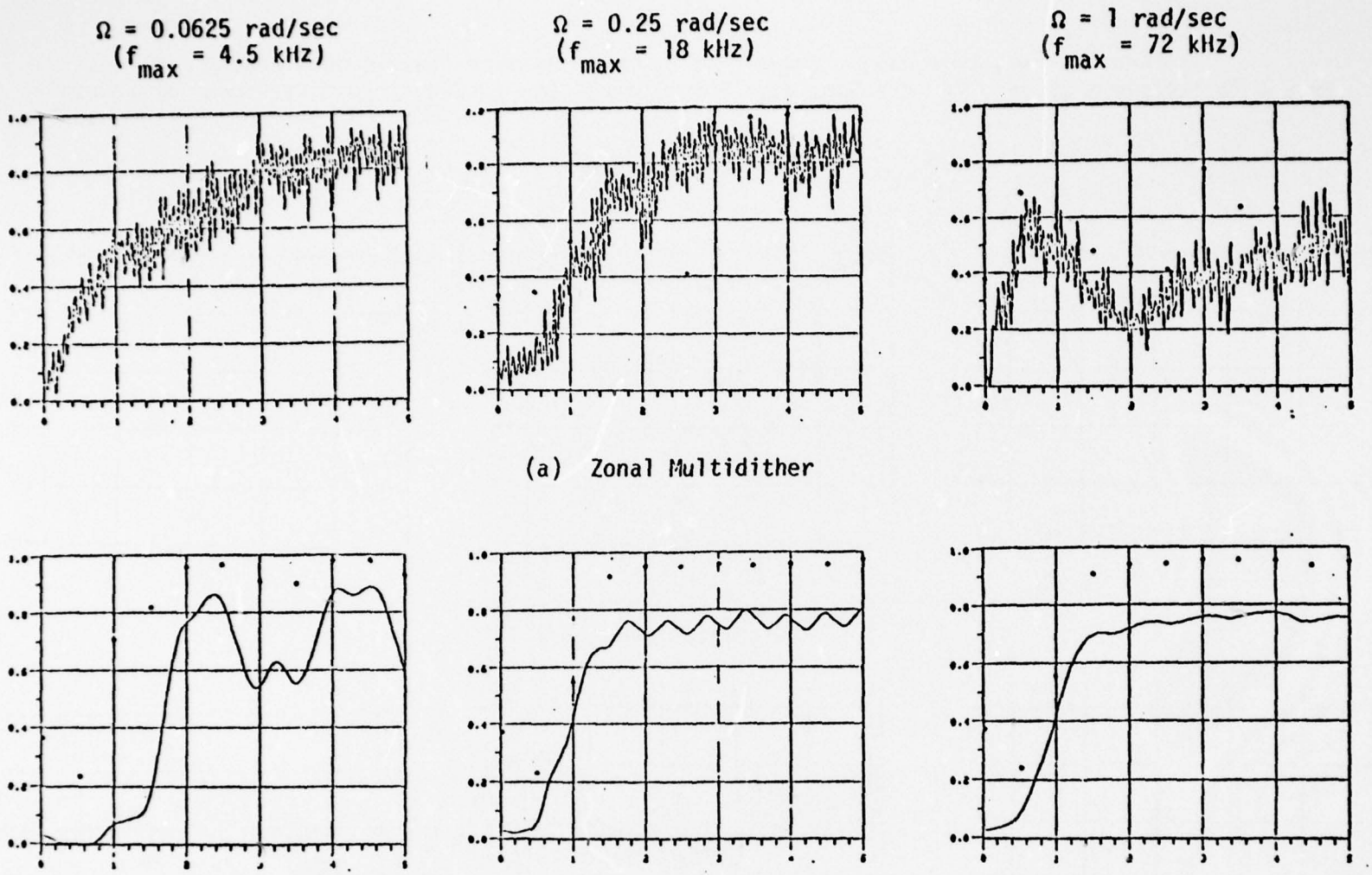

Figure 5-11. Comparison of 7-Channel COAT Performance with Target C (d_0 = 40 cm $\cong 4\lambda R/d_T$, r_c = 1 m). Curves show Strehl ratio vs. time (0 to 5 msec). Dots show beam maximum.

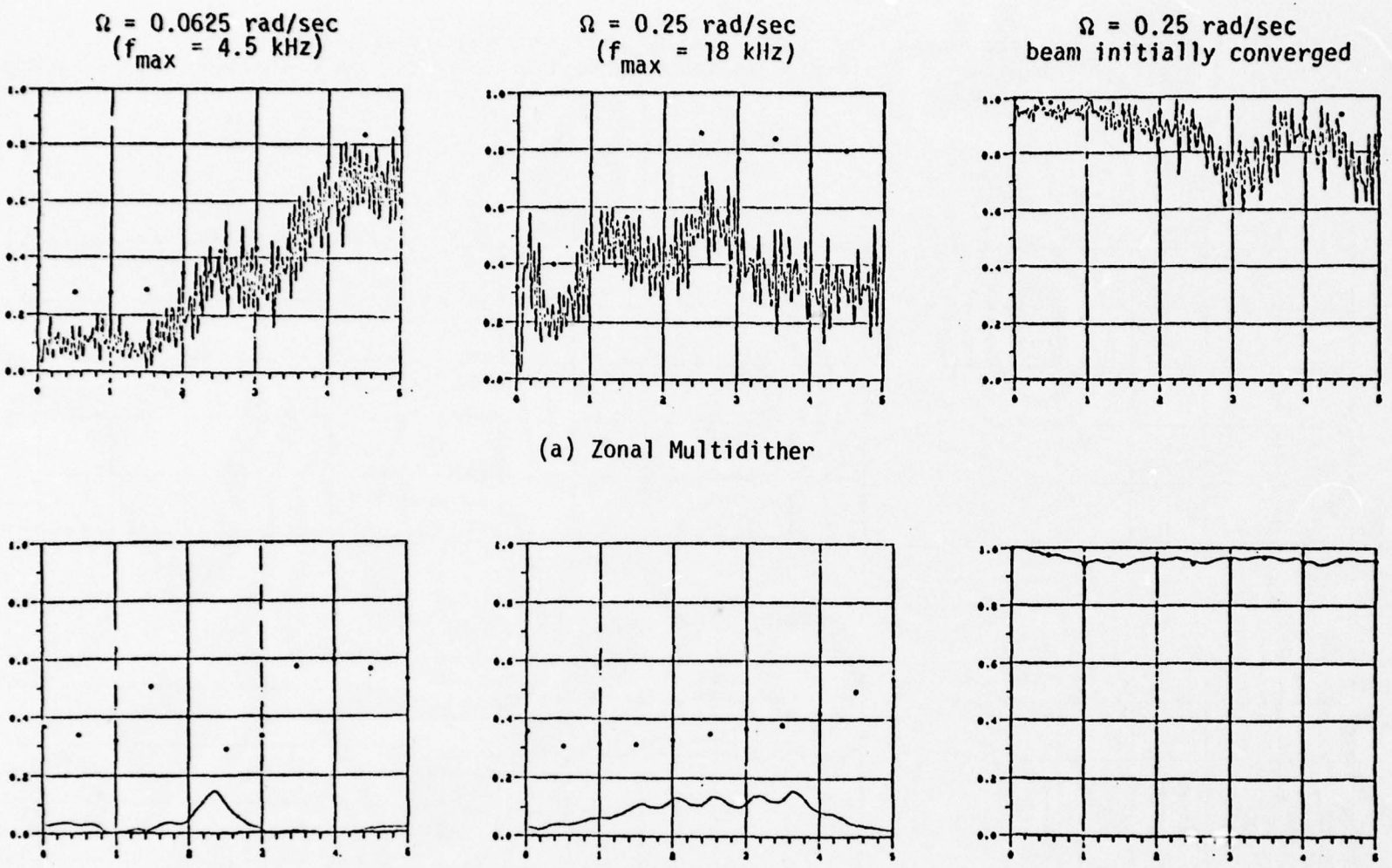

Figure 5-12. Comparison of 7-Channel COAT Performance with Target D (d_0 = 40 cm $\cong 4\lambda R/d_T$, r_c = 4 m). Curves show Strehl ratio vs. time (0 to 5 msec). Dots show beam maximum.

Ω = 0.25 rad/sec
(f_{max} = 18 kHz)

Ω = 1 rad/sec
(f_{max} = 72 kHz)

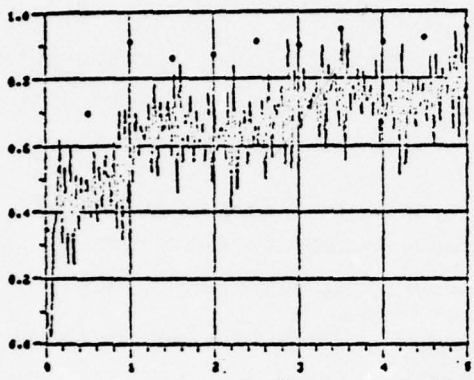

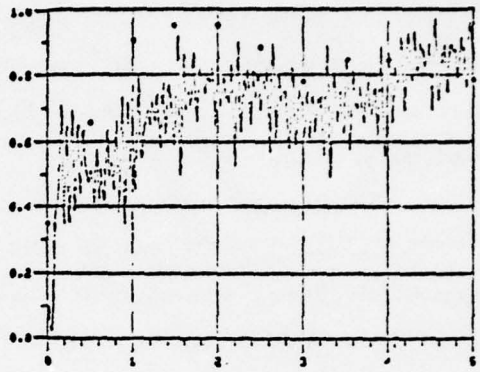

(a) Zonal Multidither

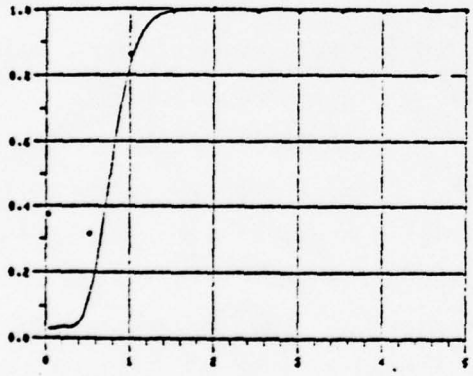

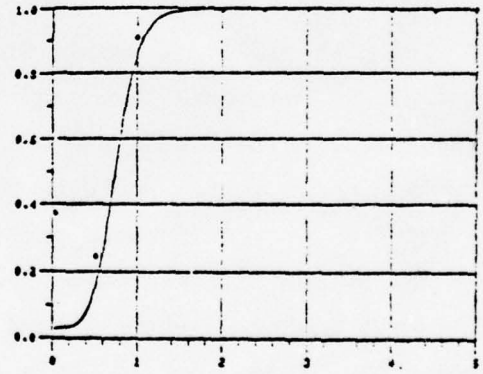

(b) Phase Conjugate

Figure 5-13. Comparison of 7-Channel COAT Performance with Target A ($d_0 = 40$ cm $\cong 4\lambda R/d_T$, $r_c = 20$ cm). Curves show Strehl ratio vs. time (0 to 5 msec). Dots show beam maximum.

Without exception, the 9-mode modal COAT performed slightly better than 7-element zonal COAT. This result is expected since it can closer represent the ideal correction for a well behaved atmospheric phase screen with its deformable surface.

Figure 5-14 illustrates performance comparisons for the stronger atmospheric turbulence. For the weaker turbulence all three systems performed equivalently (see Fig. 5-15), because this phase perturbation possessed very slight tilt error.

Closed-loop performance runs, for a point target with the phase screen atmosphere, showed that wavefront corrections were mostly applied by the first four modes of the modal transmitter, corresponding to focus and tilt. Illustrative modal simulations indicate that much of the atmospheric perturbation can be corrected by these basic low spatial order modes (see Fig. 5-16). It is understood, however, that high spatial frequency atmospheric perturbations can only be corrected using higher order modes to achieve a high level of convergence.

The possibility of design trade-offs in scenarios where target noise is a limiting factor is more substantial for modal than for zonal. If the target noise limits M-D operation to a small number of channels ($\lesssim$10), the modal system would be capable of providing greater turbulence correction and hence improved performance over a zonal system. Also, since the modal system involves whole aperture control, an adaptive system which tailors the number of channels and gain parameters to optimize power on target could be more easily implemented than a zonal system. However, these options are of interest only if optimization at less than diffraction limited intensity levels is adequate to satify the mission requirements.

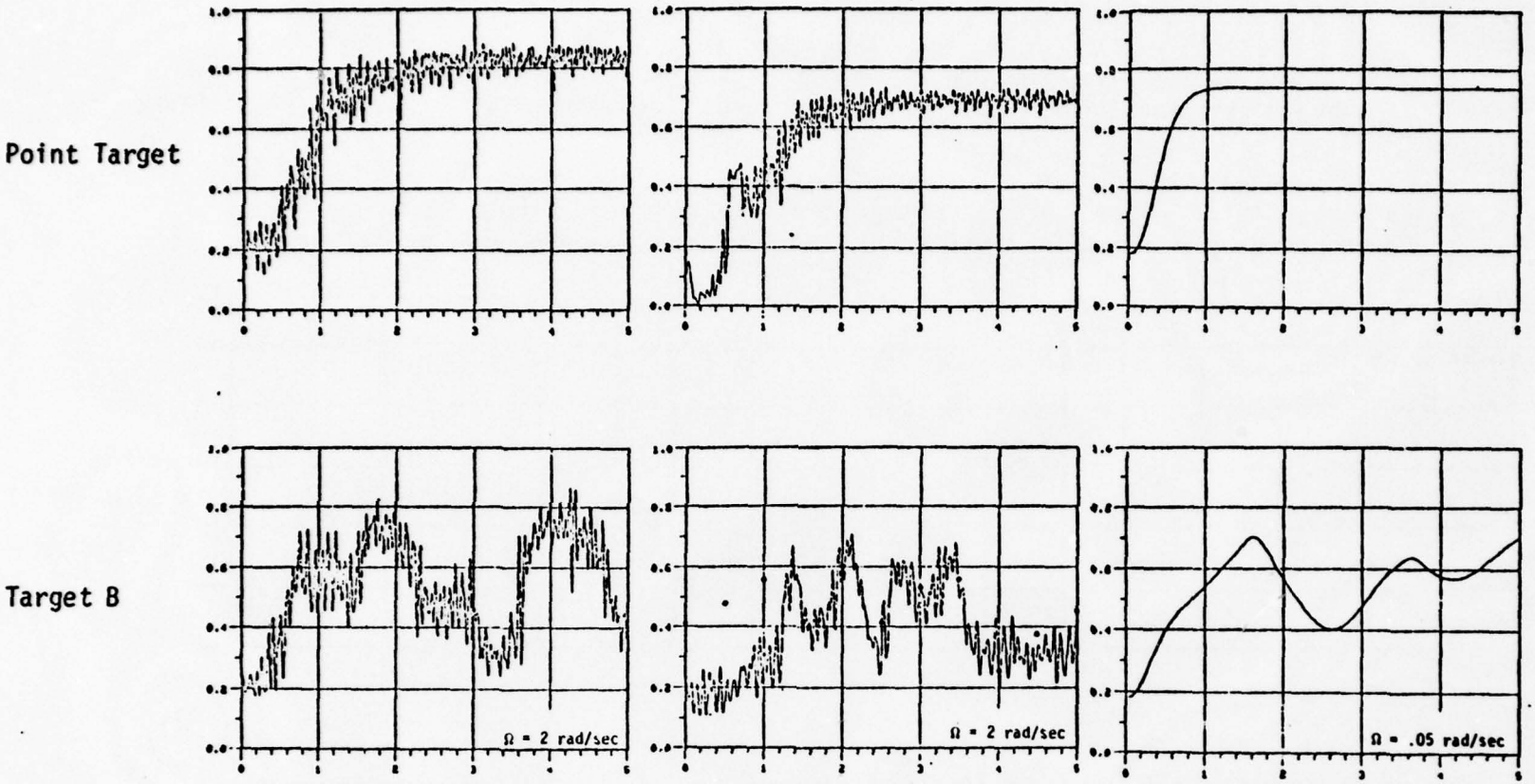

Figure 5-14. Modal, Zonal, Phase Conjugate COAT Closed Loop Simulations with a Phase Screen Atmosphere (Moderate Turbulence), $C_n^2 = 10^{-13} m^{-2/3}$). Curves are Strehl ratio vs. time (0 to 5 msec).

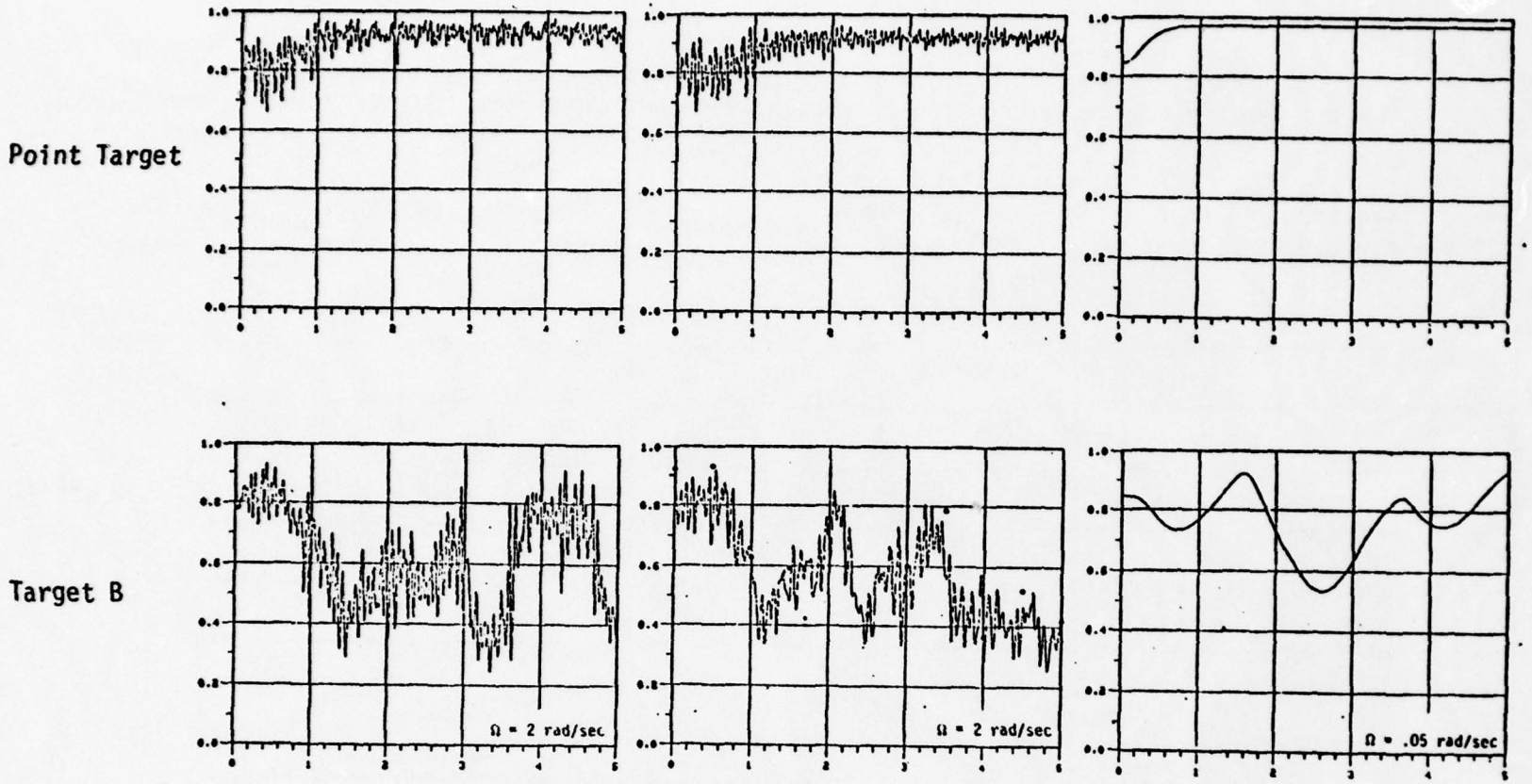

Figure 5-15. Modal, Zonal, Phase Conjugate COAT Closed Loop Simulations with a Phase Screen Atmosphere (Weak Turbulence), $C_n^2 = 10^{-14} m^{-2/3}$). Curves are Strehl ratio vs. time (0 to 5 msec).

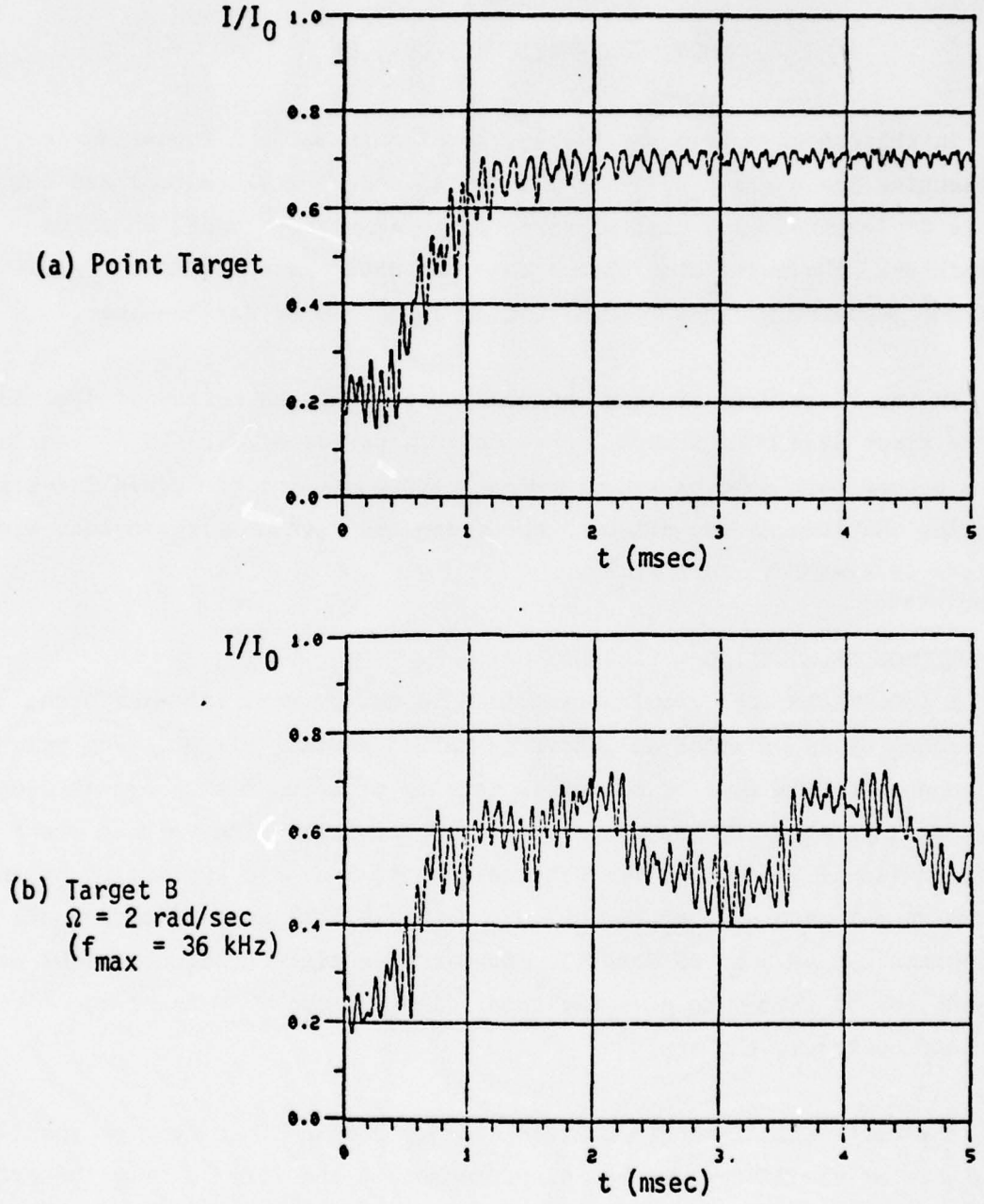

Figure 5-16. Four-Channel Modal Closed Loop Simulations with an Atmoperic Phase Screen ($C_n^2 = 10^{-13} m^{-2/3}$). Transmitter consists of only the first 4 MOWACS modes.

APPENDIX A
MODAL TRANSMITTER SIMULATION

In this section is described a general mathematical formalism for representing the vibrant structural modes of a deformable mirror and how this is implemented on a digital computer to simulate a modal adaptive transmitter. The particular choice for this study is the MOWACS (MOdal Wavefront Adaptive Control System) mirror developed by Perkin-Elmer.[1]

In the first part of this appendix we present the method of describing the first nine MOWACS modes in terms of a series of Zernike polynomials. In the second part some of the practical considerations are given for representing the transmitter for both the open- and closed-loop computer simulations presented in Sec. 5.

A.1 METHOD OF MODELING MOWACS MIRROR

A deformable mirror which is driven in one or more resonant structural modes by an array of actuators is called a modal mirror. For practical reasons, this type of mirror is usually clamped at two opposing edges to accommodate coolant; the other two edges are free. The various modes of vibration (usually sinusoidal) that can be sustained are excited by pushers located on the underside of the mirror. Virtually any set of orthogonal polynomials can be used to describe the mirror-surface displacement of each mode and can be summed to give the total displacement as a function of time and position across the surface.

The mathematical representation used by Perkin-Elmer for the spatial dependence of the mirror surface displacement is the first 22 Zernike polynomials (P_j) which are listed in Table A-1. The coefficients, a_{ij}, that accompany these polynomials in the description of the first nine modes of vibration are listed in Table A-2. Thus, the mirror surface displacement $h_i(x, y)$ of the ith mode of vibration is approximated as

[1] C. Neufeld, Modal Wavefront Control System (MOWACS) Phase II Interim Report, Perkin-Elmer Corporation Report 12700, September 1975.

TABLE A-1

MODIFIED ZERNIKE POLYNOMIALS*

$P_1 = 1$

$P_2 = 2r\cos\theta = 2x$

$P_3 = 2r\sin\theta = 2y$

$P_4 = \sqrt{3}(2r^2-1)$

$P_5 = \sqrt{6}\ r^2\sin 2\theta = \sqrt{6}\ 2xy$

$P_6 = \sqrt{6}\ r^2\cos 2\theta = \sqrt{6}\ (x^2 - y^2)$

$P_7 = \sqrt{8}\ (3r^3 - 2r)\ \sin\theta = \sqrt{8}\ y(3r^2 - 2)$

$P_8 = \sqrt{8}\ (3r^3 - 2r)\ \cos\theta = \sqrt{8}\ x(3r^2 - 2)$

$P_9 = \sqrt{8}\ r^3\ \sin 3\theta = \sqrt{8}\ y(3x^2 - y^2)$

$P_{10} = \sqrt{8}\ r^3\ \cos 3\theta = \sqrt{8}\ x(x^2 - 3y^2)$

$P_{11} = \sqrt{5}\ (6r^4 - 6r^2 + 1)$

$P_{12} = \sqrt{10}\ (4r^4 - 3r^2)\ \cos 2\theta = \sqrt{10}\ (x^2 - y^2)(4r^2 - 3)$

$P_{13} = \sqrt{10}\ (4r^4 - 3r^2)\ \sin 2\theta = \sqrt{10}\ 2xy\ (4r^2 - 3)$

$P_{14} = \sqrt{10}\ r^4\ \cos 4\theta = \sqrt{10}\ (x^4 - 6x^2y^2 + y^4)$

$P_{15} = \sqrt{10}\ r^4\ \sin 4\theta = \sqrt{10}\ 4xy\ (x^2 - y^2)$

$P_{16} = \sqrt{12}\ (10r^5 - 12r^3 + 3r)\ \cos\theta = \sqrt{12}\ x(10r^4 - 12r^2 + 3)$

$P_{17} = \sqrt{12}\ (10r^5 - 12r^3 + 3r)\ \sin\theta = \sqrt{12}\ y(10r^4 - 12r^2 + 3)$

$P_{18} = \sqrt{12}\ (5r^5 - 4r^3)\ \cos 3\theta = \sqrt{12}\ x(x^2 - 3y^2)(5r^2 - 4)$

$P_{19} = \sqrt{12}\ (5r^5 - 4r^3)\ \sin 3\theta = \sqrt{12}\ y(3x^2 - y^2)(5r^2 - 4)$

$P_{20} = \sqrt{12}\ r^5\ \cos 5\theta) = \sqrt{12}\ x(x^4 - 10x^2y^2 + 5y^4)$

$P_{21} = \sqrt{12}\ r^5\ \sin 5\theta = \sqrt{12}\ y(5x^4 - 10x^2y^2 + y^4)$

$P_{22} = \sqrt{7}\ (20r^6 - 30r^4 + 12r^2 - 1)$

*Reproduced from Neufeld, op. cit.

TABLE A-2

ZERNIKE DECOMPOSITION OF 9 MODE EXPERIMENT MODES*

Mode No.	Z_1	Z_2	Z_3	Z_4	Z_5	Z_6	Z_7	Z_8	Z_9	Z_{10}	Z_{11}
1	0.734921	0.000001	0.000002	-0.136146	-0.000000	-0.174435	-0.000000	-0.000000	-0.000000	-0.000000	0.011534
2	0.000000	-0.000000	-0.429319	-0.000000	-0.000000	-0.000000	0.037171	0.000000	0.091032	-0.000000	-0.000000
3	0.305659	0.000000	0.000001	-0.345490	0.000000	0.247649	-0.000000	-0.000000	-0.000000	0.000000	0.037565
4	0.000000	0.651998	0.000000	0.000000	0.000000	0.000000	-0.000000	-0.227033	-0.000000	-0.164120	0.000000
5	0.000001	-0.000000	0.474139	0.000001	0.000000	-0.000002	-0.329829	0.000000	0.133912	-0.000000	-0.000000
6	-0.000000	-0.311656	0.000000	-0.000000	-0.000001	-0.000000	0.000000	0.296095	-0.000000	-0.263461	0.000000
7	-0.000000	0.000001	0.000000	0.000000	0.455692	0.000000	0.000000	0.000000	0.000000	-0.000002	-0.000000
8	-0.056616	0.000001	0.000001	-0.331668	-0.000000	-0.059044	-0.000000	-0.000000	-0.000000	0.000000	0.183817
9	0.000000	-0.000000	0.044169	0.000000	-0.000001	-0.000000	0.027743	-0.000000	0.298798	-0.000000	-0.000000

Mode No.	Z_{12}	Z_{13}	Z_{14}	Z_{15}	Z_{16}	Z_{17}	Z_{18}	Z_{19}	Z_{20}	Z_{21}	Z_{22}
1	0.013670	-0.000000	0.013728	-0.000000	-0.000000	-0.000001	-0.000000	-0.000000	-0.000000	-0.000000	-0.000365
2	0.000000	0.000000	-0.000000	-0.000000	0.000000	-0.002265	0.000000	-0.003659	-0.000000	-0.005543	0.000000
3	-0.012012	0.000000	-0.054465	-0.000000	-0.000000	-0.000001	-0.000000	0.000000	-0.000000	-0.000000	-0.001597
4	-0.000000	-0.000000	0.000000	-0.000000	0.027521	0.000000	0.022494	0.000000	0.014016	0.000000	-0.000000
5	0.000000	-0.000000	0.000000	0.000000	-0.000000	0.043338	0.000000	-0.018814	-0.000000	-0.021511	-0.000000
6	0.000000	-0.000000	-0.000000	0.000000	-0.646305	0.000000	0.013226	-0.000000	0.073296	-0.000000	0.000000
7	0.000000	-0.284254	-0.000000	0.094860	-0.000000	-0.000000	0.000001	-0.000000	-0.000000	0.000000	-0.000000
8	0.012378	-0.000000	0.060743	-0.000000	-0.000000	-0.000001	-0.000000	-0.000000	0.000000	0.000000	-0.022217
9	0.000000	0.000000	0.000001	0.000000	0.000000	0.004821	0.000000	-0.027789	-0.000000	-0.114153	-0.000000

*Reproduced from Neufeld, op. cit. The Z_j coefficients for the ith mode are the a_{ij} in Eq. A-1.

$$h_i(x, y) = \sum_{j=1}^{22} a_{ij} P_j \qquad \text{(A-1)}$$

The total mirror surface displacement is the sum of the h_i. The approximation of the surface displacement by Zernike polynomials is quite accurate provided (x, y) lies within a unit circle, the range over which the Zernike polynomials are defined. Accordingly, the mirror is mathematically masked to exclude these non-defined regions. The maximum amplitude of the displacement of any mode is normalized to unity.

This Zernike polynomial formalism is conveniently represented as a transformation matrix for incorporation into the existing COAT computer simulators. This matrix, called the error signal processor (cf. Fig. A-1), calculates the total mirror displacement h(x, y) for any combination of individual mode amplitudes. The processor has nine columns corresponding to each of the MOWACS modes and n rows corresponding to the number of points describing the mirror figure.

Sample results generated by the error-signal processor are shown graphically in Figs, A-2 and A-3. In the first, each of the mode shapes is displayed, and in the second, the time evolution of modes 4 and 5 is shown.

The Zernike polynomials used in describing the mirror surface displacement were chosen not for mathematical simplicity, but because various ones are associated with aberrations of the resulting optical wavefront of the reflected beam (Fig. A-4). The expression for each aberration shown is for a Zernike polynomial given in Table A-1 and differ somewhat from the definition of the classic aberrations. The reason is that an additional set of aberrations that is equivalent to the set given here exists, but they have a rotated axis of symmetry whose rotation depends on the order of the aberration.[1] This is merely a choice of nomenclature and does not affect the results presented.

---

[1] M. Born and E. Wolf, Principles of Optics, Pergamon Press Ltd., 1970, p. 212.

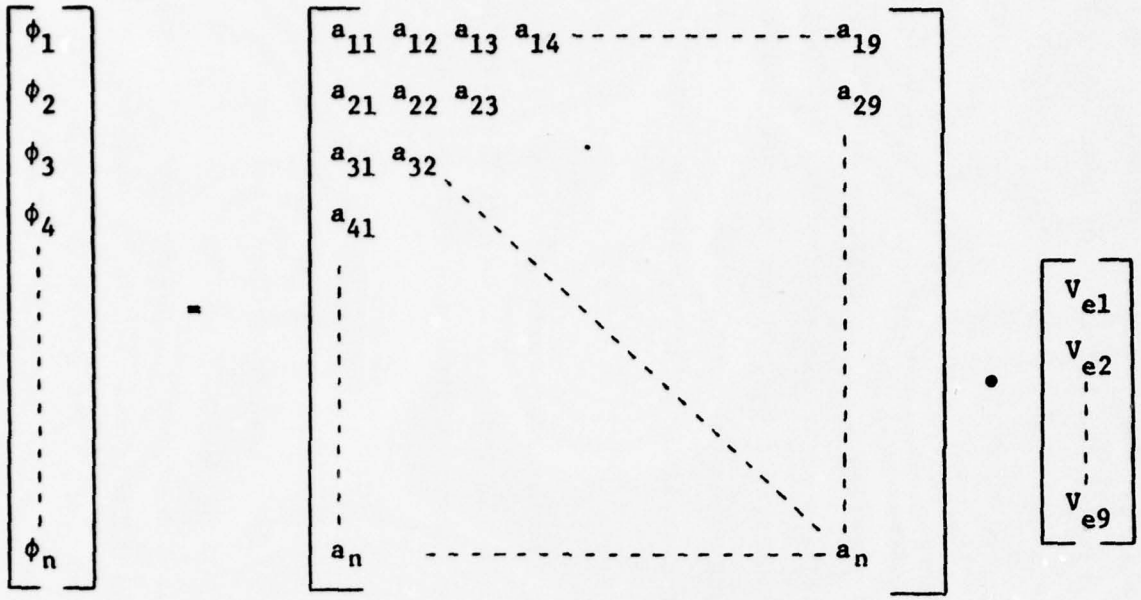

Figure A-1. The Error Signal Processor Is a Transformation Matrix Which Converts the Error Signal (V_{ei}) for Each of the 9 MOWACS Modes Into the Total Transmitter Wavefront Phase Distribution. Each column is the normalized displacement for 1 mode at ith point on the transmitter. The net phase at any given transmitter point is a weighted sum of the displacements due to each control channel. For example, the phase at the fifth point is $\phi_5 = a_{51}V_{e1} + a_{52}V_{e2} + a_{53}V_{e3} + \ldots a_{59}V_{e9}$.

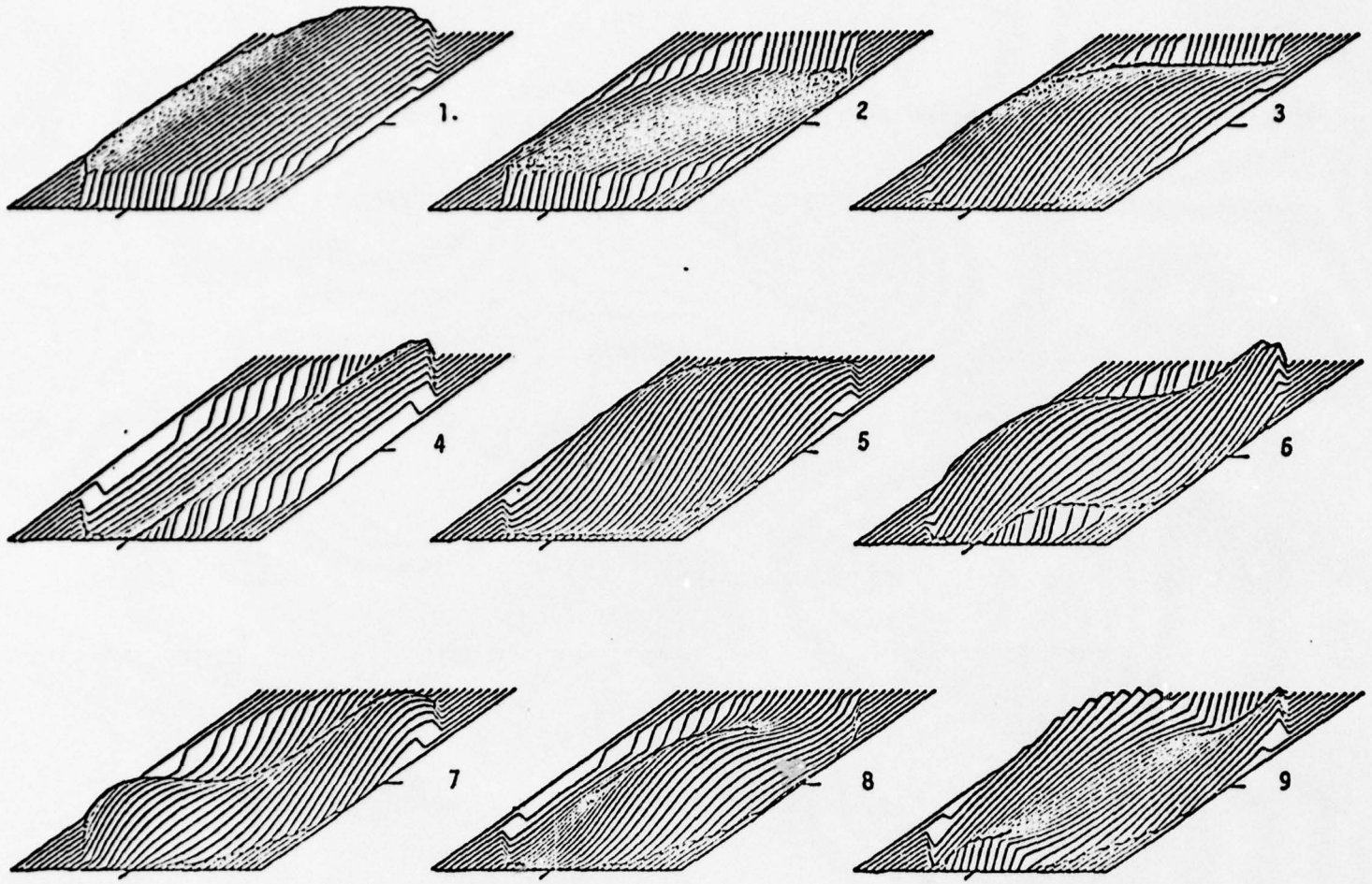

Figure A-2. First Nine MOWACS Modes.[1] Plots illustrate magnified displacement only within circular illuminated area.

[1] C. Neufeld, op. cit.

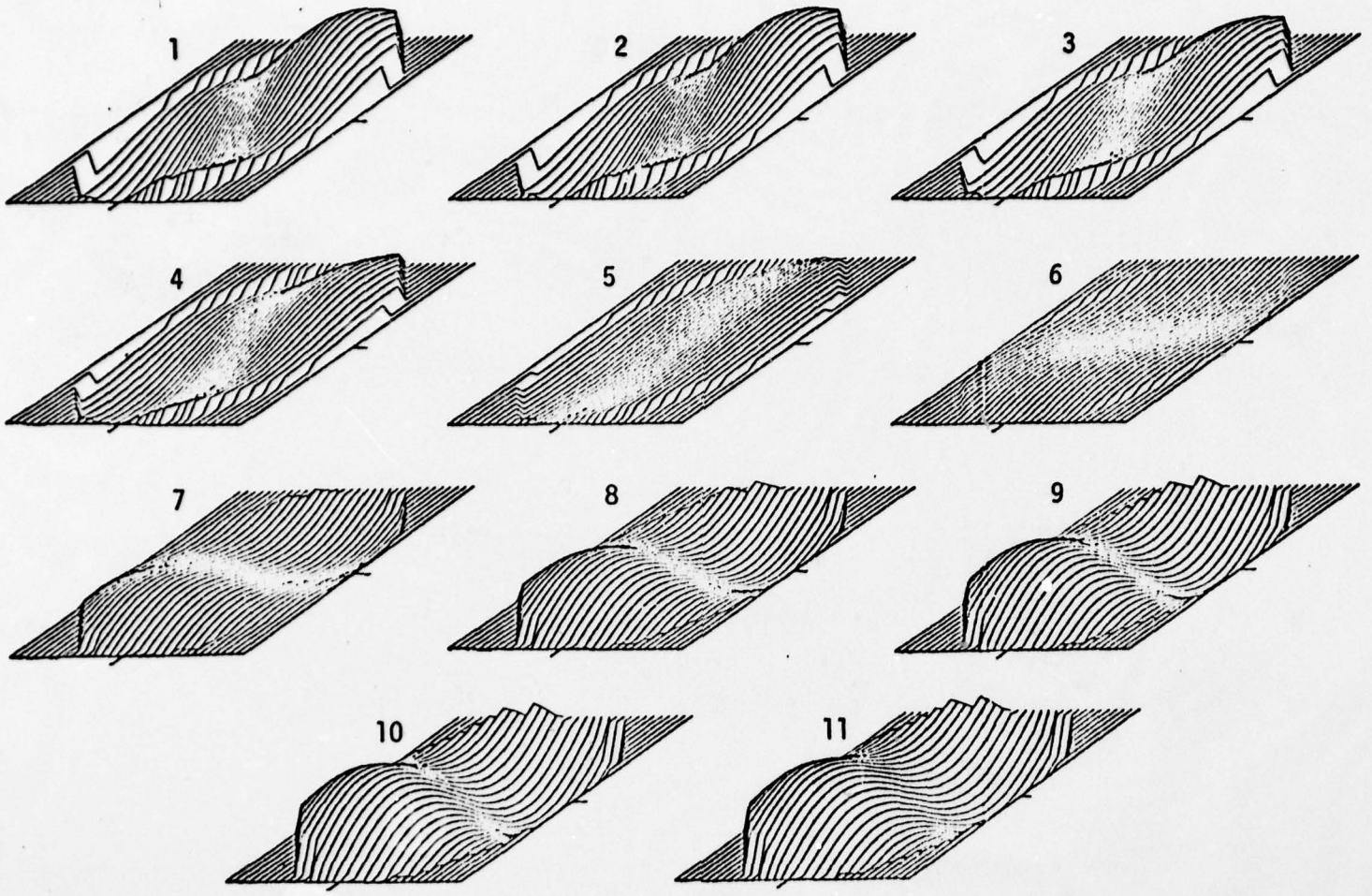

Figure A-3. Time Evolution of Superposition of Modes 4 and 5 (Frequencies 6214 Hz, 7261 Hz, Respectively) In Intervals of 18° Phase of Mode 4.

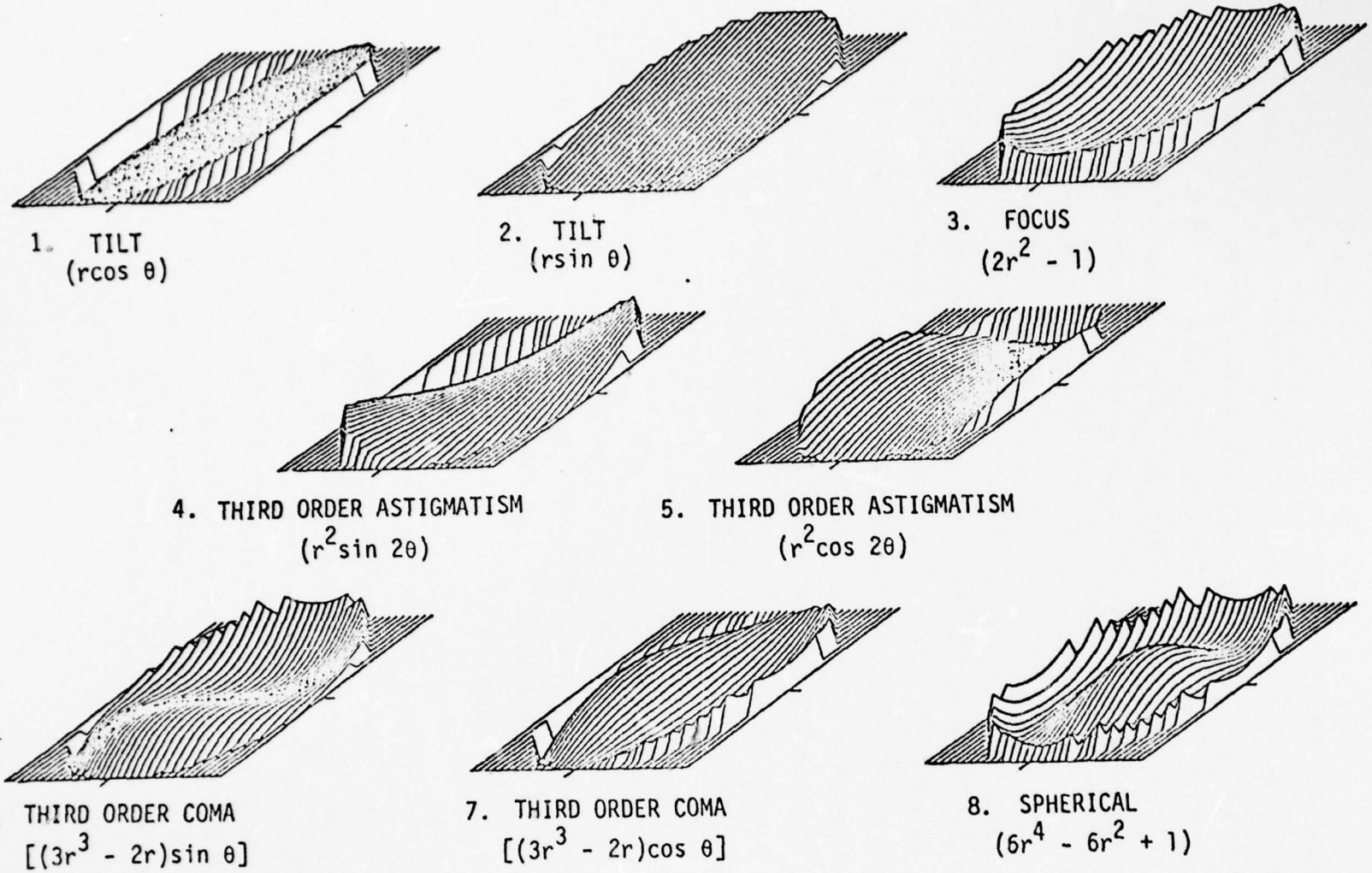

Figure A-4. Graphical Representations of Zernike Functions Associated with the Eight Lowest-Order Wavefront Aberrations. The Zernike functions are an orthogonal and complete set. Any arbitrary deformable mirror vibrant structural mode can be synthesized by a linear combination of Zernike modes. The error signal processor (cf. Fig. A-1) is generated by an outboard computer program which accepts a Zernike coefficient representation of the first 9 MOWACS modes.

A.2 SIMULATOR DESIGN FOR TRANSMITTER

Unlike the zonal transmitter, the modal transmitter has a continuous deformable surface which requires more transmitter plane points to represent the modal surface figure than the zonal case. It would be to our advantage to minimize the number of transmitter point locations and yet accurately model the modal surface from the computer simulator run time point of view.

A.2.1 Sampling Theorem

Although the MOWACS vibrational modes are a summation of Zernike polynomials which have different spatial frequencies, this may not determine the highest overall modal spatial frequency. Observing Fig. A-2, it appears that, in terms of trigometric functions, the largest number of cycles across the transmitter is not more than two. Nyquist theorem states that the minimum sampling frequency of any signal should be at least two times the highest frequency component of that signal.

A.2.2 16 × 16 Vs. 8 × 8 Transmitter

Because of the edge effects of the transmitter and the uncertainty of accurately modeling them, two transmitter configurations were considered with larger grids (16 × 16 and 8 × 8) than required by the Nyquist criterion.

Vibrational modes were compared in the far-field target plane to determine the degradation of the 8 × 8 transmitter over the 16 × 16. In Fig. A-5, Mode 7 was applied to both transmitters and a comparison was done in the far field. For a $\pi/2$ rad modal amplitude, the standard deviation (RMS) of the error observed was less than 1% with a maximum distortion of 5.7% (0.046 + 0.011). Applying all modes with random modal amplitudes ranging from $-\pi/2$ to $\pi/2$ produces an RMS error of 1.7% and a maximum distortion of 13% (cf. Fig. A-6). Based on these results the 8 × 8 grid was considered acceptable.

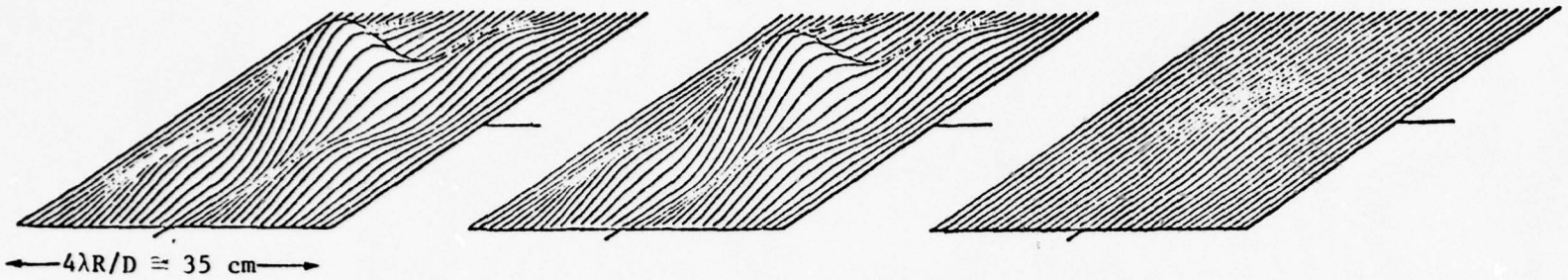

Target Plane Intensity
256-pt xmtr

Target Plane Intensity
64-pt xmtr

Difference ($\Delta I = I_{256} - I_{64}$)

$\Delta I_{RMS} = .009$

$\Delta I_{MIN}/I_0 = -.011$

$\Delta I_{MAX}/I_0 = .046$

Figure A-5. Error Calculation for Representing MOWACS Mode #7 by 64 Vs. 256 Points. Transmitter phase error is $\pi/2$. I_0 = maximum (diffraction limited) intensity.

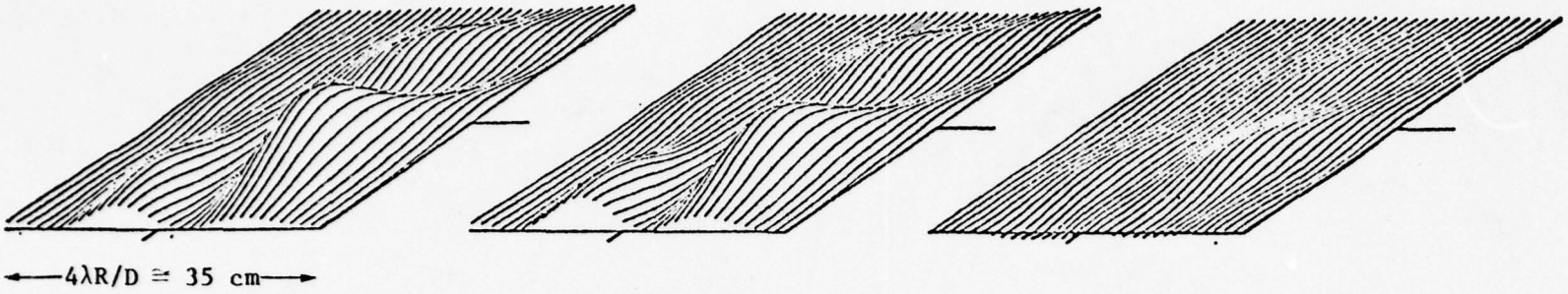

Target Plane Intensity
256-pt xmtr

Target Plane Intensity
64-pt xmtr

Difference ($\Delta I = I_{256} - I_{64}$)

$\Delta I_{RMS} = .017$

$\Delta I_{MIN}/I_0 = -.049$

$\Delta I_{MAX}/I_0 = .081$

Figure A-6. Error Calculation for Representing MOWACS Transmitter (All 9 Modes) by 64 Vs. 256 Points. Transmitter phase error is random from $-\pi/2$ to $\pi/2$ for each mode. I_0 = maximum (diffraction limited) intensity.

A.2.3 Target Plane Beam Patterns

A series of target plane beam profiles (shown in Figs. A-7 through A-9) were calculated for individual and combinations of modes for various amplitudes to determine the distribution of power on the target. Because each mode controls the entire transmitter aperture, dither amplitudes equal to those used in zonal systems give significantly larger fluctuations in target plane power distribution than a zonal transmitter.

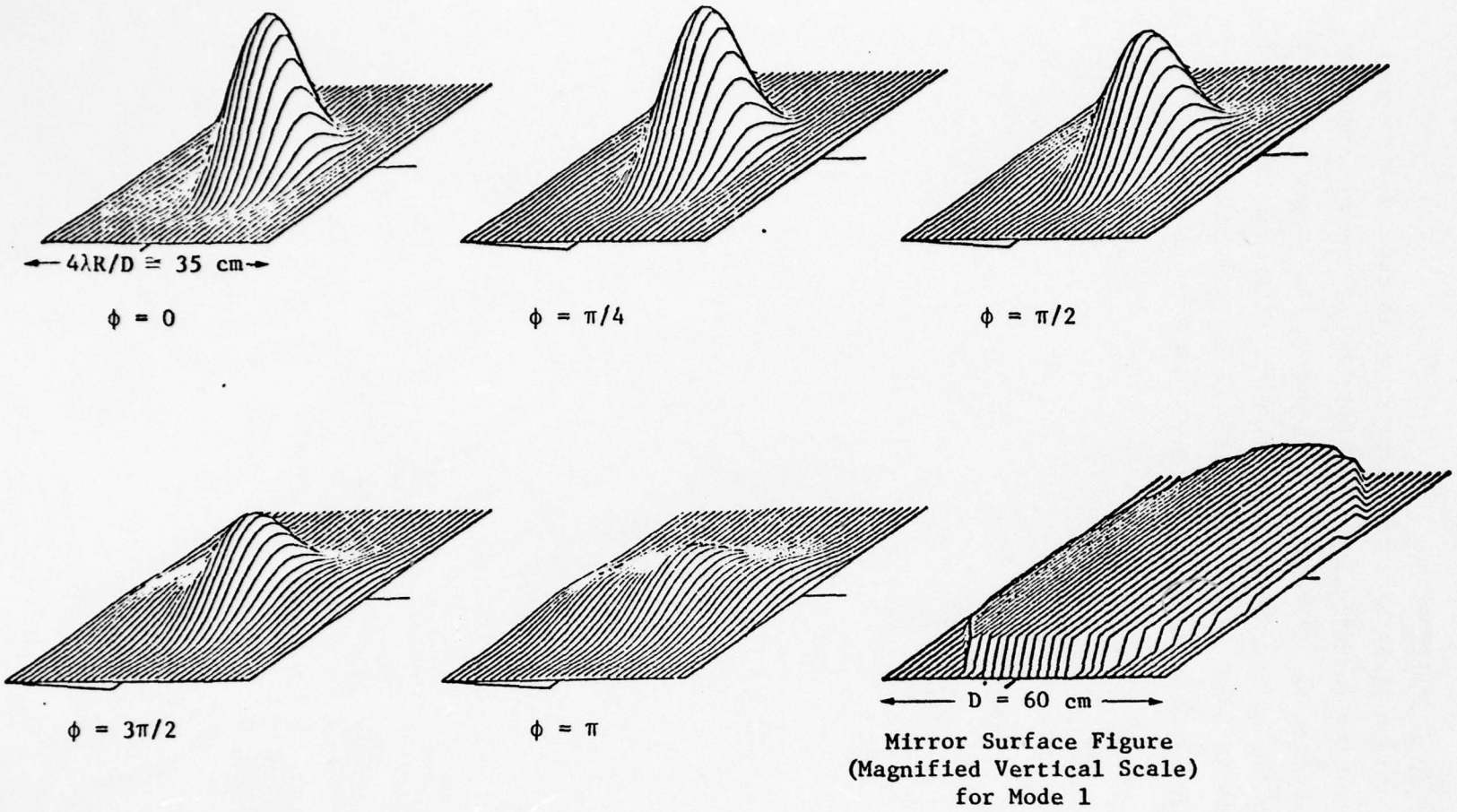

Figure A-7. Target Plane Beam Patterns for MOWACS Mode #1. Vertical displacement is intensity (linear scale) normalized to diffraction limited (ϕ = 0). Scenario parameters are: range = 5 km, λ = 10.6 μm, ϕ = transmitter phase error.

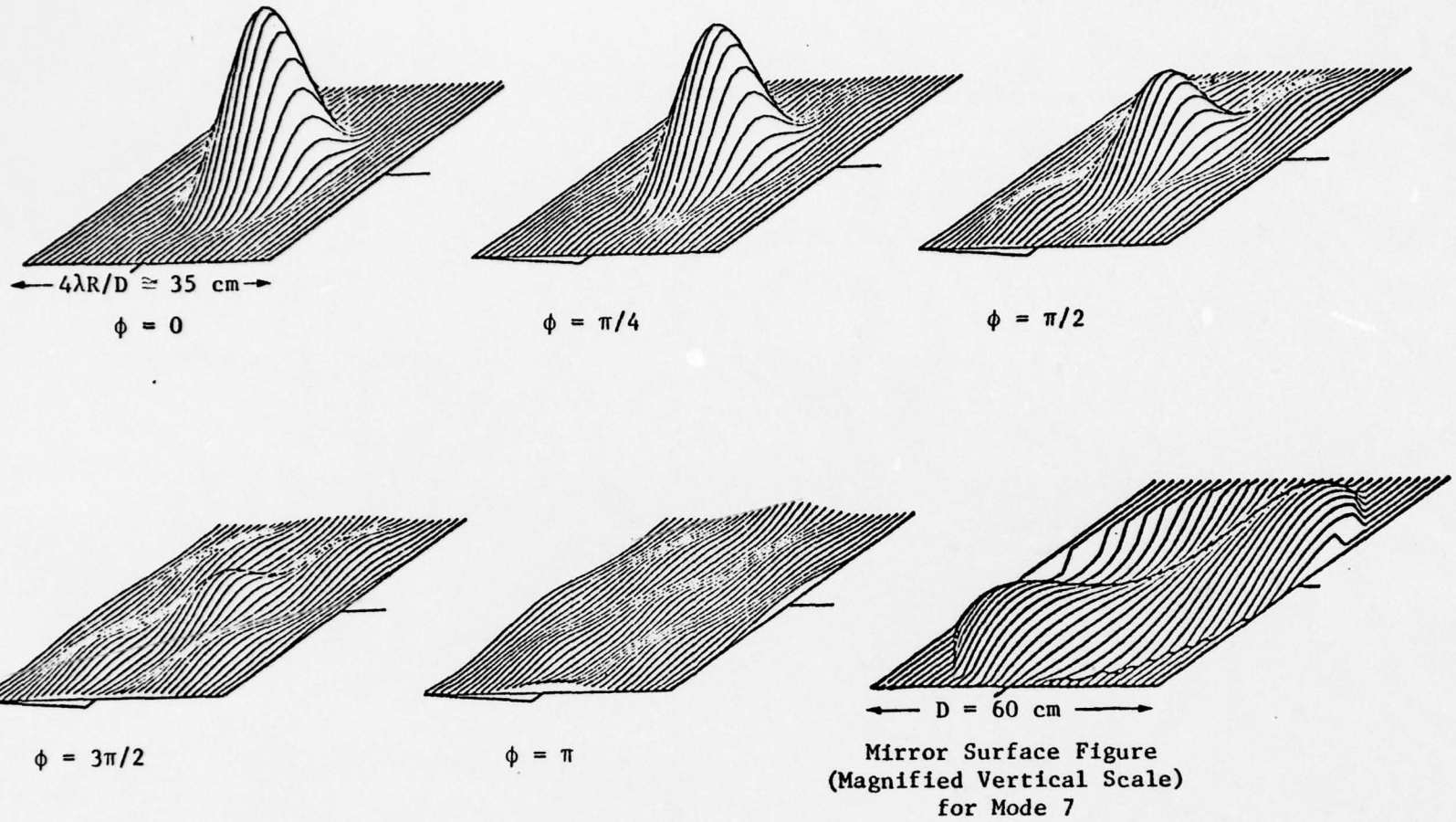

Figure A-8. Target Plane Beam Patterns for MOWACS Mode #7. Other parameters same as in Fig. A-7.

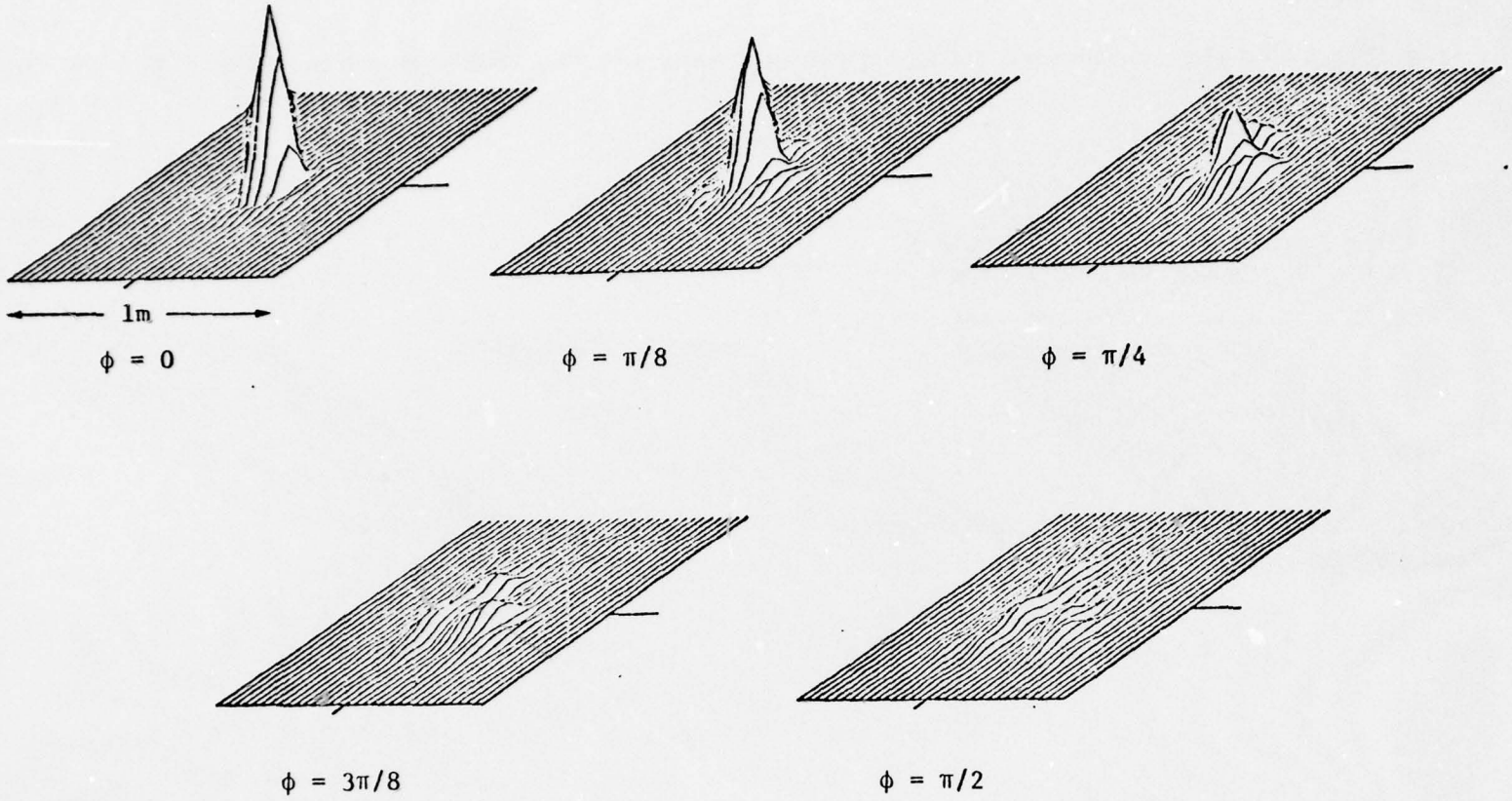

Figure A-9. Target Plane Beam Patterns for All 9 MOWACS Modes. Parameters same as in Fig. A-7 and A-8 except ϕ = initial phase error for each mode.

APPENDIX B
MODAL BASE-LINE SYSTEM EVALUATION

B.1 MODAL CORRECTION MECHANISM

Although initial perturbations are applied to the transmitter wavefront mode by mode, it is difficult to determine the mechanism by which the overall modal perturbation is corrected. It appears that a combination of both mode by mode and summation of modes approximate the conjugate of the initial perturbation. In other words, each initial mode perturbation is corrected by the negative of that perturbed mode. In addition, a combination of correcting modes may approximate the necessary correction to the wavefront, but not necessarily mode for mode. The overall effect appears to be the summation of all correcting modes working together to correct for the overall initial phase perturbation. Figure B-1 illustrates this effect, where the resultant phase error (initial mode amplitude plus correcting mode amplitude) is plotted. In case (a) an initial phase perturbation is applied only to Mode 9. Note that all modes are correcting for the perturbation caused by Mode 9. In case (b), both Modes 4 and 9 are perturbed initially. In both cases, the mode(s) that was initially perturbed contributed the maximum correction, but additional correction is provided by the other modes.

B.2 SENSITIVITY TO INITIAL TRANSMITTER PHASE ERROR

The additive property of the different modes causes an initial randomization of the modes that can produce a wavefront distortion too severe for the system to correct. Hence, proper treatment in determining the initial wavefront distortion must be exercised. This effect is demonstrated in Fig. B-2, in which the two target plane beam profiles were produced by initially unconverged transmitters with the same RMS (1.7 rad) but slightly different peak-to-peak errors (6.28 rad vs. 6.50 rad). The closed-loop performance against a point target (Fig. B-3a) shows the sensitivity of the modal performance to the assumed initial phase error.

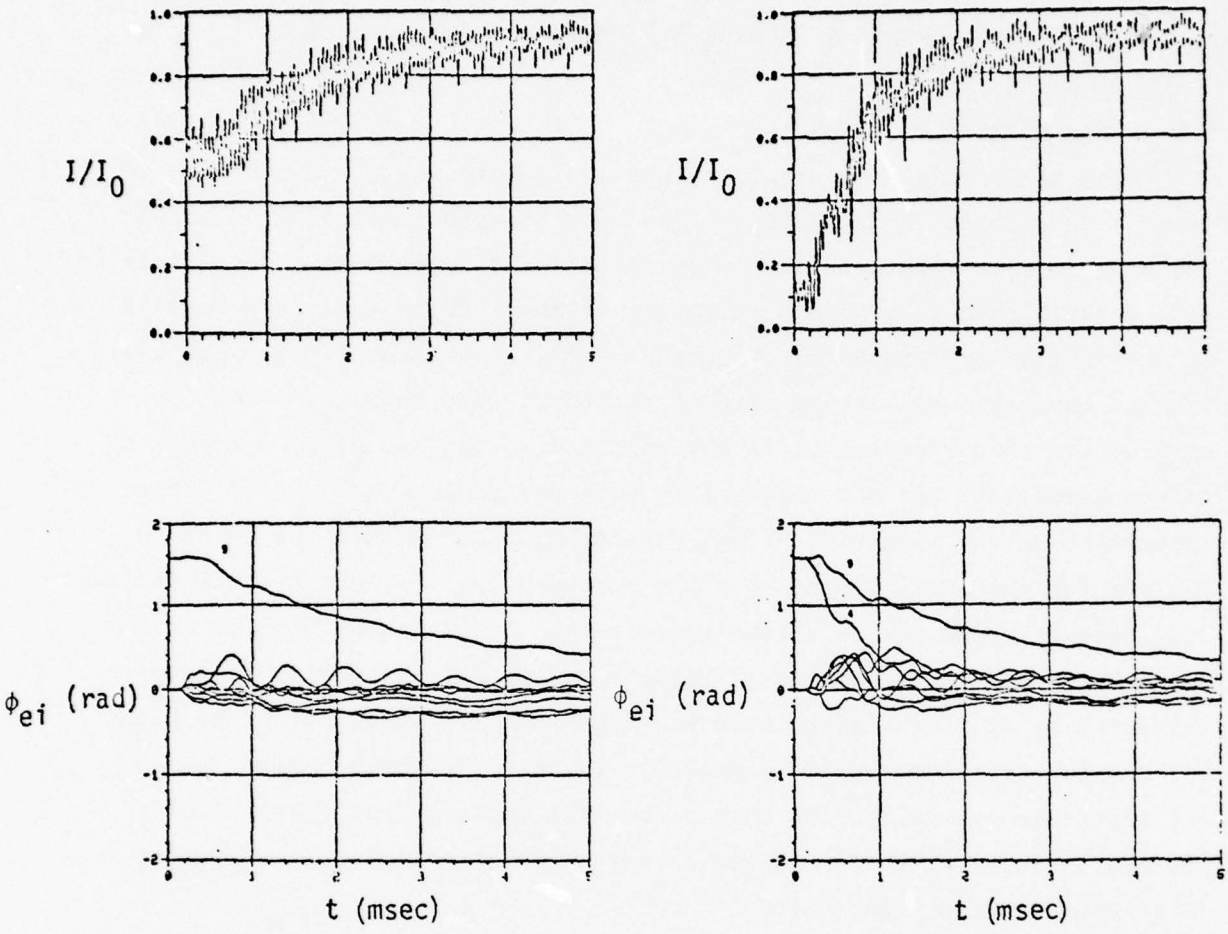

(a) initial error in mode 9 only

(b) initial error in modes 4 and 9 only

Figure B-1. Modal Multidither COAT Closed Loop Performance with a Point Target for One- and Two-Mode Initial Errors. Curves show Strehl ratio (I/I_0) and amplitude error per mode (ϕ_{ei}) vs. time. Modal transmitter consists of the first 9 MOWACS modes.

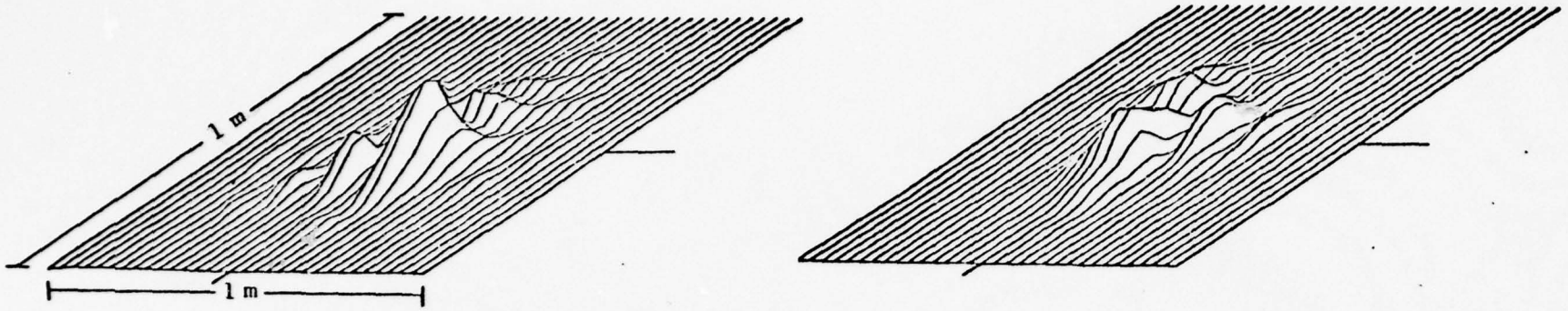

(a) ϕ_{p-p} = 6.28 rad

(b) ϕ_{p-p} = 6.50 rad

Figure B-2. Target Plane Beam Profiles for Two MOWACS Transmitters with Equivalent Phase RMS ($\cong$ 1.7 rad), but Different Peak-to-Peak Wavefront Distortion (ϕ_{p-p}). Parameters are: range = 5 km, λ = 10.6 μm, transmitter diameter = 0.6 m.

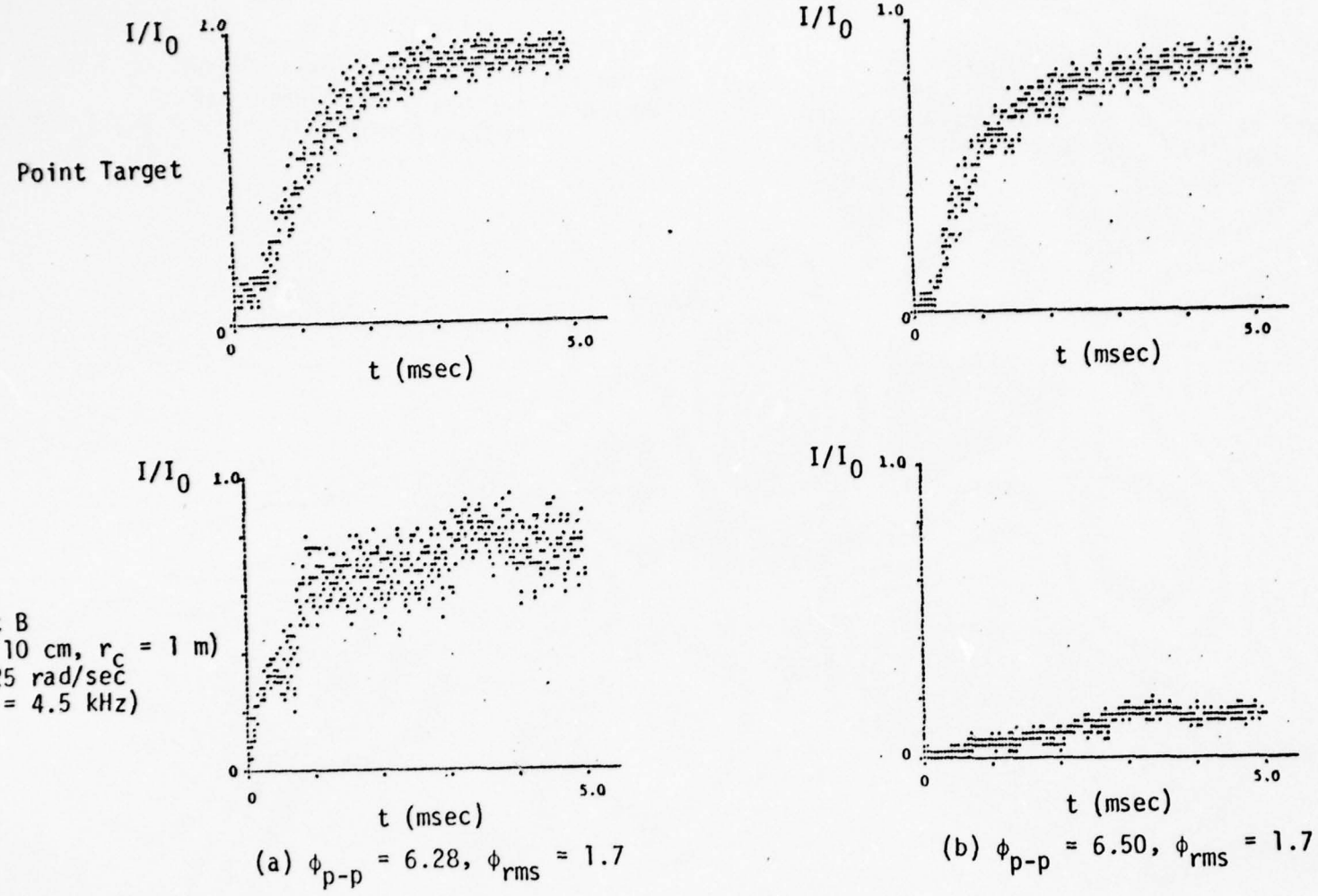

Figure B-3. Modal Closed Loop Performance for Two Initial Phase Errors. ϕ_{rms} = root mean square phase error, ϕ_{p-p} = peak-to-peak phase error.

These same initial phase errors show even more pronounced effect on a distributed target (cf. Fig. B-3b). The target is Target B (a sphere segment of 10-cm extent, 1-m radius of curvature, comprised of aircraft material) rotating at 0.25 rad/sec. The target size corresponds to half the converged beam diameter. The bandwidth of the target noise is 4.5 kHz, which is well below lowest dither frequency (8 kHz). The results with the more favorable initial beam profile show a similar level of performance to the zonal multidither system.

B.3 EFFECT OF DITHER FREQUENCIES ON SYSTEM PERFORMANCE WITH A DISTRIBUTED TARGET

A fair comparison for both multidither systems require the same dither frequencies and dither frequency separation if the same electronic signal processor is used. As dither frequencies are lowered, base-band target noise overlaps the dither bands for slower target rotations. The result is a degradation in performance due to target noise overlapping the lower dither frequencies. In addition, if the dither frequency spacing is decreased, it can be shown that the convergence will be delayed.

In Fig. B-4, a comparison in modal performance for two dither bands, the zonal equivalent (8-20 kHz) and the actual MOWACS frequencies (2.3-13.3 kHz) is presented. The target is Target B rotating at 1 rad/sec (f_{max} = 18 kHz). As expected, qualitative results indicate a degradation in performance, both in convergence level and convergence time.

With the point target, a delay in convergence time was expected for the actual MOWACS dither frequencies (2.3-13.2 kHz) due to the additional intermodulation terms. In practice, this was found not to be significant as illustrated in Fig. B-5, where similar performance between equally spaced dithers and actual MOWACS resonant frequencies is compared.

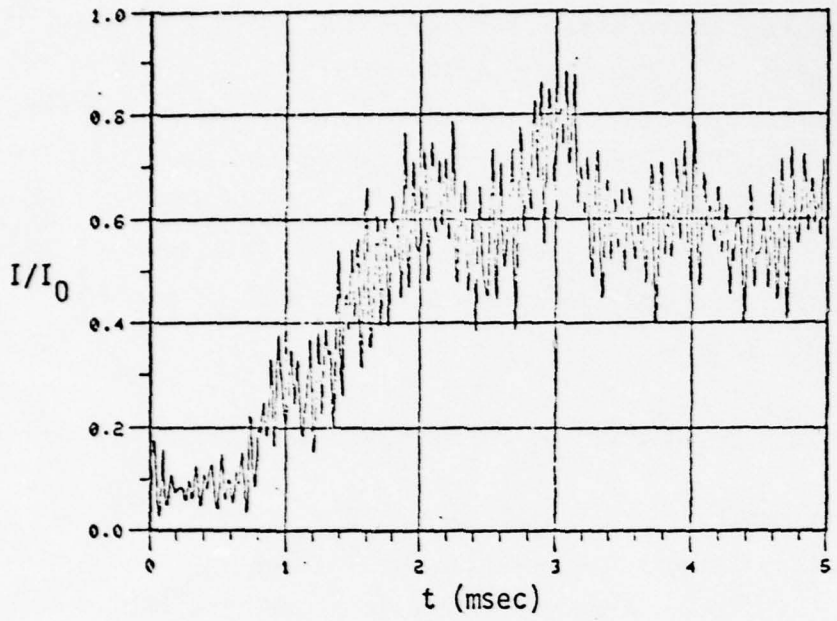

(a) f_d = 8-20 kHz, Δf = 1.5 kHz

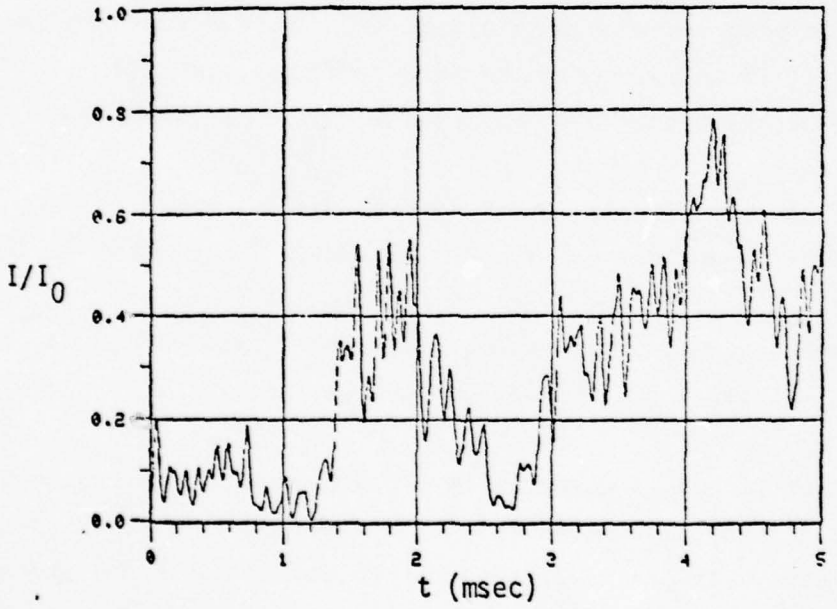

(b) f_d = 2.3-13.3 kHz (actual MOWACS frequencies)

Figure B-4. Modal Closed Loop Performance with Target B for Two Different Sets of Dither Frequencies. In (a) the dithers are equally spaced Δf apart. Parameters: number of modes = 9, range = 5 km, λ = 10.6 μm, Ω = 1 rad/sec (f_{max} = 18 kHz).

AD-A036 302 GENERAL RESEARCH CORP MCLEAN VA WASHINGTON OPERATIONS F/G 17/8
COAT: MODAL-ZONAL COMPARISON.(U)
AUG 76 J RADLEY, N NOMIYAMA, J WILSON N60921-76-C-0122

UNCLASSIFIED NL

2 OF 2
AD-A
036 302

END
DATE
FILMED
4-5-77
NTIS

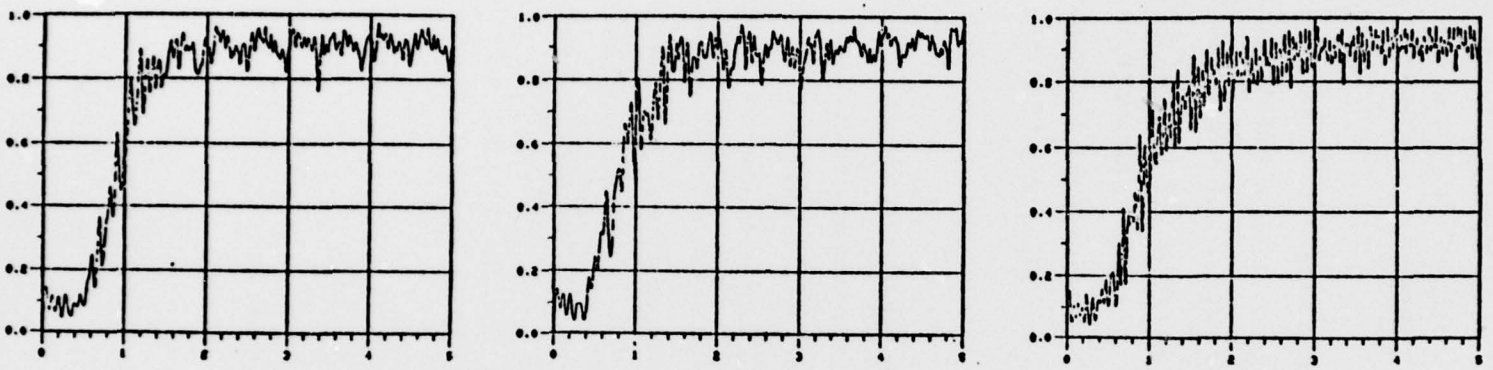

(a) f_d = 2-14 kHz, Δf = 1.5 kHz

(b) f_d = 2.3-13.3 kHz (actual MOWACS frequencies)

(c) f_d = 8-20 kHz, Δf = 1.5 kHz

Figure B-5. Modal Closed-Loop Performance with a Point Target for Three Different Sets of Dither Frequencies. In (a) and (c) the 9 dithers are equally spaced Δf apart. Curves are Strehl ratio (I/I_0) vs. time (0 to 5 msec).

APPENDIX C
ATMOSPHERIC TURBULENCE MODEL

The effect of atmospheric turbulence on a received laser beam wavefront is included in system calculations by generating a two-dimensional array of phase fluctuations induced by the atmosphere at the transceiver plane. The inclusion of such an array here accounts for most of the phase variations caused by propagation through the turbulent atmosphere. While not including amplitude variations due to propagation from turbulent layers at high altitudes, such effects are of secondary importance for the laser system and scenarios of interest.

The array of phase fluctuations is computed from the convolution of a set of zero mean, normally distributed random numbers with the autocorrelation of the spatial frequency distribution for the propagation path under consideration. This autocorrelation is the Fourier transform of the spatial frequency spectrum (assumed to be modified von Karman). For the simulation, the spectrum was approximated by a κ^{-4} dependence (where κ is the spatial frequency) with a sharp cutoff at $\kappa = 2\pi/L_0$, corresponding to the outer scale of turbulence. The variance for the phase fluctuations derived below is given by[1]

$$\sigma_n^2 = 0.0087 k^2 C_n^2 \, dL_0^{5/3} \qquad \text{(C-1)}$$

where k = wave number $2\pi/\lambda$

C_n^2 = refractive index structure parameter

L_0 = outer scale of turbulence

d = effective width of phase-perturbing region

---

[1] J. Gilbert et al., Sensor Modulation Effects, General Research Corporation, 905-01-CR, to be published.

The square root of Eq. C-1 is plotted in Fig. C-1 vs. C_n^2 for several values of d and L_0. As is illustrated by the curves, a particular value for the phase variance can be obtained from numerous sets of the other three parameters.

A great deal of experimental work has been performed to determine the parameter C_n^2. For reference, Fig. C-2 presents representative experimental data[1] on the variation of C_n^2 as obtained from thermosonde measurements.

The expression for σ_n follows. The refractive index spectrum hypothesized by Tatarski[2] has the following form:

$$\Phi_n(\kappa) = 0.033 C_n^2 \kappa^{11/3} \exp\left(-\kappa^2/\kappa_m^2\right) \qquad \text{(C-2)}$$

where C_n^2 = index of refraction structure function

κ = spatial frequency

$\kappa_m = 5.92/\ell_0$ in which ℓ_0 = inner scale of the atmosphere

In the limit as κ approaches 0, this spectrum becomes indeterminate. Strohbehn[3] added an additional term that causes the spectrum to saturate for values of $\kappa < 1/L_0$. This modified spectrum has the form

$$\Phi_n^1(\kappa) = 0.033 C_n^2 [\kappa^2 + 4\pi^2 L_0^{-2}]^{-11/6} \exp\left(-\kappa^2/\kappa_m^2\right) \qquad \text{(C-3)}$$

---

[1] P. O. Minott et al., Results of Balloon Atmospheric Propagation Experiment Flights of 1970, Goddard Space Flight Center Document X-524-72-125 (March 1972).

[2] V. I. Tatarski, The Effects of the Turbulent Atmosphere on Wave Propagation, Report TT-68-50464, U.S. National Technical Information Service, Springfield, Virginia, p. 76.

[3] J. W. Strohbehn, Proc. IEEE, 56, p. 1301 (1968).

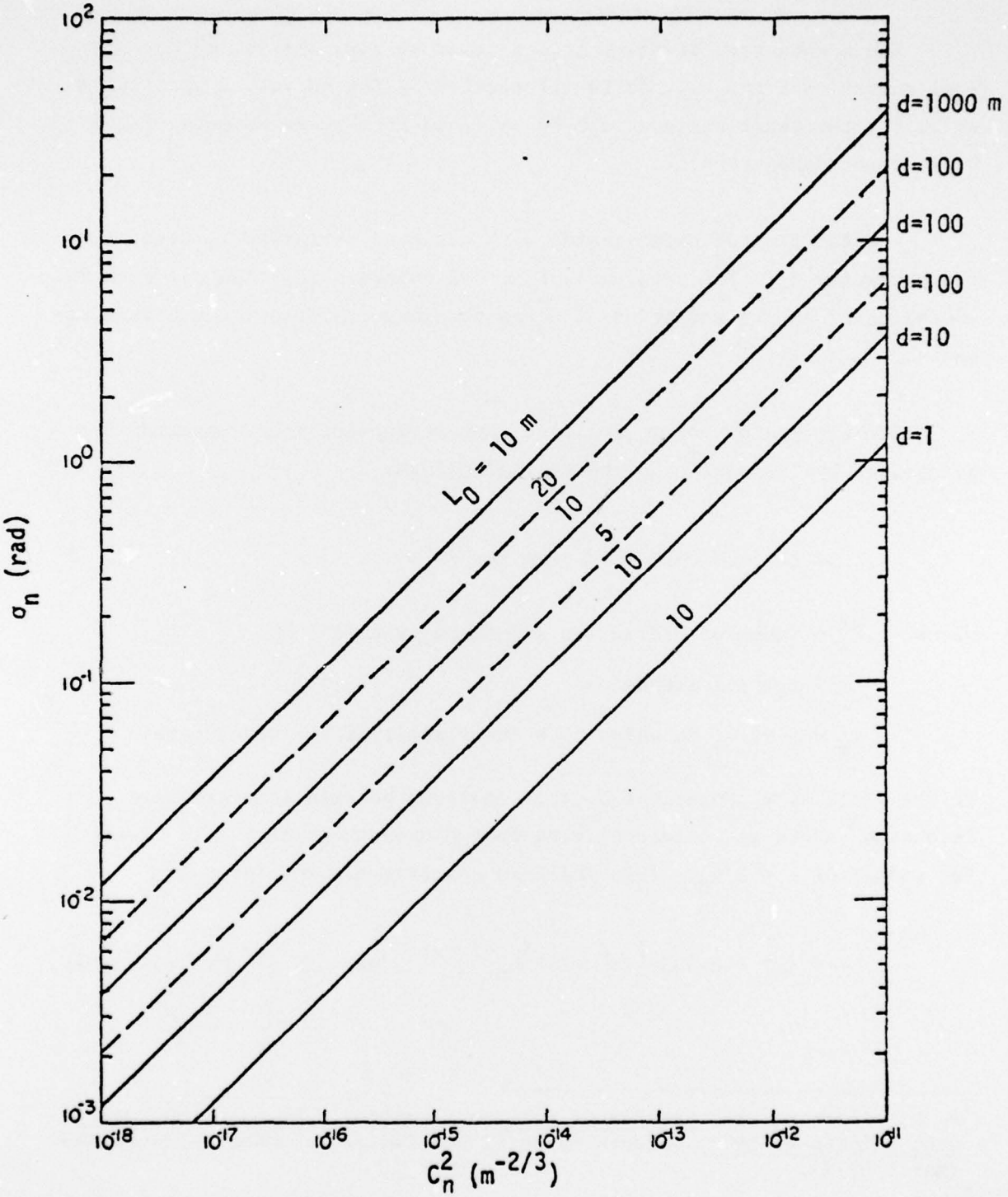

Figure C-1. Curves of RMS Phase (σ_n) of Fluctuations vs. the Refractive Index Structure Parameter (C_n^2) Showing the Effects of Model Parameters on the Magnitude of the Phase Variations: L_0 = outer scale of turbulence, d = effective width of phase screen

REFRACTIVE-INDEX-STRUCTURE CONSTANT AS A FUNCTION OF HEIGHT ABOVE GROUND LEVEL. 1:00 AM MST 21 OCTOBER 1970 AT HOLLOMANAFB NEW MEXICO. BAPE I EXPERIMENT

\+ DATA POINTS OBTAINED BY TATARSKI'S METHOD OF MEAN TEMPERATURES

● DATA POINTS OBTAINED FROM THERMOSONDES MEASUREMENT

——— EXPERIMENTAL DEPENDENCE OF C_n^2 UPON ALTITUDE

– – – MATHEMATICAL MODEL USED TO REPRESENT EXPERIMENTAL DATA

$C_n^2 = C_{no}^2 \, h^{-1/3} \, e^{-h/ho}$

$C_{no}^2 = 4.0X10^{-14}$ m.$^{-2/3}$ $h_o = 1000$ m.

GROUND LEVEL $1.2X10^3$ m. ABOVE MSL

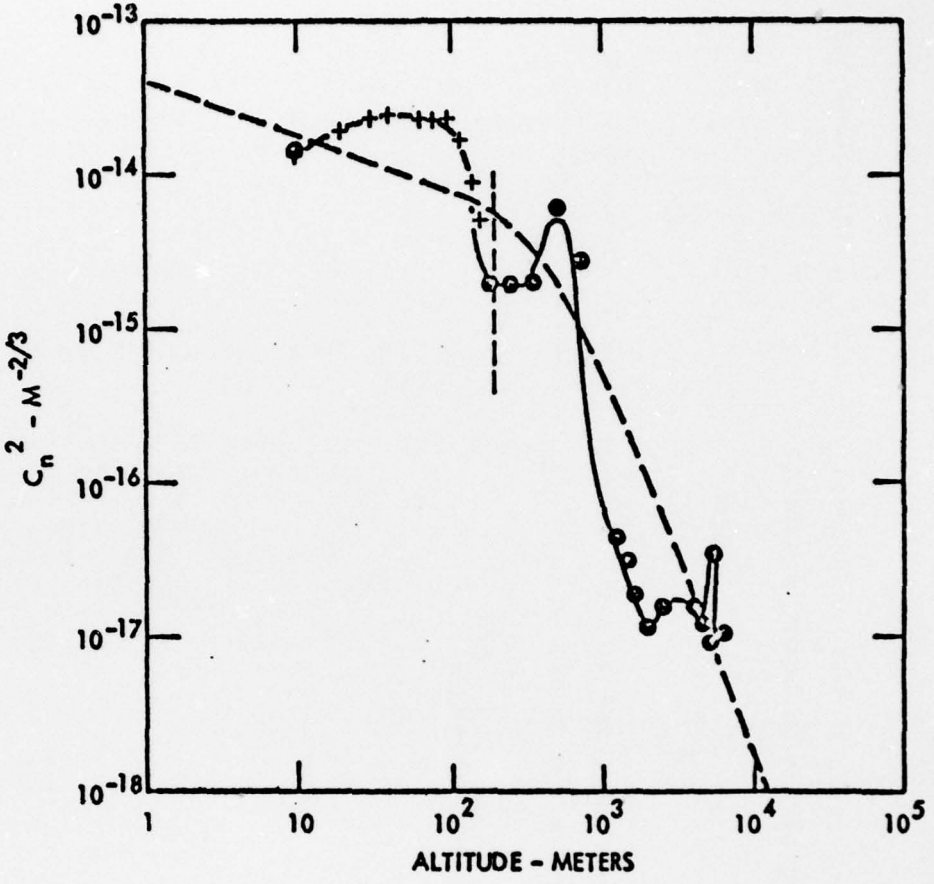

Figure C-2. Empirical Modeling of the Atmosphere

As demonstrated by Taylor,[1] the variance of the index of refraction variations is obtained by the following equation:

$$\sigma_n^2 = \pi^2 k^2 d \int_0^\infty \Phi_n(\kappa)\kappa \, d\kappa \qquad \text{(C-4)}$$

where d = width of the phase screen. This integral is tabulated, from which we obtain, for the condition $L_0 >> \ell_0$, Eq. C-1:

$$\sigma_n^2 = 0.0087 k^2 d C_n^2 L_0^{5/3}$$

[1] L. S. Taylor et al., JOSA, 65, p. 78 (1975).

APPENDIX D

EFFECT OF APERTURE AVERAGING ON SPECKLE POWER SPECTRAL DENSITY

COAT systems are degraded by target effects because the random phase and intensity pattern that is generated by the microscopically irregular target surface manifests itself as a noise signal at the COAT receiving aperture. Accordingly, it is important to know the extent and distribution in the frequency domain of this target modulation signal in comparison with the COAT sensing and bandpass frequencies.

There are two methods available to assess the COAT degradation by target noise. The direct method is the more laborious: the spatial distribution of target brightness is represented by a system of point scatterers whose speckle pattern (intensity) at the receiving plane is calculated point by point in its propagation from target to receiver; the square of the absolute magnitude of the Fourier transform of the speckle pattern gives the power spectral density; and a large number of samples provides the ensemble-averaged power spectral density of the speckle pattern at the receiver.

The second method to assess target-induced noise effects is analytical and circumvents a large amount of computation that is required by the direct method. It is simply that, by using properties of the Fourier transforms that are involved, the power spectral density of the intensity in the receiving-aperture plane is proportional to the autocorrelation of the target brightness distribution. The only assumptions necessary are that the target and receiver be in Fourier transform planes and that the target be diffuse. Several authors[1,2,3,4] have derived this relationship between speckle power spectral density (PSD) and target brightness, so only the results will be summarized here.

---

[1] R. I. Goldfischer, JOSA, 55, 247 (1965).

[2] J. W. Goodman, Proc. IEEE, 53, 1688, (1965).

[3] R. B. Crane, JOSA, 60, 1658 (1970).

[4] P. H. Dietz, JOSA, 65, 279 (1975).

The first assumption is that the target and receiver electric fields are related by Fourier transform. This is valid if either one of two conditions is met: (1) a lens is present in the receiver plane whose focal length is equal to the target range, or (2) the target is in the far field. In this report, perfect autofocus is assumed and condition #1 is satisfied. One method of deriving the desired relationship is using the autocorrelation (or Wiener-Khintchine) theorem of Fourier transform theory.[1] Displayed graphically in Fig. D-1, it states that the power spectral density of an arbitrary function may be calculated either by (1) the square of the absolute magnitude of the Fourier transform of the function, or (2) the Fourier transform of the autocorrelation of the function. Repeated application of the autocorrelation theorem to the electric field distribution at the target results in the assorted relationships that are displayed in Fig. D-2.

The final step in relating the speckle PSD to the target brightness distribution is to derive an expression for the intensity autocorrelation in terms of the autocorrelation of the field at the receiver plane. Goodman has shown,[2] in the case where the real and imaginary components of the complex electric field obey Gaussian statistics and have equal variances (which, for example, is the case for a diffuse target), that the speckle-intensity normalized autocorrelation function [$\Gamma_I(\Delta x, \Delta y)$] (the autocorrelation coefficient) and normalized field autocorrelation function [$\Gamma_E(\Delta x, \Delta y)$] are related by the following expression:

$$\Gamma_I(\Delta x, \Delta y) = \langle I(x, y)\rangle\langle I(x + \Delta x, y + \Delta y)\rangle + |\Gamma_E(\Delta x, \Delta y)|^2 \qquad \text{(D-1)}$$

Taking the Fourier transform of both sides of this expression gives the following result:

---

[1] J. D. Malick et al., Implications of Evolving Laser Technology, Phase II: Observables and Discriminants, SAMSO-TR-71-220, July 1971.

[2] J. W. Goodman, "Statistical Properties of Laser Speckle Patterns," in Topics In Applied Physics, ed., J. C. Dainty, Springer-Verlag: New York, Vol. 9, 1975.

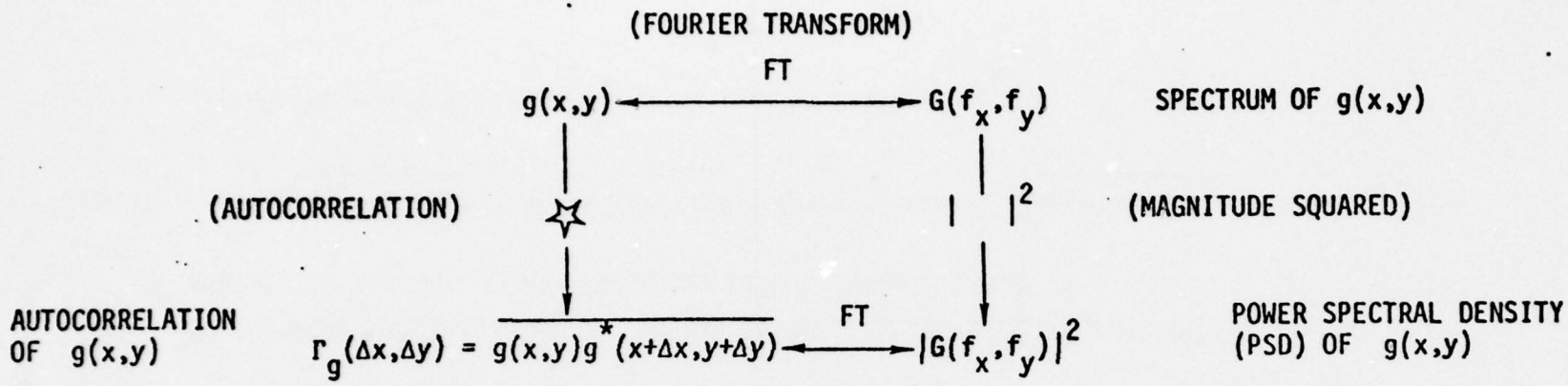

Figure D-1. The Autocorrelation Theorem. This theorem (also known as the Wiener-Khintchine Theorem) is a general result of Fourier transform theory and can be used to relate the optical properties of a target to the observables in the receiver plane.

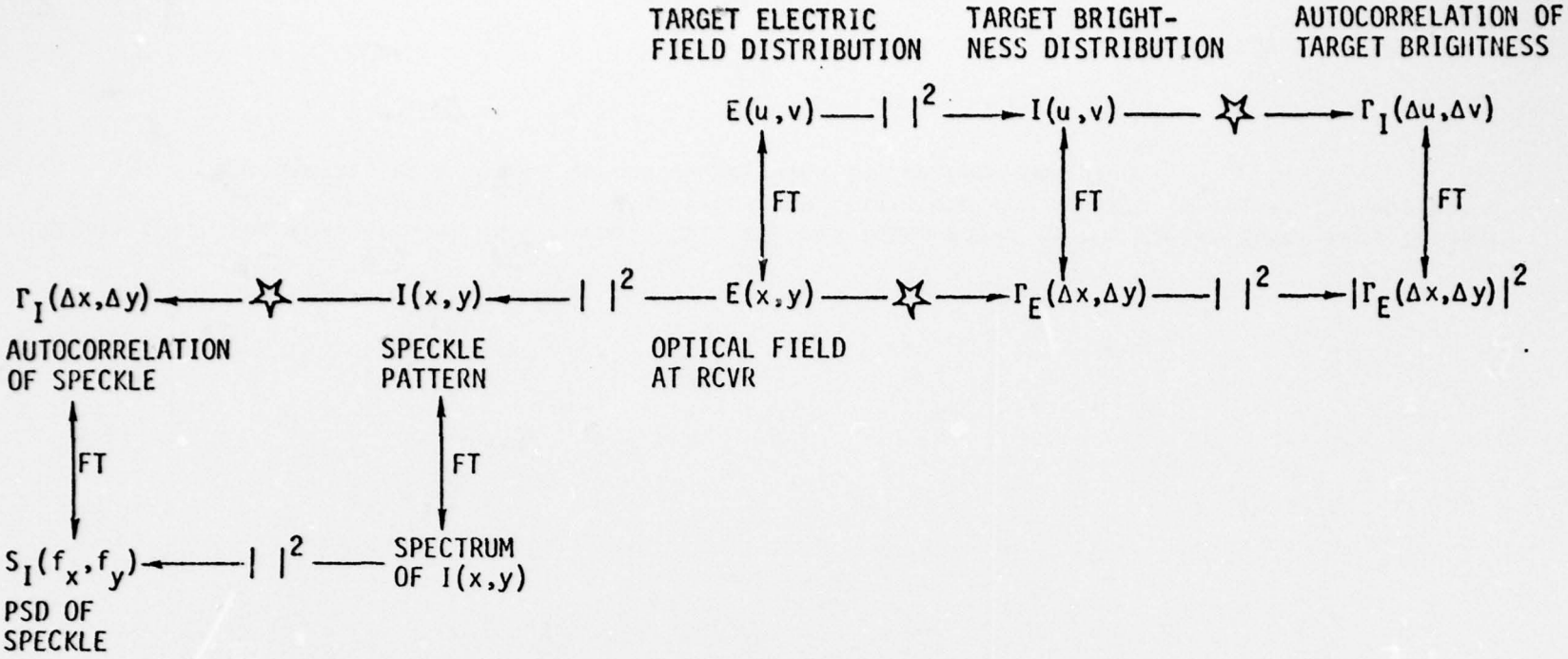

IF THE REAL AND IMAGINARY COMPONENTS OF THE COMPLEX FIELD E(x,y) OBEY GAUSSIAN STATISTICS AND HAVE EQUAL VARIANCES (i.e., DIFFUSE TARGET):

$$\underbrace{\langle \Gamma_I(\Delta x, \Delta y) \rangle}_{} = \langle I(x, y) \rangle \langle I(x + \Delta x, y + \Delta y) \rangle + \underbrace{|\Gamma_E(\Delta x, \Delta y)|^2}_{}$$

TAKING THE FOURIER TRANSFORM OF BOTH SIDES GIVES:

$$\boxed{S_I(f_x, f_y) \propto \delta(f_x, f_y) + \Gamma_I(\Delta u, \Delta v)}$$

Figure D-2. Application of Autocorrelation Theorem[1]

[1] J. D. Malick et al., op. cit.

$$S_I(f_x, f_y) \propto \delta(f_x, f_y) + \Gamma_I(\Delta u, \Delta v) \qquad \text{(D-2)}$$

where $S_I(f_x, f_y)$ is the power spectral density of the speckle pattern and $\Gamma_I(\Delta u, \Delta v)$ is the autocorrelation of the target brightness distribution, $I(u, v)$. With proper normalization, the complete relationship is as follows:[1]

$$S_I(f_x, f_y) = \langle I \rangle^2 \left\{ \delta(f_x, f_y) + \frac{\iint_{-\infty}^{\infty} I(u, v) I(u - \lambda R f_x)(v - \lambda R f_y)\, du\, dv}{\iint_{-\infty}^{\infty} I(u, v)\, du\, dv} \right\} \qquad \text{(D-3)}$$

where the receiver plane spatial frequencies in the x and y directions respectively are f_x and f_y, the mean intensity at the receiving-aperture plane is $\langle I \rangle$, the perpendicular distance between the target and receiver plane is R, and the wavelength is λ. The second term in the braces is the normalized autocorrelation function (the autocorrelation coefficient) of the target brightness. It will be therefore noticed that the total power, or the integral of the entire expression over frequency, contains equal contributions from the DC (impulse) term and from the frequency-distributed component.

With this relationship between the speckle PSD and target brightness, it is straightforward to calculate the target modulation spectrum for virtually any target geometry and adaptive illumination. The next step is to relate this PSD to the case when it is sampled by a finite size (rather than a point) receiver and how this is scaled into the temporal frequency domain to account for target rotation. Only the final relationships are presented here and the reader is referred to Radley et al.[1] for the detailed analysis.

The effects of aperture averaging on speckle are shown graphically in Fig. D-3 and are summarized below. The power spectral density

---

[1] J. Radley et al., COAT-Target Interactive Modulation Effects, GRC Report 571-02-TR, August 1976.

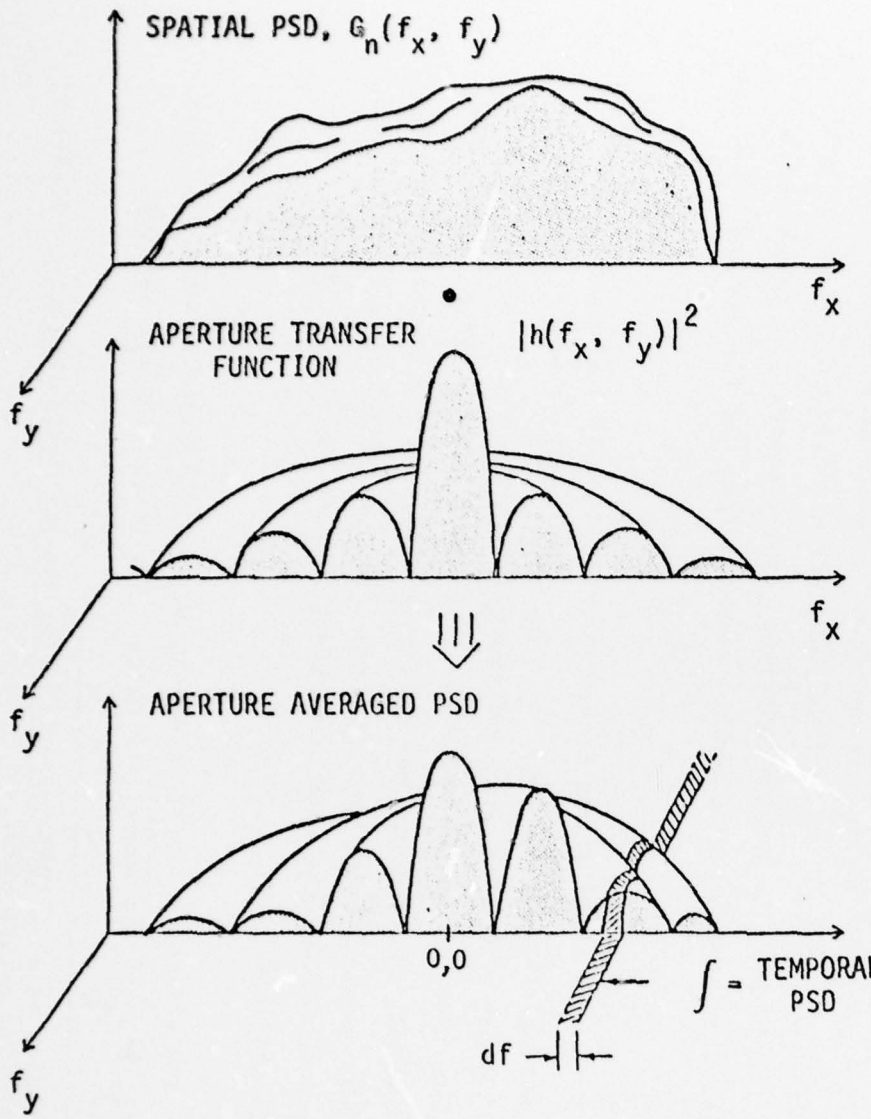

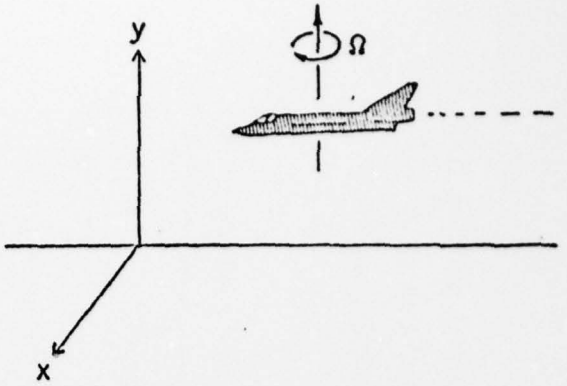

- TARGET NOISE PSD ≈ AUTOCORRELATION OF TARGET PLANE RADIANCE
- THE APERTURE TRANSFER FUNCTION $S_h(f_x, f_y)$, IS THE FOURIER TRANSFORM OF THE PUPIL FUNCTION
- THE TEMPORAL PSD OF THE DETECTED SIGNAL IS PROPORTIONAL TO THE PRODUCT OF THE ABOVE INTEGRATED ALONG THE y FREQUENCIES
- NOISE SPECTRUM CAN BE CALCULATED ANALYTICALLY
- TARGET NOISE PSD =

$$\int_{f_y=-\infty}^{\infty} S_I(f_x, f_y),\ S_h(f_x, f_y)\ df_y$$

Figure D-3. Summary of Aperture Averaging

$S_I(f_x, f_y)$ of the speckle intensity incident on the receiving aperture is related to the target brightness distribution I(u, v) and its mean <I> by

$$S_I(f_x, f_y) = \langle I \rangle^2 \left[\delta(f_x, f_y) + \Gamma_I(\lambda R f_x, \lambda R f_y)\right] \qquad \text{(D-4)}$$

where $\Gamma_I(\lambda R f_x, \lambda R f_y)$ is the autocorrelation coefficient of the target brightness, λ is the wavelength, and R is the range. The spatial frequencies f_x and f_y correspond to the x and y directions, respectively, in the aperture plane.

The power spectral density $S_0(f_x, f_y)$ of the speckle intensity that is passed by the aperture is related to $S_I(f_x, f_y)$ by the aperture transfer function $H(f_x, f_y)$

$$S_0(f_x, f_y) = S_I(f_x, f_y)\left|H(f_x, f_y)\right|^2 \qquad \text{(D-5)}$$

where $H(f_x, f_y)$ is the two dimensional spatial Fourier transform of the pupil function of the receiver aperture. The power spectral density (PSD) of the aperture response function A(x, y) is the square of the absolute magnitude of the Fourier transform of A(x, y). A(x, y) is unity within the aperture, zero elsewhere.

The probability density function p(I) of the speckle intensity I at the aperture can be found from the number M of correlation cells within the aperture

$$p(I) = (MI/\langle I \rangle)^M \, e^{-MI/\langle I \rangle}/I\Gamma(M) \qquad \text{(D-6)}$$

where $\Gamma(M)$ is the gamma function of M, and M is related to the variance of the aperture integrated speckle PSD:

$$M^{-1} = \iint_{-\infty}^{\infty} S_0(f_x, f_y)\, df_x\, df_y \qquad \text{(D-7)}$$

The speckle contrast ratio C_r, defined as the ratio of the RMS intensity variation divided by the mean intensity, is related to M very simply:

$$C_r = M^{-1/2} \tag{D-8}$$

When there is relative motion between target and aperture (e.g., a rotating target), the speckle pattern is swept across the receiving aperture in a direction perpendicular to the target's effective rotation axis, resulting in a temporal-domain PSD $S_0(f)$ that is a function of the temporal frequency f, and is given by a one-dimensional integral of $S_0(f_x, f_y)$. For rotation about the y axis, the expression for $S_0(f)$ is

$$S_0(f) = (v_x)^{-1}\left[\int_{-\infty}^{\infty} S_0(f_x, f_y)\, df_y\right]_{f_x=f/v_x} \tag{D-9}$$

where $v_x = 2R\Omega$ is the relative velocity in the x direction at the aperture and Ω is the target's effective rotation rate perpendicular to the line of sight.